Telomerase RNP: from core RNA structure to the short-telomere senescence response

By

Rachel O. Niederer

A dissertation submitted to Johns Hopkins University in conformity with the requirements for the degree of Doctor of Philosophy

Baltimore, Maryland

July 2015

Abstract

Telomerase is a ribonucleoprotein that extends the ends of linear chromosomes. The RNA component contributes to many important functions of the enzyme including providing the template for reverse transcription by TERT, presenting a flexible scaffold for accessory subunit binding and contributing to enzyme coordination during catalysis through a poorly understood mechanism. Despite these crucial roles, the structure-function relationships of the RNA have remained undefined due, in part, to the lack of detailed structural information available. Here I present refined secondary-structure models for the central cores of both the human and yeast RNA, highlighting conserved regions of flexibility adjacent to the template that likely play a role in enzyme catalysis. I also show that disease-associated mutations in telomerase RNA alter the folding equilibrium to a degree that is likely sufficient to disrupt enzyme activity. Telomerase function is critical for maintaining genome stability within the cell. When telomerase is absent or has compromised function the result is progressive telomere shortening until a specific cell-cycle arrest known as senescence. The adaptive changes undergone by the cell during this process remain unclear. Using RNA-seq I have shown that senescence is a distinct state both phenotypically and transcriptionally, although it overlaps substantially with other related conditions such as slow growth and the DNA damage response. The senescence response is consistent with many pro-survival adaptations, including initiation of a starvation response and concurrent upregulation of autophagy. These findings

place senescence within a wider context of other stress responses, while also highlighting the unique challenges faced by cells having to deal with progressively shortening telomeres.

Thesis advisor:	**Dr. David Zappulla**
Thesis committee:	**Dr. Sarah Woodson**
	Dr. Karen Beemon
	Dr. Nickolas Papadoupolos

Acknowledgements

First, I would like to thank my thesis advisor, David Zappulla, for all of the support I have received during my time in the lab. He has given me a great deal of freedom to explore topics and techniques that interest me while providing extensive enthusiasm and encouragement.

I would also like to thank my thesis committee – Dr. Sarah Woodson, Dr. Karen Beemon, and Dr. Nickolas Papadoupolos – for the helpful advice I've received over the years. Each of them has made him or herself available to me to drop by and ask questions both about science and for career advice and I greatly appreciate it.

I also thank my lab mates: Dr. Melissa Mefford, Karen McMurdie, Evan Hass and Dr. Kevin Lebo. I have grown tremendously as a scientist during my time here due in large part to the help, discussions, advice, etc. I've received from my lab mates.

I want to thank my friends in the department, in particular Kevin DeLong for numerous thoughtful discussions and code troubleshooting. I've had a lot of fun during my time here thanks to my friends, and this has made graduate school much easier to manage.

Next I want to thank my family, mostly for not laughing at me when I said I wanted to go to graduate school when I was 10 years old, but also for always encouraging my curiosity about the world around me.

Finally, I'd like to thank my husband Andrew for all the love, support, discussions and late night dinners. Truly, I could not have done this without you.

Contents

List of tables

List of figures

:

Introduction: The telomerase RNP and short-telomere induced senescence

1.1 Telomeres protect the ends of linear chromosomes

Telomeres are protective elements at the ends of linear chromosomes that contain repetitive DNA sequences and specific DNA-binding proteins. Telomeres serve a protective function in eukaryotic cells by promoting genome stability and preventing DNA ends from being inappropriately recognized as double-stranded breaks (DSBs) (Putnam, et al., 2009). This is necessary as the natural ends of chromosomes are very similar to the structures generated by DSBs. When the DSB repair machinery mistakenly targets the chromosome ends, the result is often end-to-end chromosome fusions. These dicentric chromosomes present a challenge during mitosis and are frequently torn apart during cell division. This generates additional DSBs which must be repaired in a process termed the "breakage-fusion bridge cycle" (McClintock 1941). Thus, distinguishing the natural ends of chromosomes from DNA breaks is critical for maintaining genome stability.

Telomeres accomplish this task due to a combination of telomere-specific binding proteins and a unique structural arrangement known as a t-loop (Wei, et al., 2003). Telomere-specific binding proteins are able to recognize the chromosome end due to the unique nature of the repeated sequence tracts found only at the telomere. In fact, inserting telomeric sequence at or near the site of an induced DNA break results in the recruitment of telomere-binding proteins and

subsequent misidentification of the break as a natural end (Diede, et al., 1999). Telomeric sequence is not conserved, and as a result telomere-binding proteins vary extensively between species. However, these proteins serve to prevent the recruitment of DNA repair machinery to the chromosome end (Cervantes, et al., 2002).

Telomeres present an additional problem during DNA replication as the ends of linear chromosomes cannot be fully replicated by the canonical replication machinery, leading to what is known as the end replication problem (Levy, et al., 1992). To counteract this problem most eukaryotes maintain telomeres using the enzyme telomerase, which is a ribonucleoprotein (RNP) complex that extends the telomeres via sequence-directed reverse transcription. The newly extended strand is then copied by the DNA replication machinery (Chandra, et al., 2001; Fan, et al., 1997; Qi, et al., 2000). This process prevents progressive shortening, of the telomeres and promoted genome integrity.

1.2 The telomerase ribonucleoprotein complex

Telomerase is minimally composed of a catalytic reverse transcriptase (TERT) and an RNA component (TR), which is used as the template for reverse transcription. The complex binds to the chromosome end, where the RNA component base pairs with the single-stranded portion of the telomere. TERT then catalyzes the template-directed addition of nucleotides to the telomere.

Once TERT reaches the end of the template the added sequence is known as a single telomeric repeat. At this point the telomerase complex can either dissociate or begin synthesis of additional repeats through a process that is poorly understood. In addition to the core components (TERT, TR), telomerase contains a variety of often species-specific accessory proteins. These proteins are involved in different processes, ranging from enzyme function to recruitment to the telomere.

Telomere maintenance requires precise action by the enzyme telomerase, which can be regulated at multiple levels including (1) recruitment to the telomere, (2) assembly of RNP subunits and (3) appropriate folding of the RNA component into a catalytically capable conformation. For example, studies have shown that mutations that alter the folding equilibrium of TR are associated with the disease *Dyskeratosis congenita* (Hengesbach, et al., 2012; Theimer, et al., 2003; Vulliamy, et al., 2001).

1.3 Telomerase RNA structure

Telomerase RNA is poorly conserved, and even varies dramatically in size between species ranging from ~150 nucleotides (nt) in ciliates to over 2000 nts in some yeasts. However, all TRs discovered to date do contain a shared set of structural features within a region known as the core (Lin, et al., 2004). The core can be thought of as the “central hub” of the telomerase complex as it is the

primary site of TERT binding and, therefore, contains both the active site and RNA template. The commonality of these shared structures and their location within the core suggests that all telomerase enzymes have similar structural requirements for the RNA component during catalysis. The common features consist of (1) a single-stranded template for reverse transcription, (2) a template boundary element that functions in template definition, (3) a core-enclosing helix, (4) a catalytically-important pseudoknot and (5) an Area of Required Connectivity spanning the region from the template to the pseudoknot where physical connections are required (shown in Figure 1-1) (Lin, et al. 2004; Mefford, et al., 2013).

Despite extensive structural conservation in the core, direct structural studies in differing species have been difficult. This is likely due to extensive sequence differences in regions outside of the core. For example, the yeast TR (TLC1) is over 1 kb and consists of three long stems surrounding the central core (Dandjinou, et al., 2004; Singer, et al., 1994; Zappulla, et al., 2004) while the human TR is 451 nts and consists of the core region and a box H/ACA domain at the 3' end (Chen, et al., 2000; Ramakrishnan, et al., 1997; Theimer, et al., 2005). As a result, a variety of secondary-structures have been proposed within the telomerase RNA cores based on a combination of genetic and phylogenetic information. The lack of a consensus structure has made it difficult to investigate structure-function relationships within the core. In particular, the pseudoknot models vary dramatically (yeast shown in Figure 1-2). Appropriate folding of the

pseudoknot is known to be important for function, as mutations in this region compromise activity *in vivo* in yeast, and are associated with short-telomere associated diseases in humans (Gilley, et al., 1999; Lin, et al. 2004; Ly, et al., 2003; Prescott, et al., 1997; Tzfati, et al., 2003). This underscores the need for more direct structural studies of the RNA.

Figure 1-1 The universal core model of telomerase RNA

The core of telomerase RNA contains several conserved structural elements (Lin, et al. 2004) including (1) the core enclosing helix, (2) the pseudoknot, (3) the template and (4) the template boundary element. The pseudoknot is important for catalysis and is thought to be the site of TERT-binding. The template is used to direct the sequence-specific addition of nucleotides to the telomere. The template boundary element defines the end of the template to prevent aberrant copying outside of the template. The core enclosing helix connects the neighboring elements within the ARC and may also contribute to TERT binding.

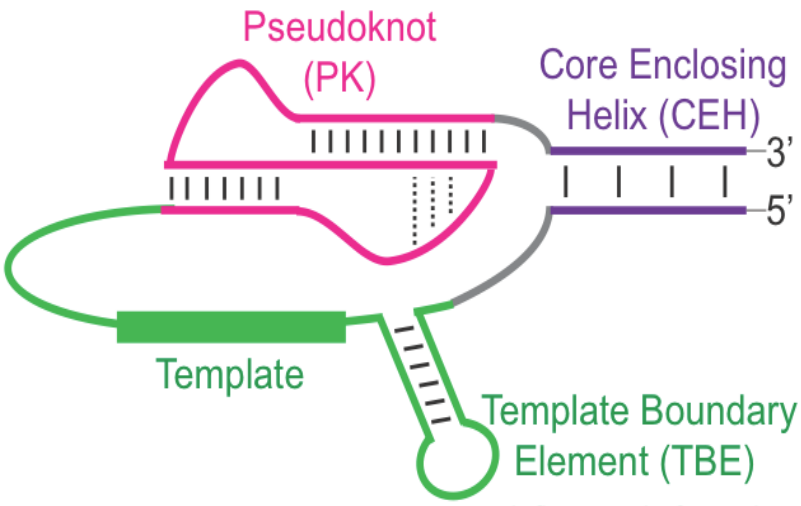

My research has focused on investigating RNA structure within the TR core. To identify any conserved features of this important region, I examined both the human and yeast TR core using chemical probing methods (discussed in Chapter 2). I have shown that both the human and yeast TR cores can adopt a catalytically-competent conformation including (1) a fully-formed pseudoknot, (2) a single-stranded template and (3) base triples in the absence of any protein binding. This is in contrast to the behavior of the ciliate TR, which requires TERT binding to form its active conformation (Mihalusova, et al., 2011). Additionally, I was able to refine the secondary structure models for both RNAs. In particular, I identified five additional base triple interactions within the yeast TR core that likely add previously unappreciated stability to the active conformation, and could play a role in positioning the template within the enzyme active site.

I also identified several shared features between the human and yeast TR cores that may play conserved roles in telomerase function. In both RNAs I observed flexible nucleotides 3' of the template and between the pseudoknot and core-enclosing helix. These flexible regions could be acting as “hinge points” during catalysis to allow movement of the template through the active site. Together, these findings further our understanding of the structure-function relationships within the enzyme core.

Figure 1-2. Previously published yeast TR pseudoknot models.

Several models have been proposed for the yeast pseudoknot, all are consistent with the available genetic and phylogenetic data. The publication where the model appeared is listed below the corresponding structure.

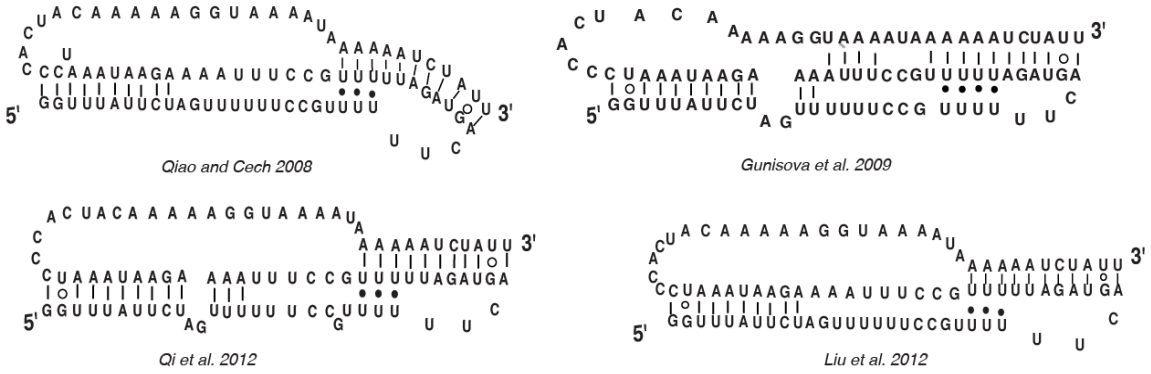

1.4 Loss of telomerase function leads to cell cycle arrest

Compromised telomerase function, either due to inappropriate folding of TR, inefficient recruitment or other defects, results in progressive telomere shortening and eventually a specific cell-cycle arrest known as senescence (summarized in Figure 1-3) (Lundblad, et al., 1989; Weinert, et al., 1988). In yeast this arrest occurs in G2/M, although the arrest is not completely uniform and cells show variable, albeit elongated, cell cycle durations (Xie, et al., 2015). Presumably this is due to transient activation of a DNA damage checkpoint,

which is consistent with previous findings from global expression studies (Greenall, et al., 2008; Mandell, et al., 2005; Nautiyal, et al., 2002), that find evidence for initiation of a DNA damage response. However, the exact nature and extent of this response remain unclear.

This arrest is eventually alleviated in rare cells by a recombination-based telomere maintenance pathway known as Alternative Lengthening of Telomeres (ALT) (Lundblad, et al., 1993) in a process that is conserved in humans and plays a role in many cancers. Cells that initiate this type of telomere maintenance are known as survivors. In yeast, two types of survivors (I and II) have been found (Chen, et al., 2001). The types can be distinguished by their distinct telomere patterns and either is sufficient to escape senescence. If telomerase-negative cells are unable to initiate either of the survivor pathways the result is progressive telomere shortening and, eventually, cell death.

Figure 1-3. Loss of telomerase function leads to senescence.

In this highly simplified model (Adapted from (Campisi 2001)), telomere length dynamics are plotted against cell divisions. In cells where telomerase is active and functional, such as in wild type yeast or in stem cells, telomere length remains relatively constant (dark blue line). However, when telomerase is either absent or nonfunctional (light blue line), as is the case in mutant yeast and most somatic cells, telomeres progressively shorten until initiating a cell cycle arrest known as senescence (red box). Due to the heterogeneity of the arrest many cells will continue to divide, resulting in progressively shorter telomeres. Eventually these cells give rise to a subpopulation of cells known as survivors that maintain their telomeres using recombination-mediated lengthening (green line).

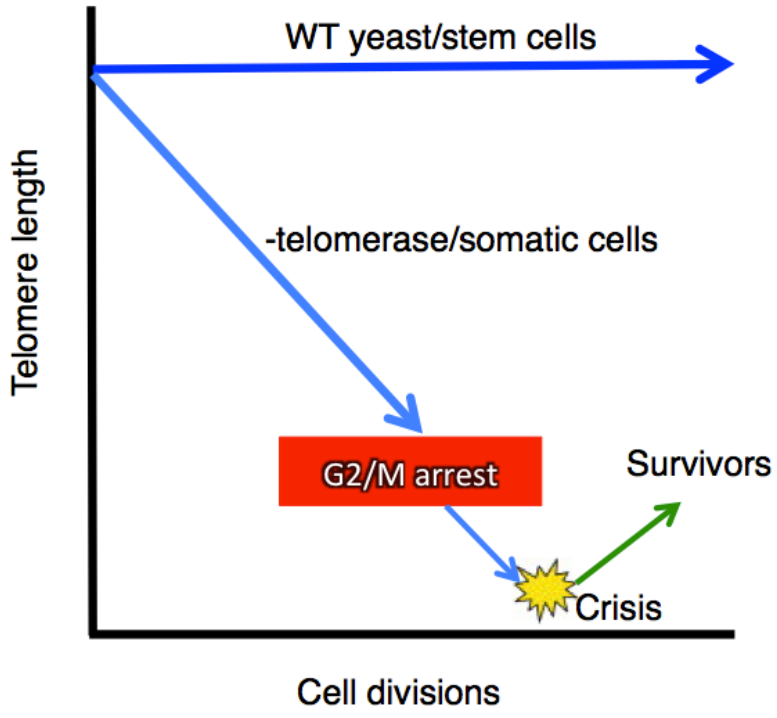

1.5 The cellular response to telomerase deletion

The adaptive changes that occur in telomerase-negative cells are poorly understood. Previous studies have examined the transcriptional response to telomere shortening using one of three approaches (1) deletion of TR (Nautiyal, et al. 2002), resulting in a complete loss of telomerase activity, (2) deletion of TERT (Mandell, et al. 2005), which also abolishes telomerase function, or (3) promotion of telomere deprotection (Greenall, et al. 2008), which leads to resection of the chromosome end and progressive telomere shortening. Each study used microarrays to examine the expression response to telomere shortening. However, there was very little overlap in the findings of the three studies so the exact nature of the cellular response to senescence remains unclear.

In particular, the extent to which senescence represents a distinct cellular state is unknown. Senescing cells share many features with other, previously characterized cell states such as slow growth, DNA damage and G2/M arrest. Each of these states can be achieved in the absence of telomerase deletion, so it is possible that senescence is simply the overlap of these conditions. All three result in a general increase in expression of stress response genes (Fry, et al., 2006; Gasch, et al., 2001; Klosinska, et al., 2011; Spellman, et al., 1998),

something which has also been observed in senescing cells (Greenall, et al. 2008; Mandell, et al. 2005; Nautiyal, et al. 2002).

1.6 Quiescence in yeast

Quiescence is generally characterized as a state where viability is maintained during growth arrest and mitotic divisions can be resumed once the arrest is alleviated (Coller, et al., 2006). By this definition senescence can be considered to be a type of cellular quiescence. However, previous studies examining quiescence in yeast have focused on nutrient deprivation, either by examining stationary phase cells that have exhausted the available supply of glucose or by removing one or more nutrients from the media. While the quiescence state remains poorly defined several distinguishing features have been identified such as increased resistance to heat and oxidative stress, a thickened cell wall, reduced translation and a specific transcriptional profile (Gray, et al., 2004; Smets, et al., 2010). Much of the previously described “specific transcriptional profile” is, in fact, a direct response to slow growth (Klosinska, et al. 2011) rather than to the quiescence state. This more general response to slow growth appears to initiate expression of many of the stress response genes and likely prepares the cells to survive future insults.

My research has focused on determining what, if any, features of senescence are unique. Using RNA-seq data generated through a collaboration

with the Papadopoulos lab, I examined the transcriptional profile of telomerase-negative cells during and after senescence. The cells show substantial temporal changes in gene expression, with each “phase” exhibiting a specific group of differentially expressed genes. Additionally, a group of genes exhibited differential expression at every time point, consistent with a previously described telomerase deletion response. These genes included many stress and DNA damage response genes and seem to be involved in the general response to life without telomerase. By comparing our transcriptional profile with published datasets for other quiescence-like states I was also able to define senescence as a distinct state. Unique features of senescence include upregulation of various meiotic proteins involved in recombination and spore formation, compromised mitochondrial function and expression of many proteins with unannotated functions. These findings further our understanding of the specific cellular response to telomerase loss or dysfunction and highlight the unique challenges posed by rapid telomere loss.

1.7 Noncoding RNA expression during senescence

With the increased usage of high-throughput sequencing technologies the expression response to senescence can now be examined in more detail. Additionally, sequencing-based studies afford the opportunity to discover novel or previously unannotated transcripts. Recent studies have shown more extensive

transcription than was previously appreciated, even in yeast (Xu, et al., 2009) and many noncoding transcripts are associated with specific cellular states such as meiosis (Lardenois, et al., 2011) or growth in limiting metal ion conditions (Toesca, et al., 2011). In many cases, transcription of these noncoding RNAs modulates expression of neighboring genes either by blocking sense transcription through the production of antisense transcripts or by recruiting histone modification machinery to the promoter region(Guil, et al., 2012). Additionally, in human cells senescence is associated with an increase in the expression of many lncRNAs, known as SAL-RNAs (Senescence Associated LncRNAs), that mediate features of the aging process(Abdelmohsen, et al., 2013). Given the importance of noncoding RNAs under these conditions it is possible that the noncoding RNAs also play a role in the senescence response.

My approach to define the transcriptional response to senescence also allowed me to examine noncoding RNA transcription in more detail. Using a bioinformatics approach, I identified 112 novel transcripts that don't overlap with any known protein-coding gene or noncoding RNA. A subset of these RNAs show correlated expression with a neighboring gene and likely represent a cis-regulatory element. Thus, like other cell states, senescence includes a specific noncoding RNA program.

Taken together, my work examining both the structure of telomerase RNA and the cellular response to senescence have underscored the importance of tightly regulated telomerase activity. Mutations that disrupt the folding equilibrium

within the core lead to senescence in yeast and can cause a diseased state in humans. This state is characterized by induction of a general stress response as well as many proteins involved in DNA recombination, likely priming the cells for survivorship. These findings further our understanding of the essential role telomerase plays in maintaining genome integrity and viability within the cell.

Refined secondary-structure models of the yeast and human telomerase RNA cores

2.1 Structure-function analysis of yeast and human telomerase RNAs by chemical probing

Despite extensive divergence of telomerase RNA in sequence and length (spanning from 147 nts in a ciliate species to >2 kb in some fungi), most telomerase RNAs share four common structural elements within the central catalytic core, including the template, a template-boundary element, a core-enclosing helix and a catalytically important pseudoknot (Lin, et al. 2004; Mefford, et al. 2013). In the core of TLC1, the elements are functionally linked by an Area of Required Connectivity (Mefford, et al. 2013). The high conservation of telomerase RNA core structures in spite of rapid evolution of the RNA overall suggests that the cores function similarly.

The pseudoknot of TLC1 and human telomerase RNA (hTR) are both large, unlike that of the small ciliate telomerase RNAs. In both *S. cerevisiae* and *H. sapiens*, the pseudoknot exists in an equilibrium *in vitro* with an alternate two-stem loop conformation (Liu, et al., 2012; Theimer, et al. 2003). Mutations that promote the stem-loop conformation are associated with the disease dyskeratosis congenita (Vulliamy, et al. 2001), which is characterized by defects in highly proliferative tissues (Dokal 2000), indicating a possible disruption of telomere maintenance. This underscores the importance of appropriate pseudoknot formation *in vivo.* Another important feature of both the human and yeast pseudoknots is a set of base triples, which have been shown to be in close

proximity to the template (Qiao, et al., 2008; Theimer, et al. 2005). In yeast, the base triples contribute directly to catalysis through an unknown mechanism (Qiao, et al. 2008). One difference between the TLC1 and hTR cores is that whereas TLC1 has both a template boundary-defining helix (Seto, et al., 2002; Tzfati, et al., 2000) and a core-enclosing helix (Dandjinou, et al. 2004; Lin, et al. 2004; Zappulla, et al. 2004), hTR has a single paired element that contributes to both of these functions (Chen, et al., 2003).

Despite the great interest in telomerase in biomedical research, the three-dimensional structure of the catalytic core of telomerase RNA remains unknown. Only the structures of isolated elements have been solved by NMR (Chen, et al., 2006; Kim, et al., 2010; Kim, et al., 2014; Kim, et al., 2008; Leeper, et al., 2003; Leeper, et al., 2005; Richards, et al., 2006; Richards, et al., 2006; Theimer, et al. 2005; Theimer, et al., 2007; Zhang, et al., 2011; Zhang, et al., 2010). Although there have been some previous chemical structure-probing analyses of telomerase RNAs (Antal, et al., 2002; Forstemann, et al., 2005), even secondary structure models have been difficult to validate or refine. In this study, I examine the entire catalytically competent core region of both the yeast and human telomerase RNA using Selective 2'-Hydroxyl Acylation analyzed by Primer Extension (SHAPE), which interrogates the flexibility of each nucleotide (Merino, et al., 2005; Wilkinson, et al., 2006). In this chapter, I use SHAPE to refine the secondary structure models for both the yeast and human telomerase RNA cores, as well as determine the structural consequences of several mutations in

the Est1-binding arm. In comparing the SHAPE-reactivity patterns of the yeast and human cores, I identified conserved patterns in reactivity with potential implications for enzyme coordination. Additionally, I was able to propose a new set of base triples in the yeast core which likely add substantial stability to the folded RNA. Using mutants in the Est1-binding arm generated by Kevin Lebo, I determined the structure rather than the sequence is important for its function.

2.2 Materials and Methods

2.2.1 RNA preparation

To obtain data at the 3' end of the RNAs, templates were designed with an additional sequence cassette at the 3' end as previously described (Wilkinson, et al. 2006). The cassette had the following sequence: 5' - gaaccggaccgaagcccgatttggatccggcgaaccggatcgagggaagttcag - 3'

The extension did not alter the SHAPE reactivity pattern (Figure 2-1). *In vitro* transcription templates of Micro-TLC1 and hTR were prepared by *FokI* digestion of the corresponding pUC19 plasmids, while templates containing the RNA structure cassette were generated by PCR amplification. RNAs were purified by excising them from denaturing polyacrylamide gels and isolated by phenol-chloroform extraction followed by ethanol precipitation.

Figure 2-1 Addition of an RNA structure cassette to the 3' end does not appear to greatly impact folding.

(a) An RNA cassette was added to obtain data at the 3' end as indicated (Wilkinson, et al. 2006). (b) The RNA cassette does not alter folding of Micro-TLC1 or hTR. **Folding was examined in RNAs with and without the cassette. Here, assayed nucleotides in common to each construct are plotted for comparison**.

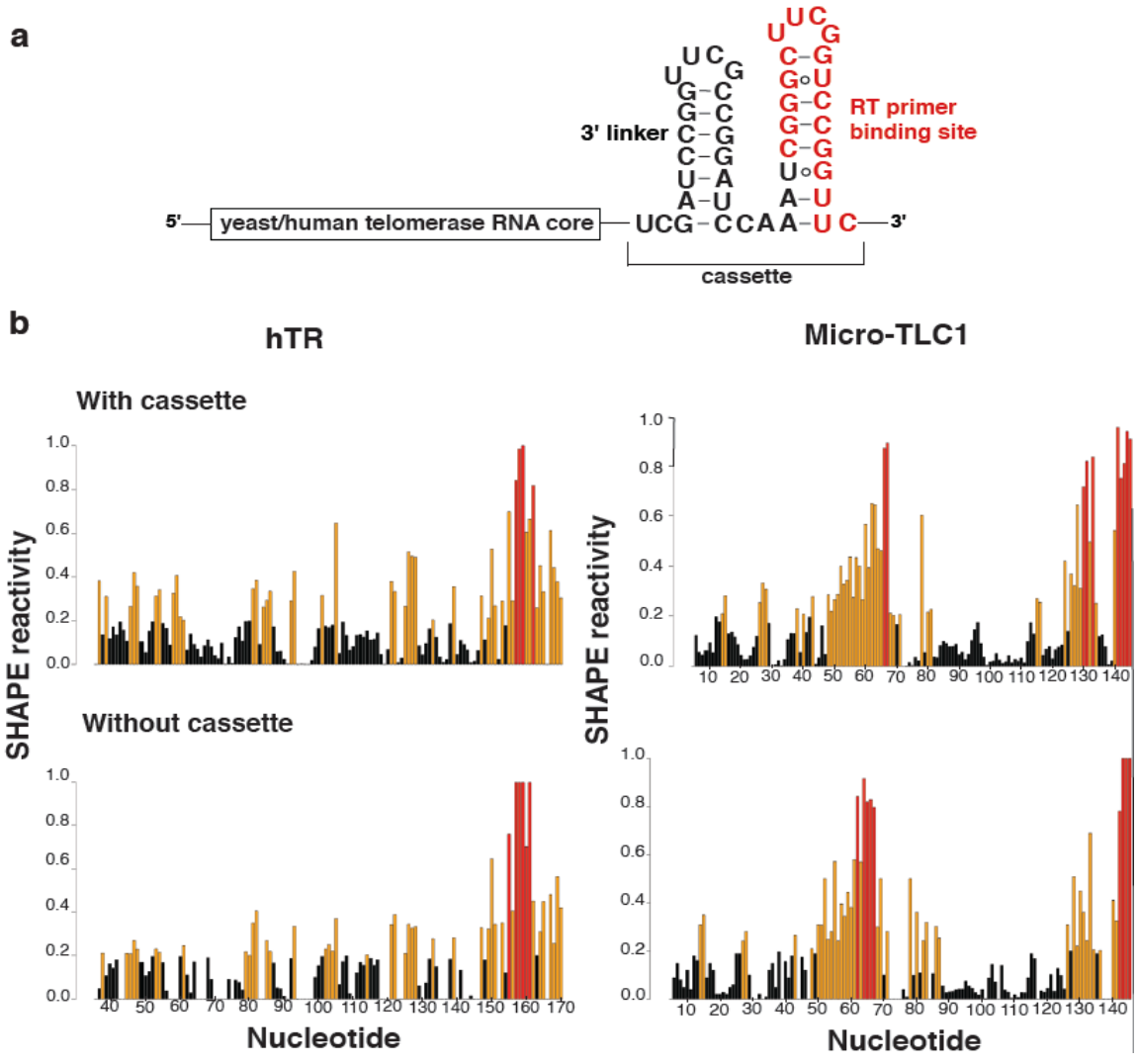

2.2.2 SHAPE chemical probing

Two picomoles of Micro-TLC1 or hTR 33–191 constructs were suspended in 12 µL 0.5x TE pH 8.0 and subsequently denatured at 95°C for 2 minutes, then cooled on ice for 3 minutes. Micro-TLC1 constructs were folded by treatment on ice with 6 µL 3.3x folding buffer (333 mM HEPES pH 8.0, 333 mM NaCl, 20 mM $MgCl_2$). hTR 33–191 constructs were folded in the same manner but with a modified 3.3x folding buffer (333 mM HEPES pH 8.0, 333 mM NaCl, 33 mM $MgCl_2$). Folded RNAs were divided and treated with either 1 µL 65 mM N-methylisatoic anhydride (NMIA) (Sigma) in anhydrous DMSO or 1 µL DMSO. Modification reactions were carried out at 37°C for 22 minutes (Steen, et al., 2012). Reaction volumes were then adjusted to 100 µL with 0.2 M NaCl, 2 mM EDTA pH 8.0 and 0.2 mg/mL glycogen; the modified RNA was then ethanol precipitated and resuspended in 9 µL 0.5x TE pH 8.0.

2.2.3 Primer extension

Primer extension reactions were carried out as described in the SuperScript III reverse transcriptase protocol (Invitrogen) with the following modifications. 1 pmol of each RNA was denatured at 95°C for 1 minute and placed on ice for 2 minutes. 3 µL of [γ^{32}P]-end-labeled primer was added and the solution was incubated at 65°C for 2 minutes followed by annealing at 35°C for

10 minutes. 6 µL of the supplied SuperScript III buffer supplemented with 5 mM DTT (final concentration) and 1 mM dNTPs (final concentration) was added to the mixture, which was then pre-heated for 1 minute at 52°C. 100 units of SuperScript III were added to each reaction at room temperature. Reactions were then incubated at 52°C for 5 minutes prior to running on a 10% polyacrylamide/1x TBE/7 M urea gel at 90 W. Gel electrophoresis was performed for between 1.75 and 4 hours to obtain appropriate resolution of each given region of the RNAs in order to quantify reactivity of individual nucleotides to NMIA. Gels were exposed on a phosphorimager screen, and imaged using a Typhoon 9410 Variable Mode Imager.

2.2.4 SHAPE data analysis

Modification intensities were measured using SAFA software (Das, et al., 2005). Results were scaled by selecting the least-variable band across lanes, calculating lane-by-lane normalization factors to make the reference band equal across all lanes and scaling each lane accordingly. Normalized SHAPE reactivity was calculated by subtracting the intensity of the corresponding DMSO-only band from the NMIA band. To quantify the SHAPE reactivity, the average of the 10 most-reactive bands was set as 100% reactivity and all other bands were scaled accordingly (negative values were set to zero). Data were averaged from multiple experiments as indicated and were obtained using RNA from at least 3

independent transcription reactions. All RNAs were folded independently as described above.

2.2.5 Secondary-structure model generation

SHAPE-guided secondary-structure refinement was achieved by first mapping relative SHAPE-reactivities onto the most recent models. Inconsistencies between the SHAPE data and the model for the RNA were resolved using SHAPE-constrained secondary structure predictions by *RNAstructure* (Deigan, et al., 2009). In the event of a mismatch (e.g., one nucleotide of a predicted base-pair is reactive while the other is not) pairing status was left as described by current models.

2.2.6 Telomerase Assays

Telomerase assays were performed essentially as previously described (Zappulla, et al., 2005). Briefly, DNA template encoding Pro-A tagged Est2 (TERT) and telomerase RNA were added to the coupled rabbit reticulocyte lysate (RRL) transcription and translation system containing T7 RNA polymerase (Promega). Telomerase was immunopurified using IgG Sepharose beads (GE Healthcare). Telomerase activity was assayed by incubating 5 µl of bead-bound

enzyme with 1 μM telomeric DNA substrate primer (DZ427), ~ 1 nM [γ-^{32}P]-labeled primer DZ428 as a recovery and loading control, 3.3 μM [α-^{32}P]-dGTP, 1 μM each dATP, dCTP, and dTTP, in 38 mM Tris pH 8, 47 mM NaCl, 4.7% glycerol, 2.2 mM $MgCl_2$, 0.5 mM spermidine, and 0.5 mM DTT. Reactions were incubated for 10 minutes at 26°C and subsequently stopped by the addition of ammonium acetate. Products were then ethanol precipitated and resuspended in 1x formamide loading buffer. The products were run through a 10% polyacrylamide/1x TBE/7 M urea denaturing gel at 90 W for 1.25 hours, exposed on a phosphorimager screen, and imaged using a Typhoon 9410 Variable-Mode Imager.

2.2.7 Native gel analysis

Renatured RNAs were mixed with non-denaturing loading dye and run on a 5% polyacrylamide/1x TBE gel for 3 hours at 70 W at 4˚C. Gels were stained using Gel Star (Lonza) and imaged using a Typhoon 9410 Variable-Mode Imager.

2.3 Results

2.3.1 The yeast telomerase RNA core adopts its active conformation *in vitro*

The SHAPE results are consistent with formation of both the pseudoknot and a single-stranded template of the yeast telomerase RNA core *in vitro*, even in the absence of TERT (Figure 2-2). This is in contrast to the reported behavior of the *Tetrahymena* RNA and the full-length human RNA (Cole, et al., 2012; Mihalusova, et al. 2011; Yeoman, et al., 2010). The predicted stems of the template-boundary element and pseudoknot show reproducibly low reactivity, as expected for base-paired nucleotides, whereas there is higher reactivity in most junctions and loops. Overall, the SHAPE-supported secondary structure model is largely consistent with the previously observed DMS-reactivity pattern in the pseudoknot of full-length, protein-bound TLC1 (Forstemann, et al. 2005), and therefore protein binding may not influence the conformation of the yeast pseudoknot to a great extent.

The junctions within the yeast core are generally reactive, with every nucleotide in J3 and J4 being modified. These regions may introduce considerable physical flexibility in the core, particularly J3, which is 16 nucleotides long and tolerates a wide variety of mutations (Mefford, et al. 2013).

However, both J1 and J2 are comparatively less reactive (Figure 2-2). Interestingly, while I observe reactivity within the template, nucleotides 44–46 (CCC) consistently did not show reactivity above background levels, suggesting they may be stacked or involved in tertiary interactions.

2.3.2 The pseudoknot in the yeast telomerase RNA core forms *in vitro*

Previous work has shown that pseudoknot formation in the ciliate telomerase RNA requires protein binding (Mihalusova, et al. 2011). To test the SHAPE-supported pseudoknot model, I designed two pseudoknot-disrupting mutants, dmPK-1 and dmPK-2. Each mutant has 7 nucleotides on each side of stem 1 changed to its Watson-Crick cognate, which is predicted to abolish base pairing with minimal disruption to proposed alternate conformations (Figure 2-3a) (Liu, et al. 2012; Zappulla, et al. 2004). Both mutants dmPK-1 and -2 showed severely reduced telomerase activity *in vitro* (Figure 2-3c) and an increase in SHAPE reactivity throughout stem 1, showing that the mutations disrupted pseudoknot formation (Figure 2-b). While both mutants disrupt pseudoknot formation, they do not appear to result in the same RNA conformation (Figure 2-b). In contrast, the double-mutant allele (dmPK-R) showed greater telomerase activity than either single mutant and NMIA-reactivity restored to that of wild type.

These results support the conclusion that the pseudoknot is forming *in vitro* and provide further evidence that it is important for activity.

Figure 2-2: SHAPE-directed secondary structure model of the core of S. cerevisiae telomerase RNA.

(a) The refined yeast telomerase RNA secondary structure model incorporating SHAPE results. GU wobble pairs indicated by open circles. Other non-Watson-Crick interactions are denoted with filled circles. Open triangles correspond to deletions relative to TLC1 and exogenous sequence is lowercase. (b) SHAPE reactivity at each position in the yeast telomerase RNA core. Values represent the average of between 5 and 18 independent trials with standard error shown.

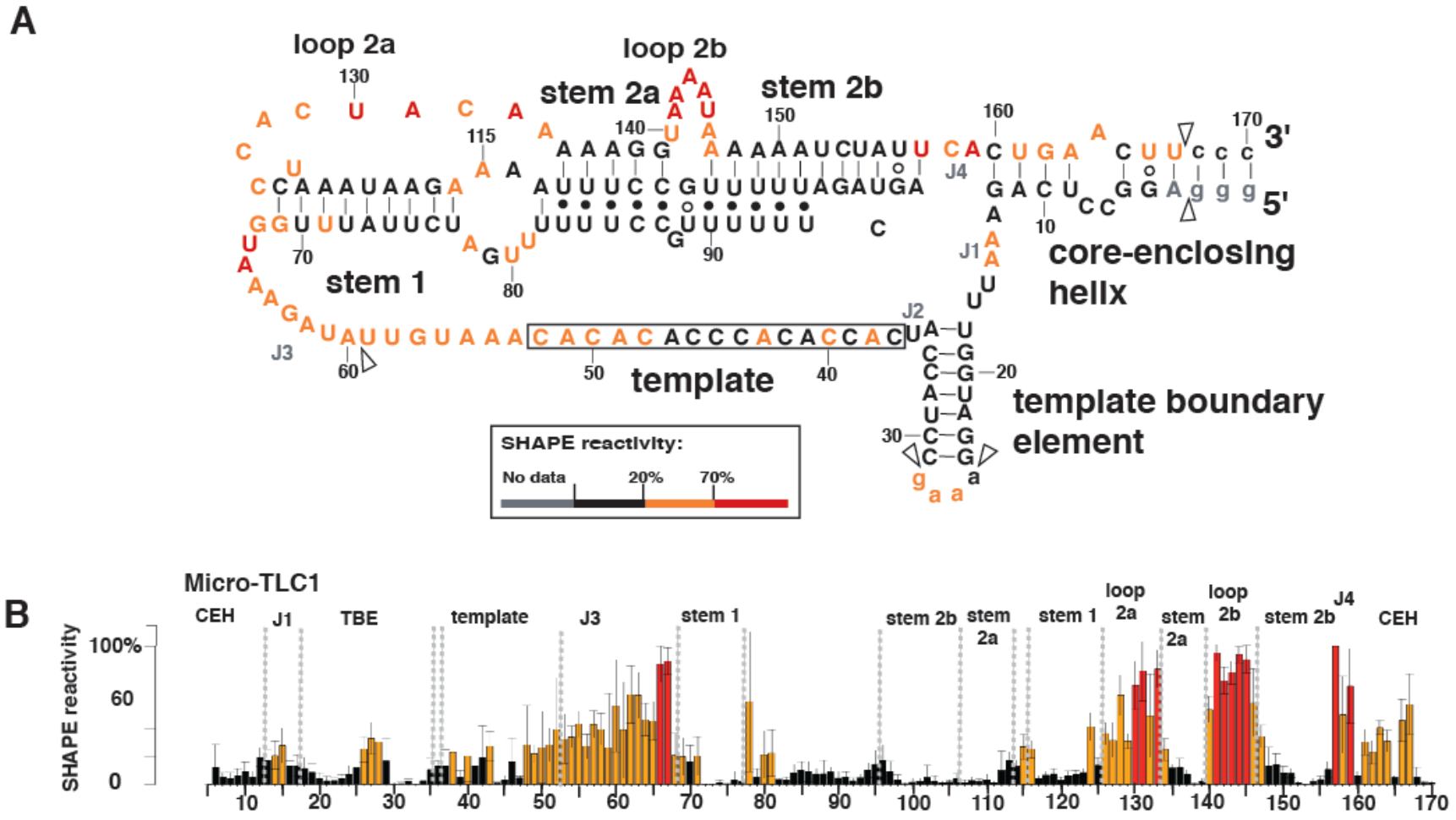
A
loop 2a
loop 2b
stem 2a
stem 2b
stem 1
core-enclosing helix
template
template boundary element
J1
J2
J3
J4
3'
5'
SHAPE reactivity:
No data
20%
70%
B
Micro-TLC1
SHAPE reactivity
100%
60
0
CEH
J1
TBE
template
J3
stem 1
stem 2b
stem 2a
stem 1
loop 2a
stem 2a
loop 2b
stem 2b
J4
CEH

Figure 2-3. Pseudoknot-disrupting mutants increase reactivity in stem 1.

(*a*) Design of pseudoknot-disrupting mutants. Seven nucleotides in stem 1 were mutated to their Watson-Crick cognate to abolish base pairing. The mutations are predicted to disrupt pseudoknot formation without affecting the alternately observed 2-stem loop conformation (Liu, et al. 2012) (right). Pseudoknot-disrupting mutants are indicated as dmPK-1 and dmPK-2. **(*b*) SHAPE reactivity in WT and PK-disrupting mutants.** SHAPE reactivity is plotted for WT (from Figure 2-2), both PK-disrupting mutants and the stem 1 restoring mutant dmPK-R. Reactivities for dmPK-1, dmPK-2 and dmPK-R correspond to the average value from between 3 and 9 independent trials with standard deviation shown. Mutated nucleotides are indicated by brackets. **(*c*) Pseudoknot-disrupting mutants decrease telomerase activity *in vitro.*** Telomerase assay testing activity of PK and compensatory mutants. Alignment of DNA primer with TLC1 is shown. TBE indicates template boundary element.

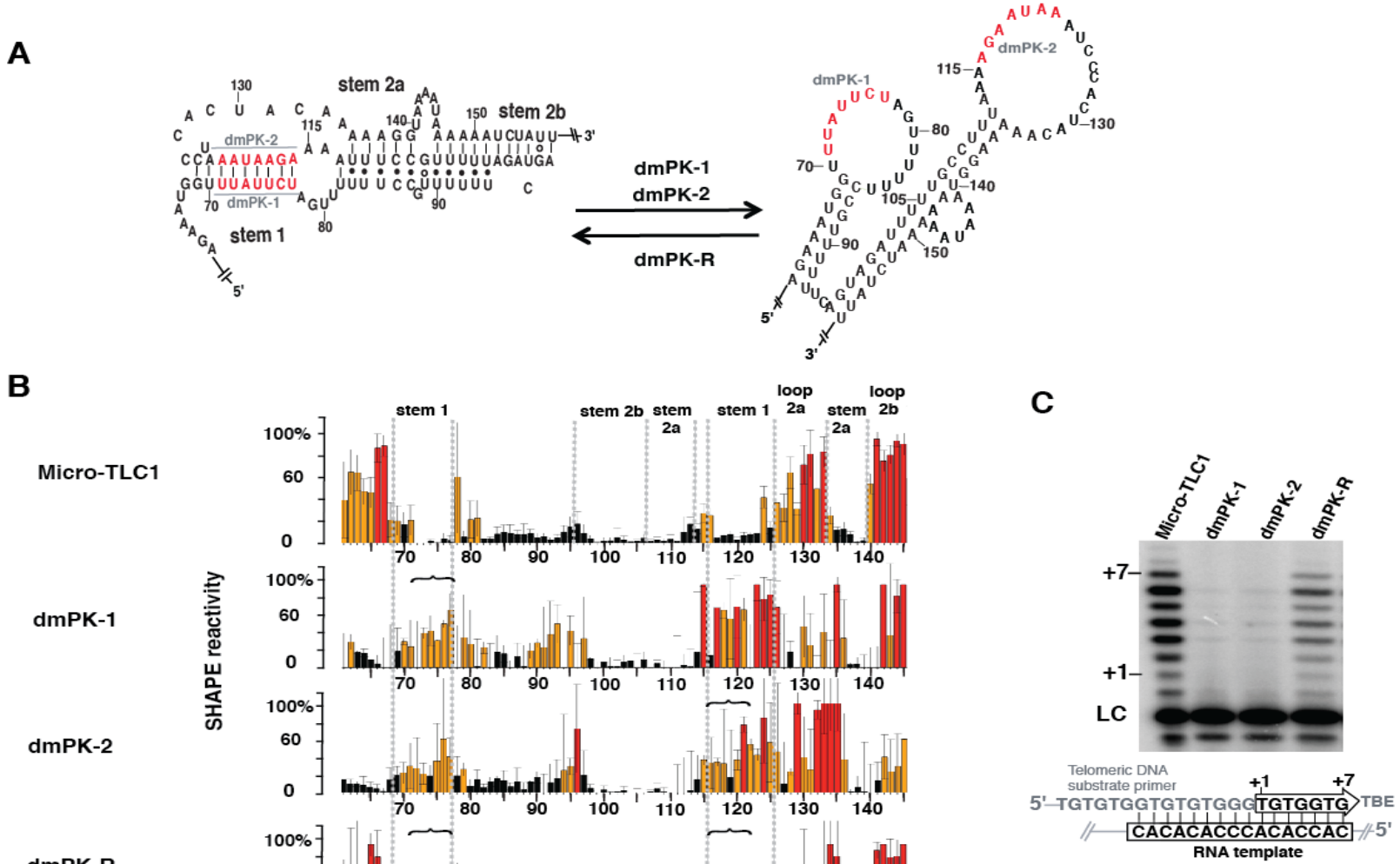
A
stem 2a
stem 2b
stem 1
dmPK-2
dmPK-1
dmPK-1
dmPK-2
dmPK-R
B
Micro-TLC1
dmPK-1
dmPK-2
dmPK-R
SHAPE reactivity
100%
60
0
stem 1
stem 2b
stem 2a
stem 1
loop 2a
stem 2a
loop 2b
70
80
90
100
110
120
130
140
Nucleotide
C
Micro-TLC1
dmPK-1
dmPK-2
dmPK-R
+7
+1
LC
Telomeric DNA substrate primer
5'-TGTGTGGTGTGTGGGTGTGGTG-TBE
CACACACCCACACCAC
RNA template
5'

2.3.3 The yeast pseudoknot contains additional base-triples

My SHAPE results strongly support the formation of 5 additional base triples within the pseudoknot (nts 83–87, 108–112 and 135–139), which I named "stem 2a". The structure is phylogenetically supported (Figure 2-4), however, mutations in this region in the context of larger yeast telomerase RNAs have resulted in only a slight decrease in activity *in vivo* and *in vitro* (Lin, et al. 2004; Qiao, et al. 2008; Shefer, et al., 2007). These base triples have been previously proposed based on thermodynamic characterization and were observed in *K. lactis* (Cash, et al., 2013; Liu, et al. 2012) and their main function is likely to favor pseudoknot formation and stability without directly contributing to catalysis.

Figure 2-4. Additional base triples are supported by SHAPE and phylogenetic data.

SHAPE reactivities are mapped onto nucleotides for each model. The model proposed in this work is shown above with 100% conserved nucleotides within stem 2a enclosed in green circles while nucleotides with variants that maintain base-pairing are in blue circles.

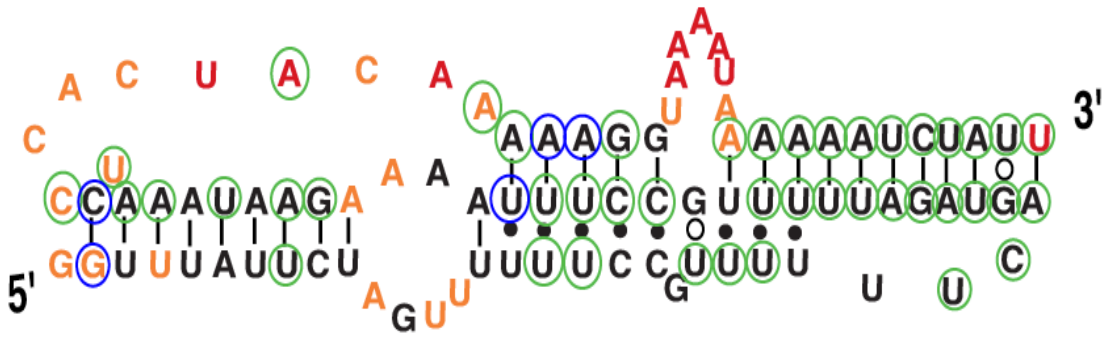

To investigate the nature and importance of the 5 base triples, I first mutated the 3′-most and middle two strands to their Watson-Crick cognate. In both cases, the mutations greatly decreased telomerase activity (Figure 2-5c). Combining these changes in a compensatory mutant reduced telomerase activity further and did not return the wild-type SHAPE-reactivity pattern, indicating the base-compensatory Watson-Crick interaction had not formed (Figure 2-5c). However, the low SHAPE reactivity of the 5′ and middle strands in the double mutant is consistent with these mutations simply lengthening stem 1 of the pseudoknot. Therefore, in the next mutation strategy, I instead changed the three U-A•U predicted triples to C-G•C, and vice versa for the other two triples to

generate the best structural mimic of the wild-type interactions. I also made the single- and double-mutant-strand combinations. Again, I observed decreased telomerase activity for many of the mutants, including for the triple-strand substitution allele (Figure 2-5c). I conclude from these results that the native sequence of each of these three strands is important for activity. X-ray crystallography and/or NMR studies on the *S. cerevisiae* pseudoknot region should help reveal the nature and geometry of these interactions more precisely. Finally, it appears that this structure is more important for telomerase function in the context of Micro-T RNA than it is in longer TLC1 alleles (Lin, et al. 2004; Qiao, et al. 2008).

Figure 2-5. Mutagenesis of proposed base triples.

(a) Mutated nucleotides are underlined. (b) SHAPE analysis of mutants. Mutants 1, 2, and the compensatory 1+2 mutant are shown. Each mutant was tested in triplicate. All mutants increase reactivity on the 3' strand with the compensatory mutations failing to restore WT reactivity pattern. **(c) Telomerase activity of base triples mutants.** Mutations in this region disrupt telomerase activity. Compensatory mutants fail to restore telomerase activity to WT levels. Each mutant was tested in triplicate.

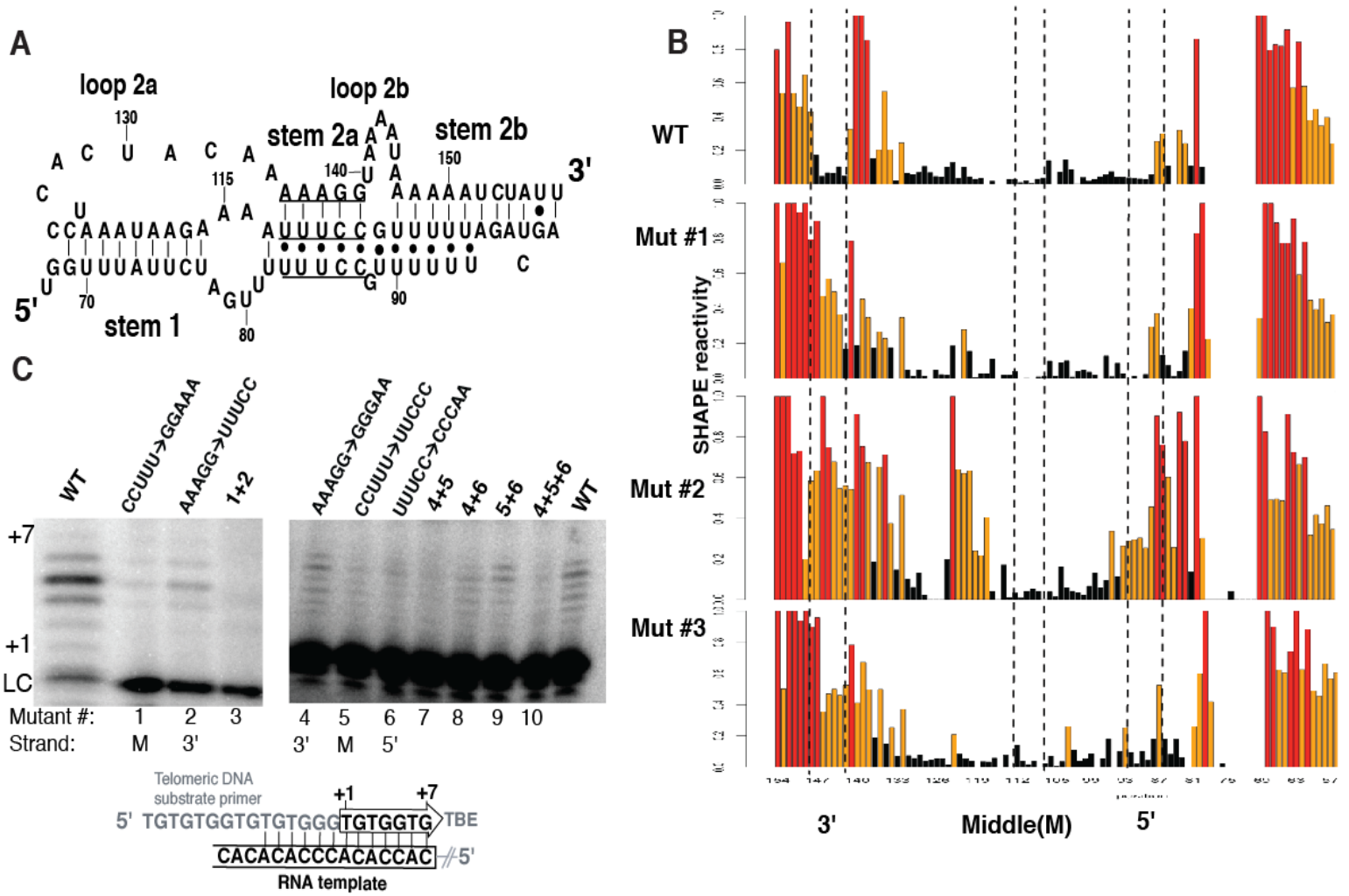
A
loop 2a
loop 2b
stem 2a
stem 2b
stem 1
5'
3'
B
WT
Mut #1
Mut #2
Mut #3
SHAPE reactivity
3'
Middle(M)
5'
C
WT
CCUUU→GGAAA
AAAGG→UUUCC
1+2
AAAGG→GGGAA
CCUUU→UUCCC
UUUCC→CCCAA
4+5
4+6
5+6
4+5+6
WT
+7
+1
LC
Mutant #: 1 2 3 4 5 6 7 8 9 10
Strand: M 3' 3' M 5'
Telomeric DNA
substrate primer
5' TGTGTGGTGTGTGGGTGTGGTG TBE
CACACACCCACACCAC //5'
RNA template

2.3.4 Folding of the human telomerase RNA core requires high magnesium

To examine the folding of the human telomerase RNA (hTR) core I focused on nucleotides 33–191, which reconstitute telomerase activity *in vitro* when expressed in a transcription-translation system with the CR4/5 domain and hTERT (Ly, et al. 2003). Pseudoknot formation in full-length hTR requires magnesium (Hengesbach, et al. 2012), so to investigate the structure of the core I next sought to identify and characterize elements that show magnesium-dependent folding. In the absence of magnesium, we observed two major RNA conformations by native gel (Figure 2-6a), suggesting the core of hTR RNA exists in an equilibrium between two folded states, consistent with previous work on the pseudoknot alone (Theimer, et al. 2003). This indicates the pseudoknot is the structural element primarily driving this equilibrium. I observe an overall decrease in reactivity in the P2b/P3 pseudoknot region as magnesium concentration increases, supporting the conclusion that Mg^{+2} promotes pseudoknot formation (Figure 2-6b). The hTR does not fold uniformly in less than 10 mM magnesium (Figure 2-6a).

Figure 2-6. Magnesium-dependent behaviour within hTR and hTR^{DKC}.

(a) hTR and hTR^{DKC} adopt two major conformations. Native gel analysis of hTR and hTR^{DKC} RNAs in increasing magnesium. High magnesium conformations favor one conformation in hTR. SHAPE reactivity is shown for each magnesium concentration as indicated. (b) Previous and proposed model for J2a.1 region (c) SHAPE reactivity by nucleotide in increasing magnesium. (d) Differential SHAPE reactivity between hTR and hTR^{DKC}. Differential SHAPE reactivity between hTR and hTR^{DKC} in 10 mM magnesium highlights regions most likely to differ conformationally.

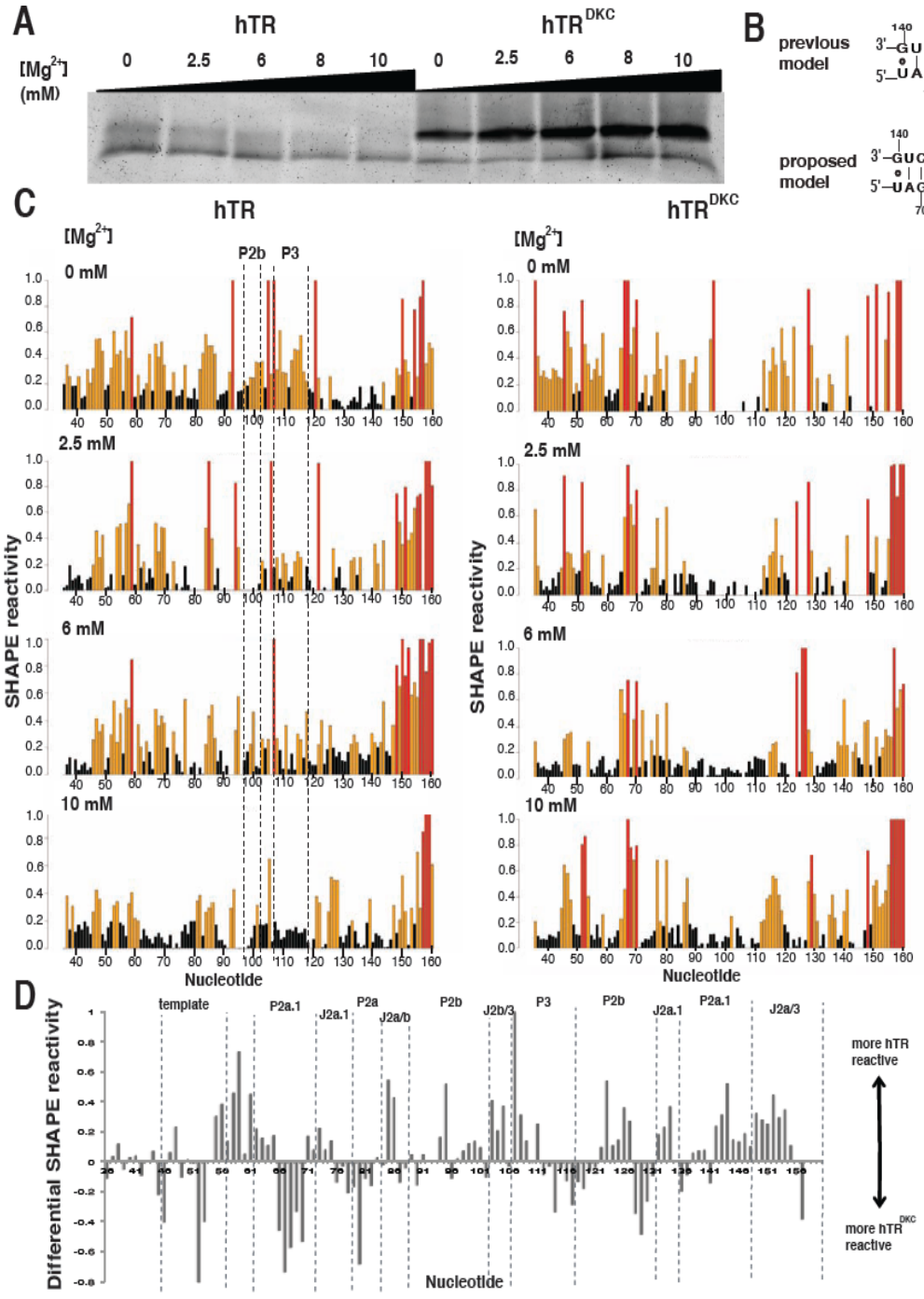
A
hTR
hTR^DKC
[Mg2+] (mM)
0 2.5 6 8 10 0 2.5 6 8 10
B
previous model
proposed model
J2a.1
C
hTR
hTR^DKC
[Mg2+]
P2b P3
0 mM
2.5 mM
6 mM
10 mM
SHAPE reactivity
Nucleotide
D
template P2a.1 J2a.1 P2a J2a/b P2b J2b/3 P3 P2b J2a.1 P2a.1 J2a/3
Differential SHAPE reactivity
Nucleotide
more hTR reactive
more hTR^DKC reactive

2.3.5 The human telomerase RNA core adopts its active conformation *in vitro*

Having determined the optimal magnesium concentration I performed SHAPE on the hTR core. The results are generally consistent with current structural models and suggest that the RNA alone is able to form a catalytically-competent structure with both a pseudoknot and a single-stranded template (Figure 2-7a) (Hengesbach, et al. 2012; Kim, et al. 2008; Theimer, et al. 2005; Zhang, et al. 2011). We observe high reactivity of nucleotides throughout J2a/3 and, reciprocally, generally low reactivity throughout each pseudoknot stem. Interestingly, the region surrounding the proposed catalytically important "hinge-point" at J2a/b (Zhang, et al. 2010) is reactive, suggesting this location may be particularly dynamic, or else held in a reactive conformation due to a unique, conserved local structure (Zhang, et al. 2010).

Additionally, the SHAPE data in optimized magnesium are consistent with a fully formed P2a.1 region leading into a surprisingly unreactive J2a.1. Here we propose three additional base pairs form, resulting in a 12-bp long P2a.1 and a smaller J2a.1, as shown in Figure 2-7a. Previous work has suggested J2a.1 can adopt alternate base-pairing conformations *in vitro*, though mutational and phylogenetic analyses indicate that any pairing is dispensable (Chen, et al. 2000; Martin-Rivera, et al., 2001; Zhang, et al. 2011).

The junctions in hTR show a similar reactivity pattern to the yeast core, with reactive nucleotides in the region 3' of the template and between P1b and P3 (J4 in yeast) (Figure 2-7a). Again, we see a region of low reactivity 5' of the template where it has been shown that length but not sequence is important for template boundary definition (Chen, et al. 2003), suggesting a potential structural role for these nucleotides in this process. Furthermore, we see nucleotides 50–52 (CCC) within the template are unreactive, which is consistent with previous work (Antal, et al. 2002) and the yeast RNA (see above and Figure 2-7).

Figure 2-7. SHAPE-refined secondary structure model of the *H. sapiens* core.

(A) hTR adopts its active structure *in vitro*. Non-Watson-Crick interactions indicated by circles with GU wobble pairs denoted by open circles. Hoogsteen-face interaction denoted with square. Dashed lines indicate reactive residues previously shown to pair *in vitro* (Zhang, et al. 2011). (B) SHAPE reactivity by nucleotide. Values represent the average of between 6 and 12 independent trials. Standard error is shown.

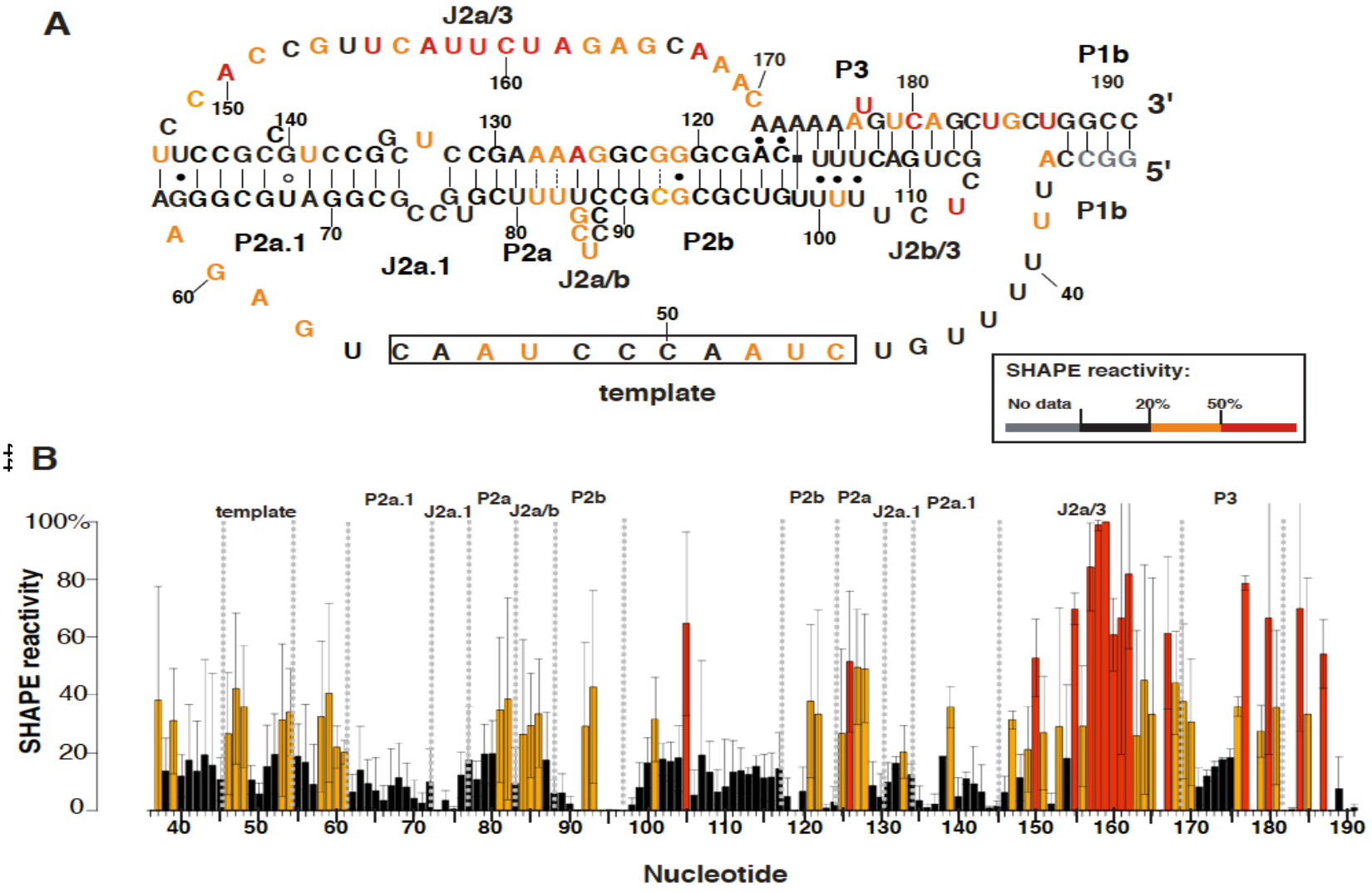
A
J2a/3
P3
P1b
3'
5'
P2a.1
J2a.1
P2a
J2a/b
P2b
J2b/3
P1b
template
SHAPE reactivity:
No data
20%
50%
B
SHAPE reactivity
100%
80
60
40
20
0
template
P2a.1
J2a.1
P2a
J2a/b
P2b
P2b
P2a
J2a.1
P2a.1
J2a/3
P3
40
50
60
70
80
90
100
110
120
130
140
150
160
170
180
190
Nucleotide

2.3.6 Mutations in the pseudoknot of the human telomerase RNA disrupt the folding equilibrium

Mutations that promote the stem-loop conformation are associated with the disease *Dyskeratosis congenita* (Vulliamy, et al. 2001), which is characterized by defects in highly proliferative tissues (Dokal 2000), indicating a possible disruption of telomere maintenance. To explore the structural consequences of these mutations we generated one disease-associated allele, hTR^{DKC} (nts 108 and 109, CG→GA), in the context of the hTR core. Native gel analysis reveals two bands present like those in wild-type hTR, although equilibrium between the two appears unaffected by magnesium (Figure 2-6a).

2.3.7 A potentially structured element within the template of yeast and human telomerase RNA cores

My SHAPE results revealed a common region of low reactivity in the template of both the human and yeast TRs, consisting of a CCC motif. To determine if these nucleotides are involved in previously unknown base-pairing interactions I performed DMS probing, which preferentially modifies the watson-crick face of unpaired C or A residues. I found that for both the human and yeast

RNA the nucleotides were reactive (Figure 2-8), suggesting they are likely unpaired but involved in some kind of tertiary interactions that limit flexibility.

Figure 2-8. DMS reactivity within the yeast template.

Every C or A nucleotide within the template appears to be highly DMS-reactive. Additionally, A residues within the GAAA tetraloop of the TBE are also reactive.

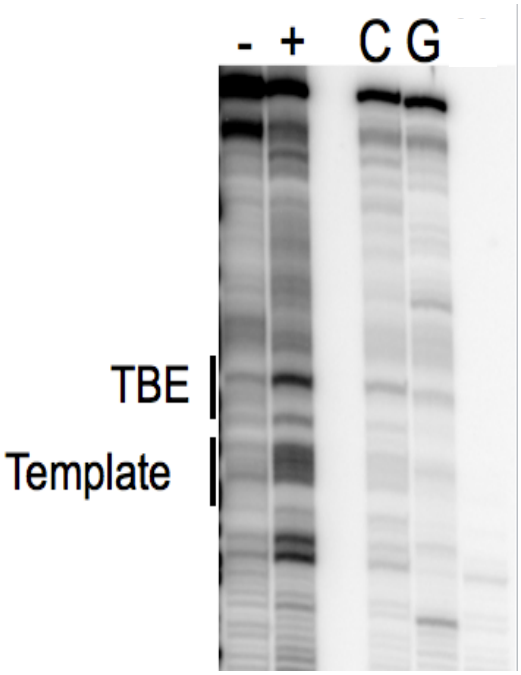

2.3.8 The structure of the Est1-binding arm is important for SEED function

Previous work in the lab identified a Second Essential function of the Est1-binding Domain (SEED) in the yeast telomerase RNA (Lebo, et al., 2015). To determine whether mutations in this region were disrupted due to structural or sequence changes I performed SHAPE analysis on the 108-nt Est1-arm fragments corresponding to both the WT arm and three mutant sequences.

In the WT arm, nucleotides predicted to comprise apical loops of the two hairpins and the 5-nt bulge in the secondary structure model were highly reactive, showing that they are flexible and suggesting that they are indeed unpaired (Figure 2-9). Correspondingly, nucleotides within predicted helices were nearly all unreactive. These data strongly support the secondary structure model for the Est1 arm, which was based on phylogenetic information as well as computational modeling that maximizes free energy (Dandjinou, et al. 2004; Seto, et al. 2002; Zappulla, et al. 2004). Interestingly, SHAPE reactivity revealed flexibility at every nucleotide in the internal loop of the Est1 arm, suggesting they are not paired and, therefore, that this conformation is favored.

I examined three mutants generated by Kevin Lebo (5-1, 5-2 and 5-3) within the internal loop region by SHAPE. All mutants target the internal loop region, and of the three only 5-1 maintains SEED function(Lebo, et al. 2015). Both 5-2 and 5-3 show considerable changes in reactivity within the internal loop

(Figure 2-9) consistent with a structural disruption in this region. Since all three mutants have altered sequences relative to WT but only the structurally disruptions abolish SEED activity we concluded that the structure and not the sequence is essential for SEED function.

Figure 2-9. SHAPE reactivity within the Est1 arm.

(a) SHAPE reactivity in the WT Est1 arm. SHAPE reactivity is largely consistent with previous models, and supports a large internal loop. (b) SHAPE reactivity in SEED mutants. SHAPE analysis of internal loop nucleotide sequence substitution mutants shows that mutants 5-2 and 5-3 have altered internal loop structures. Left, graphs showing relative normalized SHAPE reactivity of TLC1 Est1-arm nucleotides. Blue text above indicates Est1 arm structural elements. Asterisks indicate non-wild-type nucleotides in the mutants. Orange arrow indicates residue U604, with high SHAPE reactivity in mutant 5-2. Dotted lines indicate base pairs predicted to form by *Mfold* in mutant 5-3.

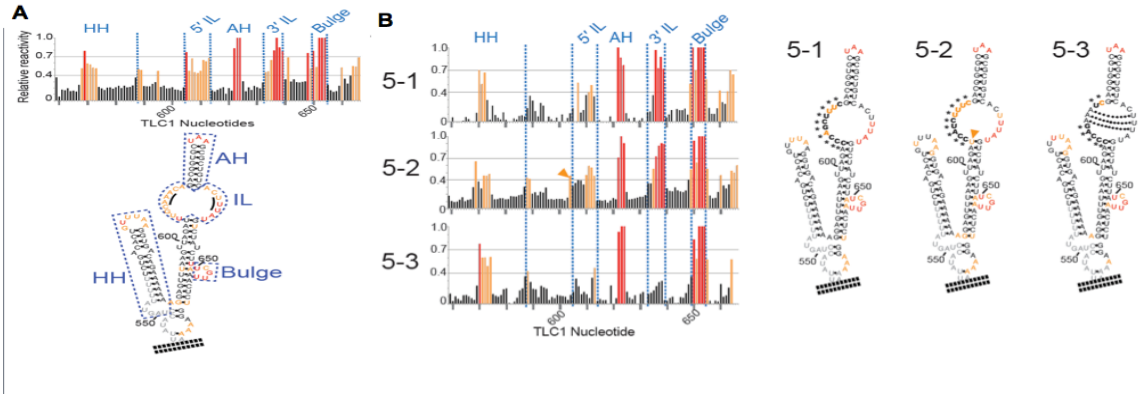

2.4 Discussion

Comparing the reactivity patterns in hTR and Micro-TLC1, we note several similarities (Figure 2-10). Both RNAs exhibit comparatively low reactivity 5' of the template with higher reactivity 3' of the template and between the pseudoknot and core-enclosing helix. These elements could coordinate the positioning of the template near the catalytically important base triples with the reactive regions serving as flexible points while the potentially structured area 5' of the template acts as an anchored template-boundary element.

In summary, I have presented secondary-structure models refined by SHAPE analysis that include base-triple interactions in the yeast core in addition to those previously implicated in catalysis(Qiao, et al. 2008) and an alternate conformation within hTR J2a.1. In so doing, we have also shown that the cores of both yeast and human telomerase RNAs independently adopt their native conformation, as indicated by formation of the pseudoknot, base triples, and a single-stranded template. This is in contrast to the *in vitro* folding of the *T. thermophila* telomerase RNA, which was shown to require TERT to adopt an active conformation. The ciliate pseudoknot is small and may lack stable base triples, potentially making it more protein-dependent(Cole, et al. 2012; Mihalusova, et al. 2011). Finally I also identified a conserved region of low reactivity within the template of telomerase RNAs suggesting a mechanism to

favor substrate binding and subsequent positioning near the catalytically important base triples within the TERT active site.

Figure 2-10. Models of the yeast and human TR cores.

(A) Micro-TLC1 and the hTR core show similar reactivity patterns. Summary diagram of general reactivity patterns for each core. Regions of low reactivity common to both hTR and Micro-TLC1 are shown in black, while common regions of high reactivity are colored red. (B) A general model for telomerase RNA core domain coordination with TERT. A generic telomerase RNA core with common structural elements is shown. Regions that may introduce physical flexibility based on SHAPE data are highlighted in red. The potential conserved structural element consisting of CCC nts in the template is drawn in proximity to the catalytically important base triples and ending in the active site, shown as an open oval. The template is indicated by a thick line. Telomeric DNA is shown in blue.

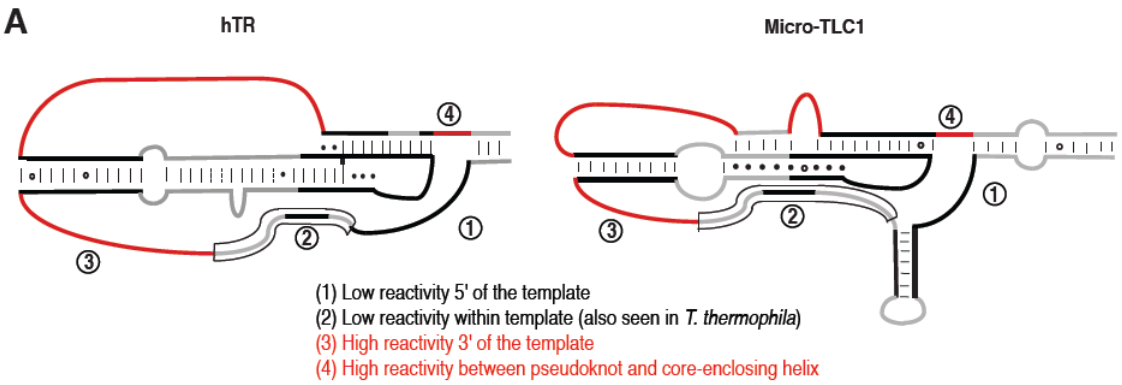
A
hTR
Micro-TLC1
④
①
②
③
(1) Low reactivity 5' of the template
(2) Low reactivity within template (also seen in T. thermophila)
(3) High reactivity 3' of the template
(4) High reactivity between pseudoknot and core-enclosing helix

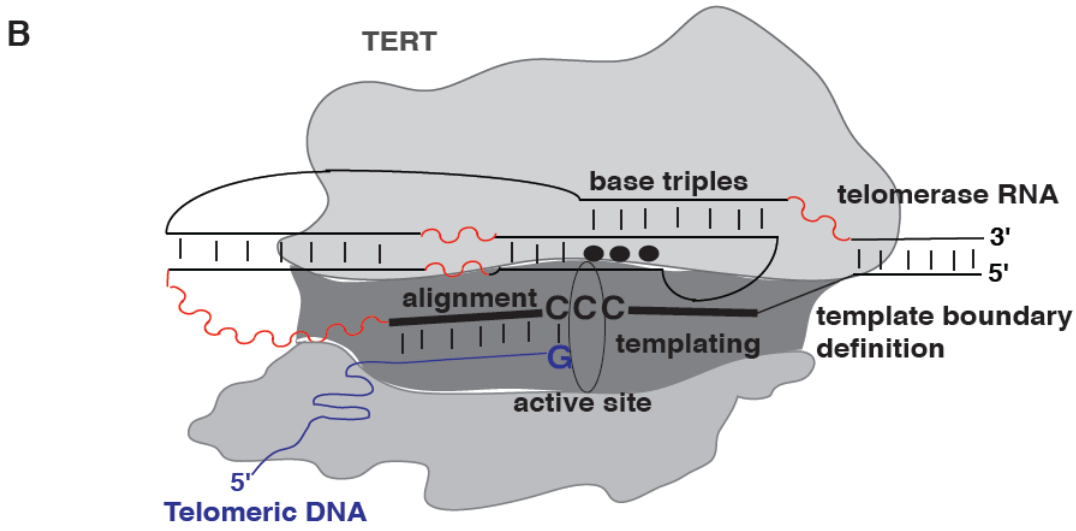
B
TERT
base triples
telomerase RNA
3'
5'
alignment
CCC
G
templating
template boundary
definition
active site
5'
Telomeric DNA

Telomerase-negative cells express a specific set of novel lncRNAs

3.1 Identification of novel lncRNAs in telomerase-negative yeast

Upregulation of telomerase is associated with approximately 90% of cancers and is thought to be required for cells to undergo limitless divisions. In contrast, telomeres have been shown to shorten with aging in mammals as a result of telomerase being largely inactive in somatic cells. Long noncoding RNAs (lncRNAs) have been implicated in both aging and cancer development (Abdelmohsen, et al. 2013; Yang, et al., 2014) but a specific link between telomerase and changes in lncRNA expression has not been established. Previous work has examined the transcriptional response to both telomerase deletion and telomere decapping using microarray technologies(Greenall, et al. 2008; Nautiyal, et al. 2002), however these studies did not include examination of lncRNA expression.

High-throughput technologies have revealed pervasive transcription in *S. cerevisiae*, indicating that approximately 85% of the genome is transcribed (Jacquier 2009; Nagalakshmi, et al., 2008). Among the transcripts are several classes of noncoding RNAs (ncRNA) including Xrn1 Unstable Transcripts (XUTs), Cryptic Unstable Transcripts (CUTs), Nrd1-Unterminated Transcripts and Stable Unannotated Transcripts (SUTs) (reviewed in (Wu, et al., 2012)). In many cases, the function of these transcripts is unknown, although they can regulate gene expression by influencing histone modifications or by interfering

with transcription of nearby genes. There are additional classes of ncRNAs only expressed under specific circumstances, such as meiosis (MUTs) (Lardenois, et al. 2011), or in the absence of nonsense-mediated decay (CD-CUTs) (Toesca, et al. 2011), underscoring the potential importance of ncRNAs in regulating adaptive changes in *S. cerevisiae.*

To identify novel noncoding RNAs associated with telomerase-negative cells, we monitored the transcriptome of yeast cells after deleting the telomerase RNA gene. I identified 113 putative new lncRNAs, 40 of which are only upregulated in telomerase-negative cells and we have termed TMLs (Telomerase-Mutant LncRNA), whereas the remainder represent novel additional SUTs (Stable Unannotated Transcripts)(Xu, et al. 2009). Approximately half of the novel lncRNAs show strongly correlated expression with the adjacent genes, suggesting these lncRNAs may influence expression of neighboring genes.

3.2 Materials and methods

3.2.1 Growth and characterization of yeast strains

The TLC1/*tlc1*::kan^r heterozygote(Mozdy, et al., 2006) was sporulated and dissected to generate the WT and *tlc1Δ* strains (*MAT*a *his3Δ1/his3Δ1*

leu2Δ0/leu2Δ0 LYS2 MET15 ura3Δ0/ura3Δ0). Genotyping was confirmed by replica plating on appropriate media.

Cells were passaged every 12 hours in YPAD media to maintain constant logarithmic growth. Small aliquots were removed for bud indexing and CFU plating. The remaining cells were harvested by vacuum filtration and the filters subsequently frozen in liquid N_2 and then stored at -80°C.

3.2.2 RNA isolation

RNA isolation was carried out using hot-phenol method, as previously described (Kohrer, et al., 1991).

3.2.3 RNA-seq data analysis

Reads were aligned to the UCSC SacCer3 genome (April 2011) using Tophat (Trapnell, et al., 2012) with the following parameters "-G SacCer3_SGD.gtf -I 2000 -i 40 --no-coverage-search UCSC/sacCer3/Bowtie2Index/genome". Transcript boundaries and quantification were determined using cufflinks(Roberts, et al., 2011; Trapnell, et al. 2012; Trapnell, et al., 2010). Data visualization was carried out in R Studio (http://www.R-project.org/)(Team 2014).

3.2.4 Telomere-length analysis

Southern blotting was used to evaluate telomere length, as previously described (Lebo, et al. 2015)

3.3 Results

3.3.1 Characterization of the senescence time course of telomerase-mutant yeast cells

To identify novel lncRNAs associated with telomerase-negative cells, I generated a strain lacking the telomerase RNA subunit (*tlc1*Δ) by sporulation and subsequent dissection of a TLC1/*tlc1Δ* heterozygote. Biological-replicate haploids were passaged every twelve hours to maintain logarithmic growth. To identify time points of interest, viability and budding index were examined at each passage. Additionally, DNA and RNA samples were collected to determine telomere length and perform RNA-seq, respectively. Consistent with the onset of senescence, cellular division potential decreased while the percent of G2/M-arrested cells increased early in the time course, reaching a maximum between 2–3 days after the start of culturing (Figure 3-1). After this point, both viability and doubling time began to return to wild-type levels, concurrent with the appearance of survivors. Analysis of the telomere Southern blot confirms the formation of type-II survivors, which is expected in liquid culture (Chen, et al. 2001; Teng, et al., 1999) (Figure 3-). Based on the phenotypic characterization, 5 time points were chosen for further analysis by RNA-seq corresponding to the following stages: (1) presenescence, (2) early senescence, (3) late senescence, (4) early

survivor and (5) survivor. Nutrient-matched wild-type *TLC1* cells were generated as controls to identify changes in transcription specific to telomerase-negative cells.

Figure 3-1. Phenotypic characterization of senescing and postsenescent tlc1 cells.

(a) Doubling time between passages. (b) Percent G_2/M cells, monitored by cellular bud indexing. (c) Cell viability as measured by ability to form a colony per unit of cell density in culture (optical density based on absorbance of 600-nm light (A_{600})). *tlc1*Δ replicate A shown in red, replicate B shown in blue, nutrient-matched wild-type A and B replicates shown as grey circles or a black 'x' respectively.

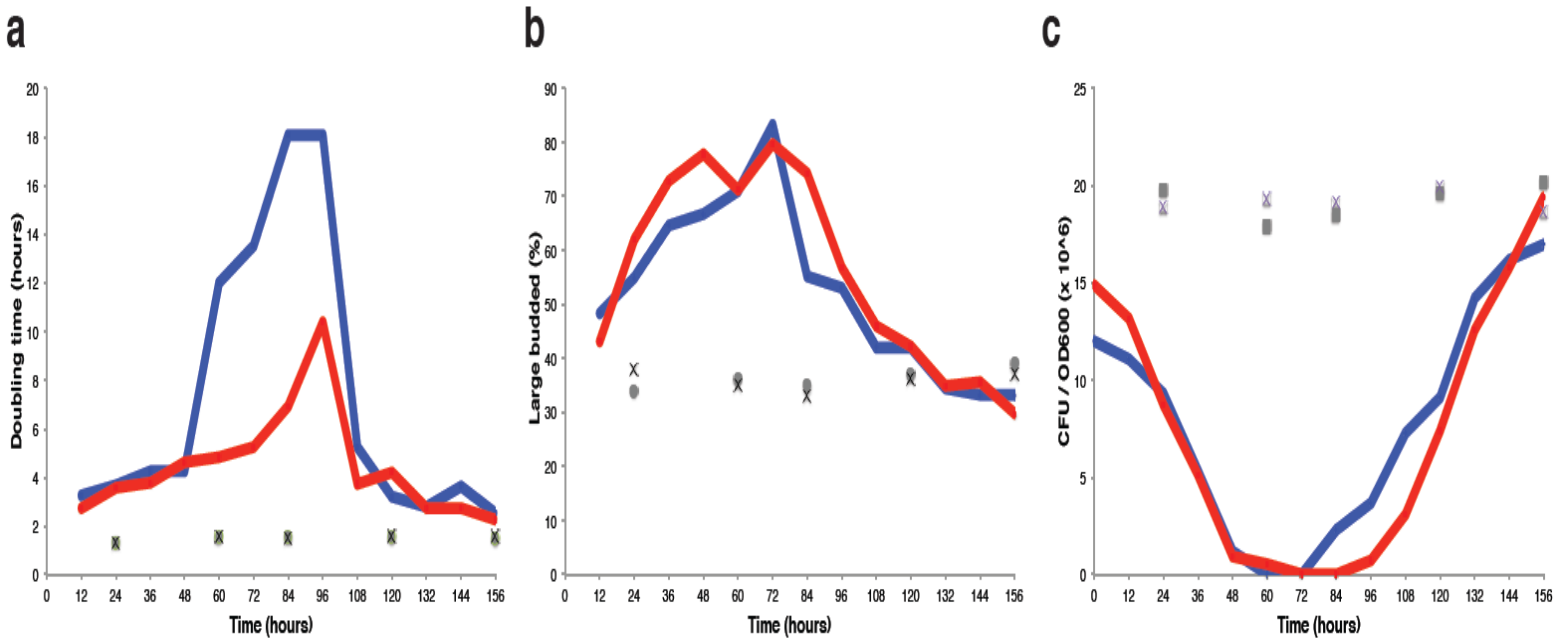
a
Doubling time (hours)
Time (hours)
b
Large budded (%)
Time (hours)
c
CFU / OD600 (x 10^6)
Time (hours)

Figure 3-2. Telomere Southern blot.

Representative telomere Southern blot of tlc1Δ cells. Increasing time is indicated by a black triangle. Samples are labeled according to the categorized time point used for sequencing.

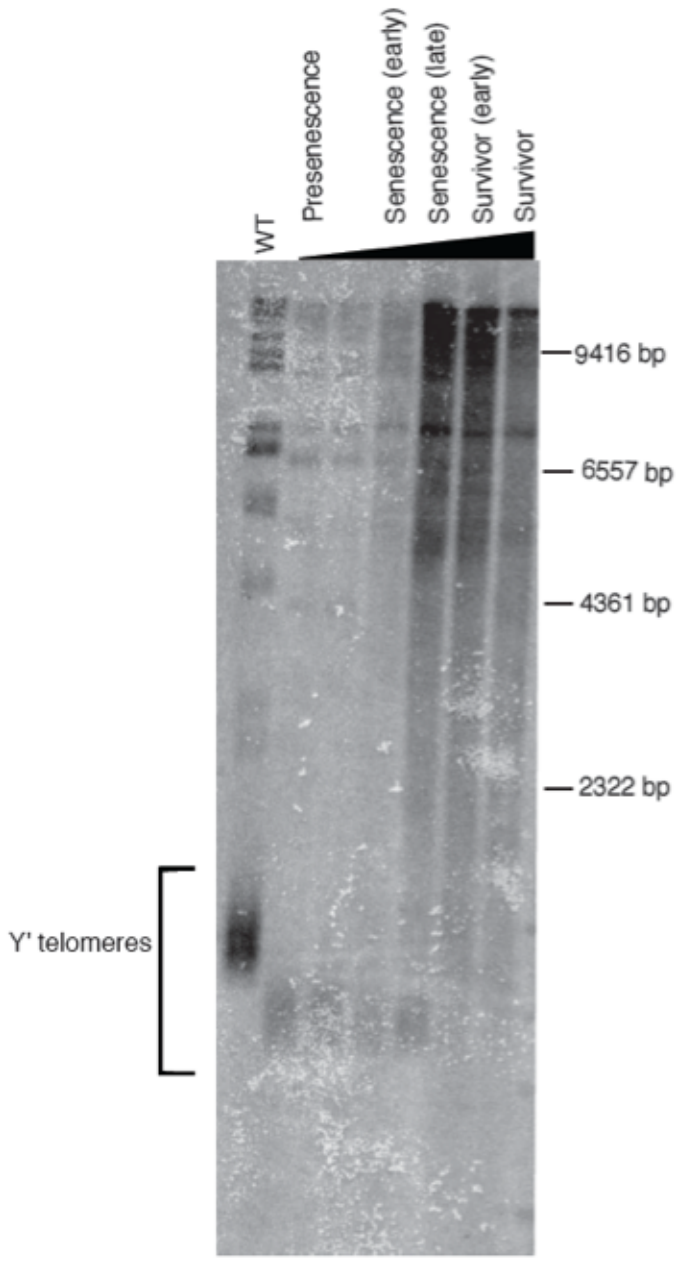

3.3.2 Identification of 112 novel lncRNAs in yeast

RNA-seq reads from biological-replicate samples were mapped to the yeast genome and analyzed using the Tuxedo software suite(Langmead, et al., 2012; Roberts, et al. 2011; Trapnell, et al. 2012; Trapnell, et al. 2010). Briefly, aligned reads underwent *de novo* assembly using Cufflinks prior to assembly into a consensus transcriptome using CuffMerge. In total, 161 intergenic transcripts were identified and then compared with previously annotated genes; any transcripts that overlapped with known genes or annotated untranslated regions (UTRs) were removed (Figure 3-3a). After this step, 112 potentially novel transcripts remained (Table 3-1). I also compared the results with previous transcriptome-profiling experiments and found that none of the candidates correspond to observed transcripts, although some were contained within larger unannotated transcripts (Kavanaugh, et al., 2009; Nagalakshmi, et al. 2008; Samanta, et al., 2006; Yassour, et al., 2009).

Widespread transcription of the yeast genome has been reported previously, with the majority of unannotated transcripts corresponding to several classes of unstable transcripts (XUTs, CUTs, NUTs)(Wu, et al. 2012). Often, the transcripts cannot be detected without depletion of either components of the exosome or stabilizing RNA-binding proteins. I did not observe any changes in Xrn1, Nrd1 or Rpp1 expression that could explain the novel transcripts in telomerase-negative cells (Figure 3-5a). Given that none of the candidates have

been previously reported and they are not associated with any known pathways that increase transcript levels, they represent a potentially novel group of noncoding RNAs in *S. cerevisiae.* In addition, 40 of the noncoding RNAs are only expressed in telomerase-negative yeast and are therefore a novel class of transcripts, which we termed TMLs (Telomerase-Mutant LncRNAs).

Figure 3-3. Characterization of novel intergenic transcripts.

(a) Experimental workflow and analysis for analyzing RNA-seq data from *tlc1*Δ and nutrient-matched wild-type cells. (b) Intergenic transcripts show low coding potential. Comparison of the coding potential of known protein coding and noncoding genes with the intergenic transcripts calculated using CPC software. (c) Intergenic transcripts show a distinct length distribution. Length distribution of intergenic transcripts as well as known protein-coding and noncoding genes ($P < 0.0001$). Intergenic transcripts have a median length of 467 nts. Data points above 5000 nt are not shown. P value calculated using the two sample t-test.

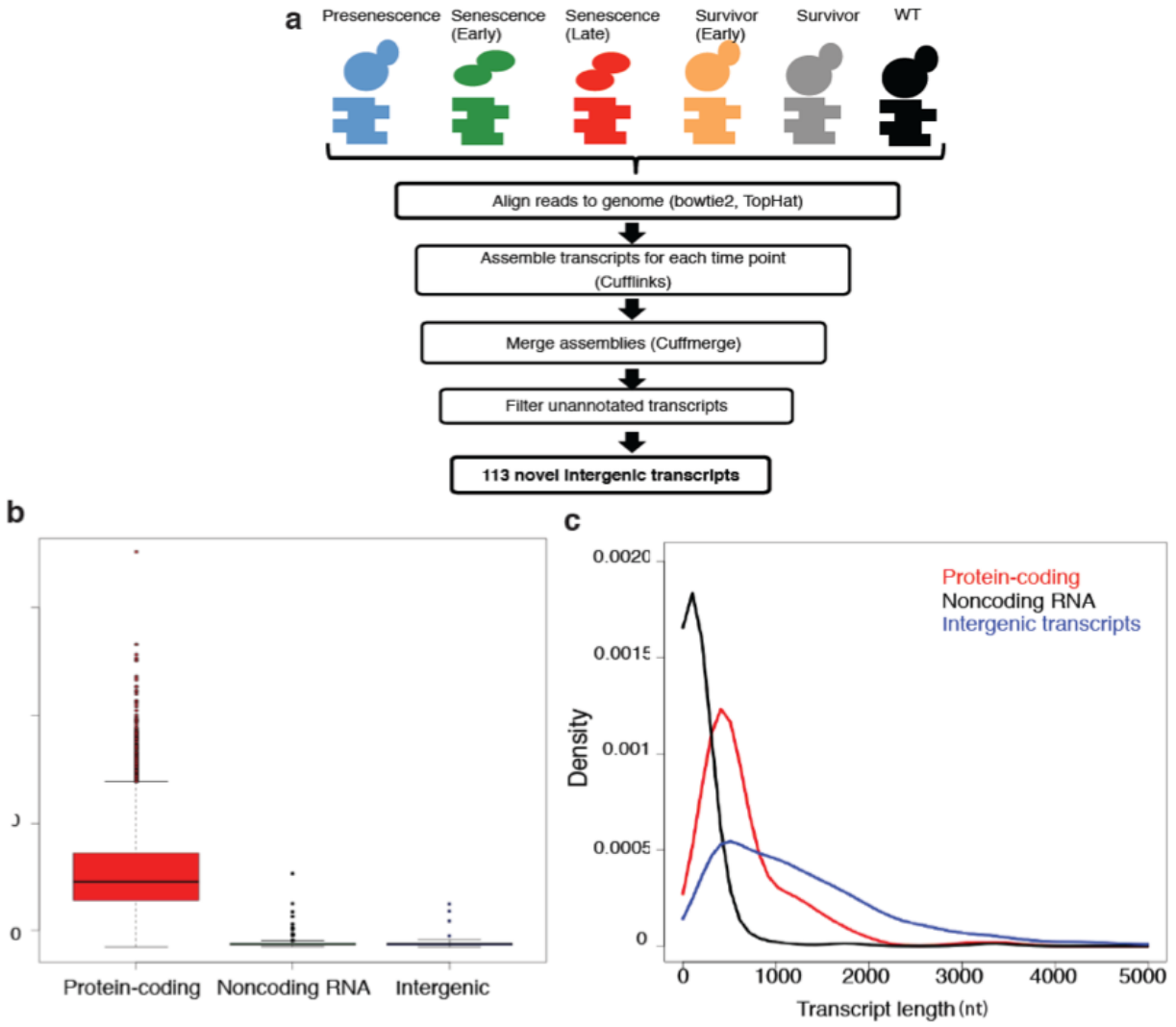
a
Presenescence
Senescence (Early)
Senescence (Late)
Survivor (Early)
Survivor
WT
Align reads to genome (bowtie2, TopHat)
Assemble transcripts for each time point (Cufflinks)
Merge assemblies (Cuffmerge)
Filter unannotated transcripts
113 novel intergenic transcripts
b
0
Protein-coding
Noncoding RNA
Intergenic
c
0.0020
0.0015
0.001
0.0005
0
Density
Protein-coding
Noncoding RNA
Intergenic transcripts
0
1000
2000
3000
4000
5000
Transcript length (nt)

3.3.3 Characterization of putative lncRNAs

To examine whether our candidates are likely to encode proteins, we used the Coding-Potential Calculator (CPC) (Kong, et al., 2007) to measure the coding potential and ORF size in each transcript. The unannotated transcripts show similarly low coding potential to known noncoding RNAs in *S. cerevisiae* (Figure 3-3b); significantly lower than that of protein-coding genes ($P < 0.0001$). This strongly suggests that the candidates do not encode a protein. Since lncRNAs are generally defined as transcripts greater than 200 nt, we also examined the length distribution of the intergenic transcripts. They are longer than annotated ncRNAs (median length = 467 nts) (Figure 3-3c) and, therefore, we conclude that the candidates represent a group of novel lncRNAs.

To determine whether the candidates represented distinct transcripts rather than extensions of nearby genes, I selected a subset of the most highly expressed lncRNAs to examine by northern blot analysis (Figure 3-4a), but was still only able to detect one candidate in this manner. This lncRNA did appear as independent transcript and therefore does not represent extended transcription from neighboring genes. The expression of an additional 10 candidates was validated using RT-PCR (Figure 3-4b, Table 3-1) although we did not confirm whether these represented independent transcripts.

Figure 3-4. Validation of lncRNA candidates.

(a) Tested candidates appear as discrete transcripts. Northern-blot analysis of one lncRNA candidate. Transcript appears as a distinct band and therefore likely has well-defined boundaries. (b) All tested candidates can be detected by RT-PCR. RT-PCR analysis of one candidate. (c) Mapped RNA-seq reads for one lncRNA candidate. Reads shown were visualized with Integrative Genomics Viewer software. (a,b and c) correspond to different transcripts.

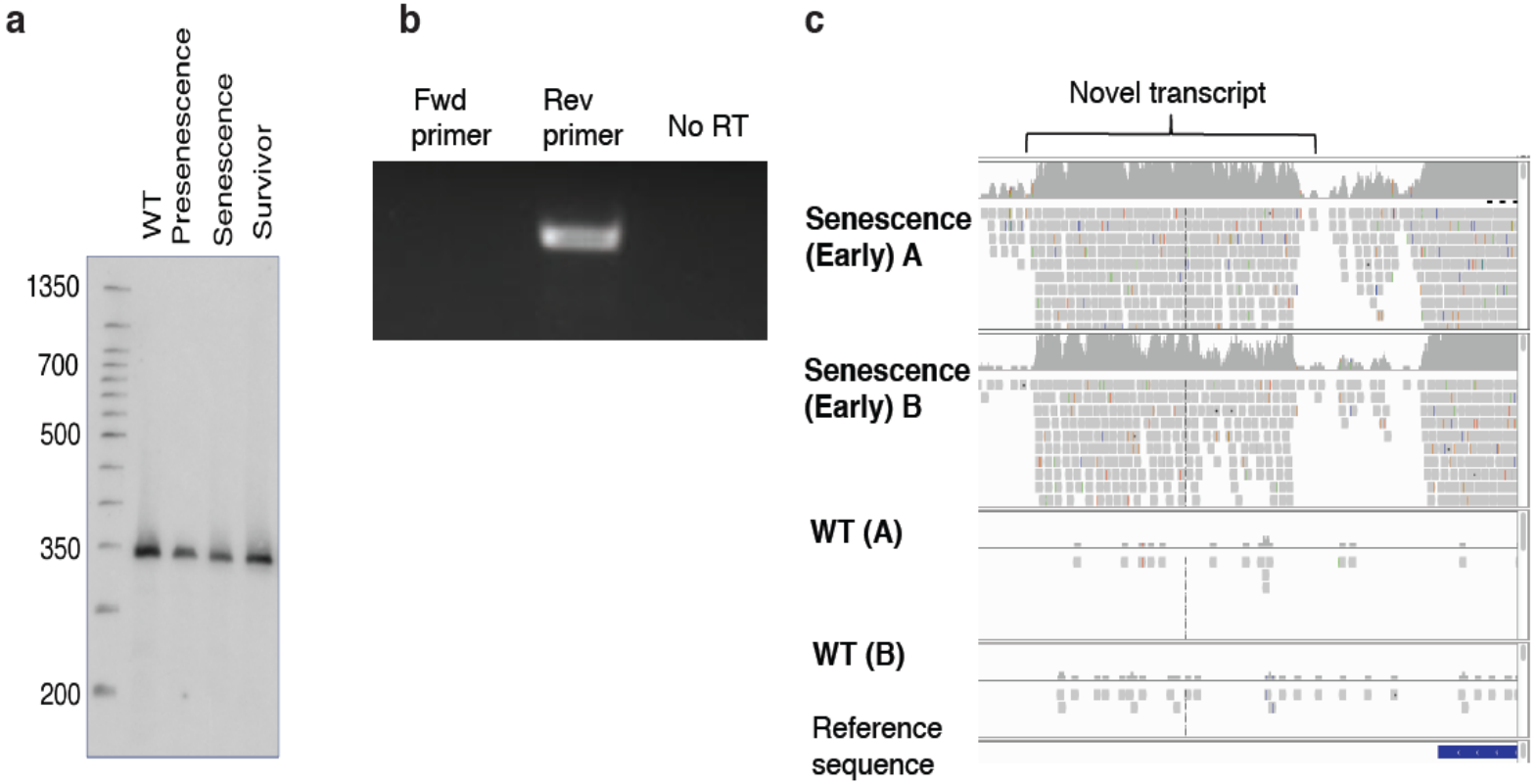
a
WT
Presenescence
Senescence
Survivor
1350
700
500
350
200
b
Fwd primer
Rev primer
No RT
c
Novel transcript
Senescence (Early) A
Senescence (Early) B
WT (A)
WT (B)
Reference sequence

Table 0-1. Genomic coordinates of novel lncRNAs.

Expression levels are given as FPKM based on cufflinks output for each time point. Transcripts that have been validated by RT-PCR are indicated. SUTs indicate transcripts that appear at equal or greater levels in WT cells, while TMLs are primarily expressed in the telomerase mutant.

tracking_id	Category/name	WT_presenescent_matchFPKM	WT_early_senescent_matchFPKM	WT_late_senescent_matchFPKM	WT_early_survivor_matchFPKM	WT_survivor_matchFPKM	presenescence_FPKM	early_senescence_FPKM	late_senescence_FPKM	early_survivor_FPKM	survivor_FPKM	Length	Chromosome	Start	End	Validated?
TCONS_00000004	SUT	0	0	0	0.99043	0	0	0	0.160552	0	2.83534	375	chrI	6578	6952	
TCONS_00000058	SUT	3.81251	11.466	7.74754	7.74374	5.568	13.2211	10.3255	9.84182	8.9381	15.1565	1143	chrI	177426	178568	RT-PCR
TCONS_00000243	SUT	3.84098	5.47287	5.9857	2.83204	8.86705	7.15674	8.69588	7.19884	6.81435	13.0766	960	chrII	288236	289195	
TCONS_00000382	SUT	0	0	0	2.15394	6.61234	1.36704	2.82835	1.64883	0.604528	14.1223	322	chrII	702057	702378	
TCONS_00000389	SUT	5.42602	1.3667	1.15181	4.40079	3.67054	5.30343	7.26095	6.1635	5.15235	16.85	573	chrII	718195	718767	
TCONS_00000722	SUT	0	0	0	0	0	0	0	0.177785	0.0119274	7.7496	472	chrIII	8611	9082	
TCONS_00000735	TML1	21.6798	9.41328	3.91949	17.2821	34.9273	48.2982	58.3914	42.4808	45.2504	17.0997	288	chrIII	41059	41246	RT-PCR
TCONS_00000764	SUT	15.8154	7.25653	6.20899	11.6958	17.0008	16.3913	34.8049	26.5446	25.0216	42.4222	510	chrIII	125339	125848	
TCONS_00000765	SUT	3.17835	5.80866	1.64385	1.88149	4.75093	5.42645	19.369	8.22193	6.71815	25.188	569	chrIII	126937	127505	
TCONS_00000773	SUT	0	0	0	0	0	0	0	0	0	18.1827	313	chrIII	157823	158135	
TCONS_00000775	SUT	0	0	1.82898	0	0	0	0	0	0	4.38712	480	chrIII	166864	167343	
TCONS_00000944	SUT	1.43448	2.17675	3.05864	1.56034	0.741529	0.959884	1.24804	1.54965	1.46161	1.10555	1193	chrIII	273097	274289	
TCONS_00000955	TML2	8.71218	10.6378	15.0893	7.08346	8.13582	19.3353	35.5174	21.5344	15.0525	33.3109	602	chrIII	308441	309042	
TCONS_00000956	SUT	0	0	0	0	0.1686	0	0.908892	0	0.064727	9.76532	346	chrIII	310333	310678	
TCONS_00001325	SUT	6.55947	19.4763	24.5637	13.1281	0	0.177248	33.0505	26.3311	20.9055	26.0648	552	chrIV	1049679	1050230	
TCONS_00001459	TML3	10.0108	28.8358	23.9016	19.7637	26.3384	40.0021	47.3254	33.2814	28.1783	2.48358	355	chrIV	1459342	1459696	
TCONS_00001652	TML4	0	0	0	0	0	0	0	0	0	16.9871	442	chrIV	443904	444345	RT-PCR
TCONS_00001679	TML5	0	0	0	0	0	0	0	0	0	17.9134	458	chrIV	505798	506255	
TCONS_00001680	TML6	0	0	0	0	0	1.07353	3.50075	0.0100503	0	20.154	842	chrIV	506525	507366	
TCONS_00001730	SUT	3.38446	0	3.33783	0	2.38572	0	0	0	0	7.76812	586	chrIV	651984	652569	
TCONS_00001809	SUT	0	0.75719	0	1.5283	0	1.61876	2.99849	1.04558	0.930351	5.23621	426	chrIV	889082	889507	
TCONS_00001818	SUT	34.0328	37.9022	34.8241	13.2262	74.3795	35.4674	26.6596	24.9876	23.7022	33.2807	384	chrIV	909514	909897	
TCONS_00001858	TML7	0	0	0	0	0	0.404289	0.731124	0	0	44.5229	1849	chrIV	1017349	1019197	RT-PCR
TCONS_00001937	SUT	27.7632	44.6435	36.2773	17.0388	7.52421	16.8881	37.9269	41.4744	32.6097	0.00827	470	chrIV	1252028	1252497	
TCONS_00001965	SUT	5.64483	8.11844	4.35187	3.95935	4.50555	6.49739	8.9201	7.91026	8.01732	1.97346	1261	chrIV	1340847	1342107	
TCONS_00002051	TML8	3.42781	4.67438	8.37903	5.79232	5.45902	12.5361	19.1976	13.573	15.6879	16.041	948	chrIX	29294	30241	
TCONS_00002052	SUT	17.5041	13.6121	31.4959	21.3325	28.5418	25.2726	26.827	27.9449	29.0364	2.05305	390	chrIX	30362	30751	
TCONS_00002053	SUT	0	2.0802	0	0	0.160912	0	0	0	0	2.92987	440	chrIX	33012	33451	
TCONS_00002114	TML9	0	0	2.40997	2.33646	9.32673	1.12995	12.3158	7.71282	7.91527	19.6711	268	chrIX	245678	245945	
TCONS_00002186	SUT	0.957938	2.52082	3.05513	0.694403	1.69568	2.84659	1.74671	3.44998	4.1911	12.5986	3478	chrIX	426813	430290	
TCONS_00002187	SUT	0	0.485852	0	0	0	0	0.00231165	0	0	28.7557	550	chrIX	432678	433227	
TCONS_00002190	TML10	0.895708	0.879716	0.828388	2.5411	0.929236	4.38159	5.16376	3.28156	3.54999	8.48495	721	chrIX	436477	437197	
TCONS_00002388	TML11	0.293853	0.438351	0.22815	0.558286	0.382461	1.63998	2.27601	1.72254	1.21939	17.4929	971	chrV	23290	24260	
TCONS_00002389	SUT	11.9379	5.18962	4.37362	2.66057	8.16763	13.467	10.5028	7.7832	8.28482	3.02657	297	chrV	24627	24923	
TCONS_00002430	SUT	11.6519	12.6803	5.89691	6.0984	12.0394	9.13713	11.5019	11.2539	11.5912	23.7365	464	chrV	110627	111090	
TCONS_00002491	SUT	3.97744	8.44518	5.85094	6.18814	11.1237	3.69039	3.2516	3.6959	4.28525	14.2284	439	chrV	284487	284925	
TCONS_00002525	SUT	8.82106	11.5311	11.4276	9.06817	9.12007	10.7301	8.09478	11.2233	9.72482	12.8191	449	chrV	377980	378428	
TCONS_00002636	SUT	302.968	176.084	152.473	177.128	940.729	297.818	305.15	302.636	353.787	27.3866	192	chrV	130762	130953	RT-PCR
TCONS_00002693	TML12	0	0	0	0	0	0	16.0055	9.70688	0.234567	18.6441	251	chrV	298152	298402	
TCONS_00002738	SUT	10.0322	8.06378	7.05254	6.92862	5.13168	1.15719	8.33083	4.45762	5.7486	3.66954	454	chrV	416682	417135	
TCONS_00002791	SUT	66.621	94.1696	70.304	39.8408	43.1189	29.8329	59.7457	46.9094	54.2315	25.648	271	chrV	362758	363028	
TCONS_00002821	TML13	0	0	0	0	0	2.60287	11.3584	4.30325	2.16445	26.9196	271	chrVI	100965	101235	
TCONS_00002914	SUT	29.7291	19.247	13.5958	24.8518	74.0034	23.8512	7.51886	11.9426	23.0032	5.19984	377	chrVI	110188	110564	
TCONS_00002915	SUT	5.94374	3.69181	1.15283	3.90522	8.98168	6.2938	4.70538	6.33672	5.73427	1.44626	1166	chrVI	111144	112309	
TCONS_00002928	TML14	2.55898	6.22214	3.17262	0.897051	2.4862	7.35371	18.7592	12.7793	7.96807	29.6816	393	chrVI	168538	168930	
TCONS_00003321	TML15	1.25371	1.10096	0.636333	2.06628	2.5307	6.61982	13.3942	8.70403	7.5837	24.1571	1029	chrVII	1066052	1067080	
TCONS_00003558	SUT	0	4.35774	14.7764	3.46713	6.89832	3.96959	13.7738	7.48197	5.70301	3.37419	451	chrVII	712601	713051	
TCONS_00003656	SUT	7.5971	0	1.83131	6.29928	4.31112	9.75035	7.31894	15.3433	16.6602	10.4091	395	chrVII	986830	987224	
TCONS_00003700	TML16	0	0.426662	0	0.430586	0.821117	1.57645	2.4851	1.77558	1.32528	15.853	598	chrVII	567999	568596	
TCONS_00003853	SUT	32.3293	53.0861	43.0332	55.63	164.285	31.6599	129.19	110.622	105.876	24.0329	165	chrVIII	429462	429626	
TCONS_00003919	SUT	24.0879	5.84198	7.74528	5.61295	36.0237	22.2246	17.5859	10.3252	12.4067	13.432	417	chrVIII	48248	48664	
TCONS_00004062	TML17	3.02109	4.1164	3.18989	3.11379	3.29141	10.3054	14.6517	12.0246	9.12948	13.8709	588	chrVIII	458228	458815	
TCONS_00004063	SUT	23.0456	4.52992	12.7996	14.9125	37.3111	5.73742	3.62428	5.92642	6.71436	12.2424	270	chrVIII	461768	462037	
TCONS_00004090	SUT	0.897918	0	1.69327	0	0	0	0.844823	0.931154	0.625643	17.6711	455	chrVIII	302109	302563	
TCONS_00004092	TML18	1.42339	0.494424	0.514669	0.49897	0	6.49159	10.4767	6.99107	5.44943	11.5003	544	chrVIII	531075	531618	
TCONS_00004284	SUT	10.4991	7.5561	9.53037	6.84477	21.2887	9.67211	10.076	11.4291	9.88475	163.757	1513	chrX	605916	607428	
TCONS_00004413	TML19	0	0	0	0	0	1.00774	0.198214	0.00472046	0	14.9595	1132	chrX	223741	224872	
TCONS_00004440	SUT	15.7027	25.8479	19.168	19.551	39.025	22.8009	19.0933	20.1308	21.481	5.25292	847	chrX	322262	323108	
TCONS_00004575	TML20	5.51879	9.42874	4.08434	3.33147	10.9746	15.3785	24.9732	15.6865	15.1414	15.0073	331	chrX	740355	740685	
TCONS_00004737	TML21	2.19836	4.76008	0	4.57046	9.17245	11.5448	13.2031	9.3725	8.8453	55.0854	409	chrXI	468880	469288	
TCONS_00004885	SUT	19.0191	26.4391	20.7601	21.7205	32.5535	33.0624	37.0459	31.787	31.0446	7.79585	1507	chrXI	303604	305110	
TCONS_00004886	SUT	0	0	1.17441	3.14477	0.593444	0.930656	1.76156	0.833267	0.632593	46.2802	502	chrXI	308316	308817	
TCONS_00005012	TML22	2.35658	3.04849	3.1701	2.70734	3.03644	6.56023	11.2708	7.96833	6.77651	25.6211	3051	chrXI	642964	646014	

TCONS_00005013	SUT	24.3971	17.0652	25.1507	21.327	57.9352	45.9852	58.8718	41.3115	31.2399	25.1975	318 chrXI	649995	650312
TCONS_00005017	TML23	0	0	0	1.5319	0	13.1214	15.352	10.0109	6.73596	4.14485	312 chrXI	664285	664596
TCONS_00005018	TML24	0	0	0	0	0	2.92689	7.05222	2.02539	1.01361	1.7879	200 chrXI	665674	665873
TCONS_00005023	SUT	24.3474	0	28.2484	20.1596	85.7052	33.1052	35.2994	40.5916	42.5861	12.6899	185 chrXII	16330	16514
TCONS_00005246	SUT	782.62	370.117	447.579	304.357	723.209	558.043	655.163	495.441	456.456	6.91389	129 chrXII	752012	752140 RT-PCR
TCONS_00005543	SUT	39.2948	37.3751	25.4692	35.5424	17.2461	10.0696	22.2893	22.6997	18.8755	18.4489	258 chrXII	510373	510630
TCONS_00005721	TML25	0	0	0	0	0	0	0	0	0	28.1985	448 chrXII	1030149	1030596
TCONS_00005734	TML26	0.893204	0.12583	0.63627	0.961545	1.05584	4.26302	5.666	3.52299	2.98903	14.1051	1540 chrXII	449707	451246
TCONS_00005735	SUT	8.64005	0	1.23272	4.21158	4.34553	0	0.498569	2.04644	0.827603	14.8593	345 chrXII	1043192	1043536
TCONS_00005736	TML27	0	0	0.447868	0	0.186356	2.80741	1.25185	0.846245	0.244367	11.7542	1153 chrXII	1061465	1062617
TCONS_00005741	SUT	8.50081	7.68907	17.07	11.0546	24.4905	15.3735	18.6411	13.4202	14.6976	11.8764	576 chrXIII	13488	14063
TCONS_00005949	SUT	13.3302	22.7027	4.81993	3.56076	2.01998	9.89899	6.23297	5.00564	4.60553	22.4571	268 chrXIII	625448	625715
TCONS_00006006	SUT	16.7612	8.59834	16.0767	9.03896	2.85005	6.46943	20.596	20.5175	14.8648	9.53109	315 chrXIII	782176	782490
TCONS_00006016	SUT	37.1167	19.0892	16.7708	31.4048	51.7772	27.0997	31.1396	36.7431	37.3997	42.5529	523 chrXIII	807587	808109
TCONS_00006063	SUT	43.523	28.0099	32.0984	54.7319	71.8626	20.8187	14.5382	13.2447	17.1047	17.1968	390 chrXIII	45980	46369
TCONS_00006189	TML28	6.31572	7.99823	6.36746	9.46547	10.2967	14.2782	14.6157	10.5793	12.2697	14.395	1323 chrXIII	433148	434470
TCONS_00006300	TML29	2.27925	4.38402	3.53214	4.4392	4.517	7.43878	9.36425	8.55828	7.68227	20.3943	841 chrXIII	769540	770380 RT-PCR
TCONS_00006422	TML30	0	1.07759	1.12171	1.37242	5.8481	2.04076	2.39883	1.60198	1.76709	15.7866	516 chrXIV	174763	175278
TCONS_00006466	SUT	3.73111	0	1.84088	3.61228	3.85746	5.23953	2.68427	3.2444	3.09378	16.6147	394 chrXIV	301892	302285
TCONS_00006496	SUT	29.7629	14.0195	17.4354	23.3816	28.7371	32.882	21.353	23.2028	25.263	16.7172	327 chrXIV	373826	374152
TCONS_00006581	SUT	5.24749	3.80342	1.85498	0.913584	4.05439	4.84479	5.8158	3.63625	3.66967	13.1599	487 chrXIV	599344	599830
TCONS_00006636	SUT	77.63	81.3557	73.2196	105.902	33.7969	50.5193	61.3647	88.5682	89.1801	13.0942	392 chrXIV	730241	730632
TCONS_00006643	SUT	7.87855	7.39315	4.8839	9.07536	18.6449	10.2715	4.71474	18.1392	15.0475	15.6654	325 chrXIV	759525	759849
TCONS_00006648	TML31	0	0	0	0	0	0	0	0	0	35.7491	733 chrXIV	776354	777086
TCONS_00006924	SUT	1.36507	0	0	2.00317	0.961181	0.206525	0.931136	0	2.88177	1.58958	677 chrXV	21663	22339
TCONS_00006987	SUT	24.0422	17.8045	6.86042	6.65116	18.4339	28.7909	33.6614	19.2518	20.1093	19.702	239 chrXV	226185	226423
TCONS_00007230	TML32	5.71986	5.68981	4.75546	6.14722	7.37028	10.9869	7.54911	8.16812	8.8548	28.8576	1676 chrXV	978347	980022
TCONS_00007242	SUT	4.98766	4.13508	2.88641	3.65589	4.26559	4.35766	10.3133	8.03306	4.8346	15.7709	741 chrXV	1018991	1019731
TCONS_00007294	SUT	2.11077	6.04211	2.14267	4.91354	10.3174	9.19963	10.4654	6.33784	4.29993	15.4207	449 chrXV	73448	73896
TCONS_00007328	SUT	5.3874	3.8756	7.92505	8.6145	15.0791	12.2251	10.0039	6.64683	8.45079	26.3447	551 chrXV	170071	170621
TCONS_00007390	SUT	8.79765	7.04798	7.30415	1.67827	0	0	1.82021	0.695101	0.847512	11.9377	377 chrXV	343415	343791
TCONS_00007402	TML33	3.67477	3.49981	3.73957	3.83417	7.32062	7.70929	9.8952	10.9272	9.69442	62.9295	1521 chrXV	385095	386615
TCONS_00007459	TML34	37.9095	20.6806	35.3634	24.8358	34.9516	60.3945	93.5078	51.1064	52.9724	16.4058	404 chrXV	518528	518931 RT-PCR
TCONS_00007647	SUT	9.96525	11.2507	7.24468	25.3437	7.77537	27.395	20.348	27.8463	25.2845	14.5535	518 chrXV	1044674	1045191
TCONS_00007649	SUT	161.979	71.0603	37.5045	81.3852	54.0184	132.043	71.5989	45.4224	48.0795	40.0199	209 chrXV	1048204	1048412 RT-PCR
TCONS_00007652	TML35	4.70555	2.82317	4.05769	4.2453	4.6876	6.31365	13.0174	9.27632	7.9343	25.0301	931 chrXV	1054436	1055366
TCONS_00007655	SUT	7.91752	15.7574	20.7058	13.4653	7.63925	7.4534	28.952	21.197	15.2881	18.0272	693 chrXV	1063864	1064556
TCONS_00007835	TML36	0	0	0	0	0	0	0	0	0	1.42607	407 chrXVI	581591	581997
TCONS_00007837	TML37	7.61074	14.5663	8.49308	8.18969	12.0782	16.3854	27.4253	33.4804	36.8784	25.3805	569 chrXVI	586591	587159
TCONS_00007838	TML38	3.52229	3.76909	8.55163	7.09135	7.1895	17.5988	14.8566	14.078	15.0209	19.5055	891 chrXVI	587779	588669
TCONS_00007839	TML39	1.30095	0.903788	2.55371	1.60712	2.29587	10.133	14.4191	7.998	5.73625	16.7142	576 chrXVI	588868	589443
TCONS_00007840	TML40	0	0	2.58617	0	0	13.757	17.2274	9.24741	8.13019	11.7595	436 chrXVI	591271	591706
TCONS_00007846	SUT	6.10681	7.67773	7.51849	6.39726	7.44372	4.79373	6.00214	6.29799	5.1907	29.2287	1155 chrXVI	607541	608695
TCONS_00007978	TML41	0.942999	5.20695	1.46431	4.29299	1.35361	7.64889	10.028	7.57901	6.85277	19.3851	443 chrXVI	22200	22642
TCONS_00007981	SUT	7.54613	5.99232	12.3669	6.12366	11.8742	28.3531	12.619	12.9725	12.5514	61.0746	580 chrXVI	40283	40862
TCONS_00008144	SUT	13.6675	9.85992	12.6888	21.0532	19.6828	19.4402	31.53	23.1939	24.0353	328.384	395 chrXVI	520566	520960 RT-PCR
TCONS_00008232	SUT	178.638	122.083	92.1631	80.1394	3.01956	23.6039	41.6507	87.0694	77.1189	25.1849	168 chrXVI	771346	771513
TCONS_00008236	SUT	13.5685	15.0482	12.4787	16.1098	34.3721	16.3581	19.603	20.1422	20.005	1.94984	1362 chrXVI	780443	781804
TCONS_00008296	SUT	11.3288	20.1144	14.2999	14.6492	21.2702	19.2599	19.845	20.3475	18.6117	5.94764	2024 chrXVI	929288	931311

3.3.4 Novel lncRNAs show altered expression in telomerase-negative cells

I first examined the expression pattern of the lncRNAs in *tlc1*Δ cells relative to wild type. Over half of the novel lncRNAs are differentially expressed by two-fold or more in at least one of the time points tested (Figure 3-5a). The majority of the differentially expressed lncRNAs were upregulated relative to wild type and in many cases the transcripts were not even detectable in wild-type cells. Thus, many of the lncRNAs are specific to telomerase-negative cells, providing an explanation as to why they have not been identified as lncRNAs previously.

Next, to identify senescence or stage-specific lncRNAs, I compared the upregulated lncRNAs from each time point (Figure 3-5b). This analysis identified 12 transcripts found only in at least one of the senescence time points. Interestingly, the survivors exhibited even more stage-specific lncRNAs (17).

However, the expression level of the lncRNAs was generally quite low, with a median value of 19.9 FPKM (fragments per kilobase of transcript per million mapped reads), so despite the strong fold-change between the telomerase-negative and wild-type cells for many of the lncRNAs, only a small subset (between 5 and 22, depending on the time point) can be considered significantly differentially expressed without further analysis.

Figure 3-5. Many lncRNAs are differentially expressed in telomerase negative cells.

(a) Heatmap analysis of lncRNA candidate expression. Most lncRNAs are upregulated by two-fold or more (red). Any color (red or blue) indicates differential expression of at least two-fold. Differential expression of commonly mutated exosome and RNA-binding proteins is shown below black line. Differential expression is calculated by $\log_2(\frac{tlc1\Delta_{exp}}{WT_{exp}})$ (b) Comparison of upregulated lncRNAs at each time point. Most lncRNAs (58/86) are upregulated in more than one time point.

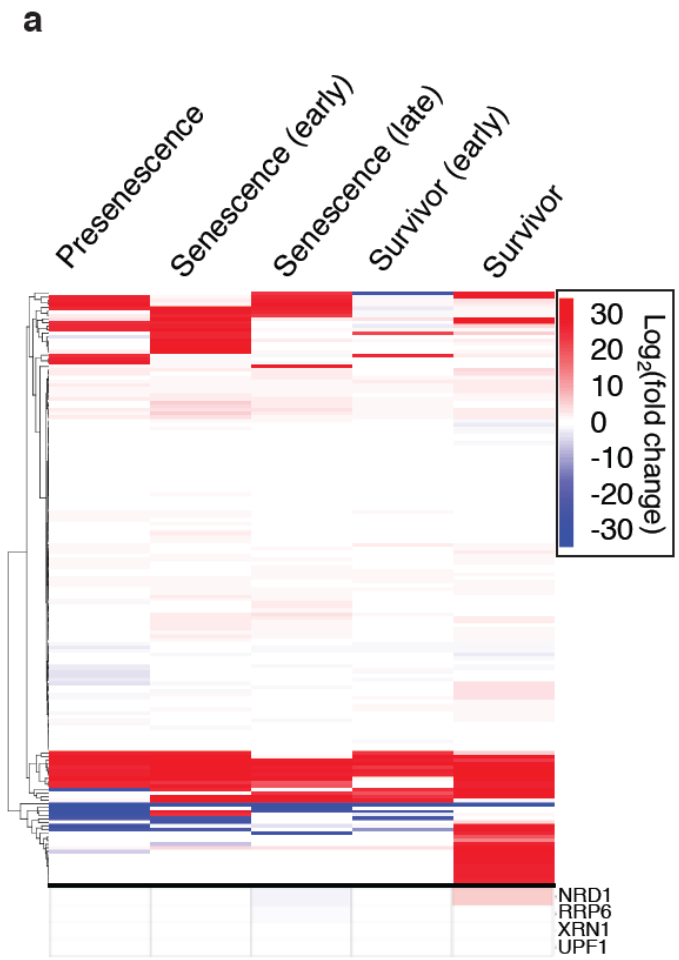
a
Presenescence
Senescence (early)
Senescence (late)
Survivor (early)
Survivor
30
20
10
0
-10
-20
-30
Log2(fold change)
NRD1
RRP6
XRN1
UPF1

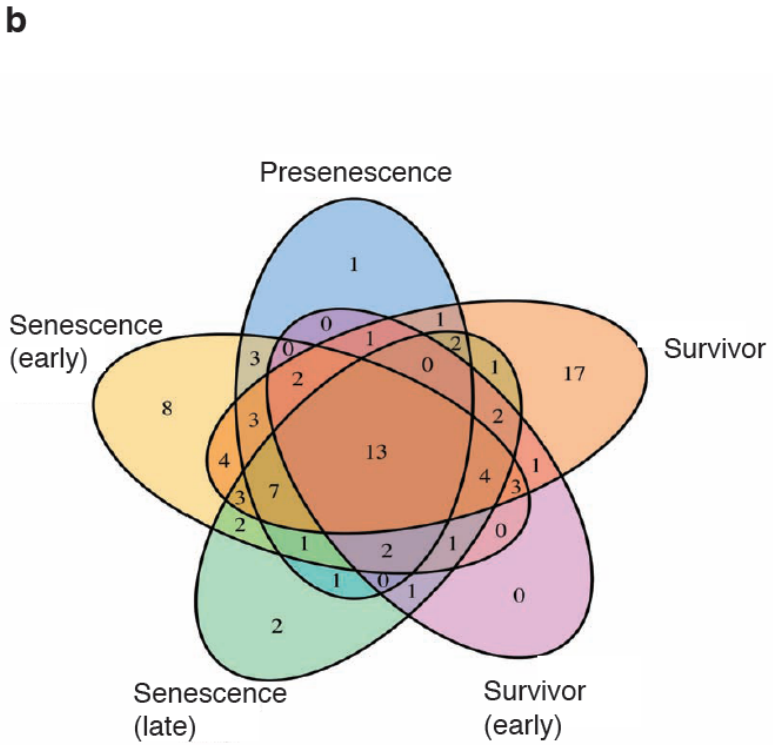
b
Presenescence
Senescence (early)
Survivor
Senescence (late)
Survivor (early)
1
0
1
3
0
1
2
2
0
1
17
8
3
2
13
4
4
3
1
3
7
2
1
2
1
0
1
0
1
0
2
0

3.3.5 A subset of the novel lncRNAs show correlated expression with a neighboring gene

Since lncRNAs can regulate the expression of neighboring genes(Guil, et al. 2012), I examined correlation of each lncRNA differential expression with that of its adjacent genes at each time point (Figure 3-6a, 3-7). For most time points, approximately one-third of the lncRNAs show strong correlation (R^2 0.79 – 0.99) with at least one neighboring gene while, in the late-senescence samples, over half are correlated. Interestingly, the lncRNAs showing the largest differential expression relative to wild type show almost no correlation with either adjacent gene ($R^2 < 0.015$, Fig. 5a).

To determine whether these correlations may be significant I generated a random dataset for comparison. Using this dataset as my expected distribution, I calculated the probability of making these observations by random chance ($P < 0.001$). Deviations from expectation are summarized in table 3-2.

Of the correlated lncRNAs, we observe more positive relationships than negative, indicating expression of the lncRNAs may promote expression of the neighboring gene. It is also possible that the correlation is the result of gene-transcript extensions being misidentified as lncRNAs, but because of the low expression levels it was difficult to distinguish between these possibilities.

Figure 3-6. The lncRNA candidates may regulate expression of nearby genes.

(a) Highly differentially expressed candidates do not show correlated expression with neighboring genes. 2D plot showing differential expression of lncRNAs and each adjacent gene. Late senescence time point is shown. Candidates fall into two groups (1) low differential expression, correlated with one or more adjacent gene and (2) high differential expression, no correlation with adjacent genes. (b) Correlated expression between a subset of lncRNAs and adjacent genes. Differential expression of lncRNAs showing either positive (red, $R^2 = 0.91$) or negative (blue, $R^2 = 0.92$) correlation with an adjacent gene plotted against differential expression of the adjacent gene. Differential expression is calculated by $\log_2(\frac{tlc1\Delta_{exp}}{WT_{exp}})$ (c) Correlated genes are enriched with extracellular proteins. Functional enrichment analysis performed using DAVID and plotted using qplot in the ggplot2(Wickham 2009) package in R studio. Proteins with an extracellular domain are enriched at each time point.

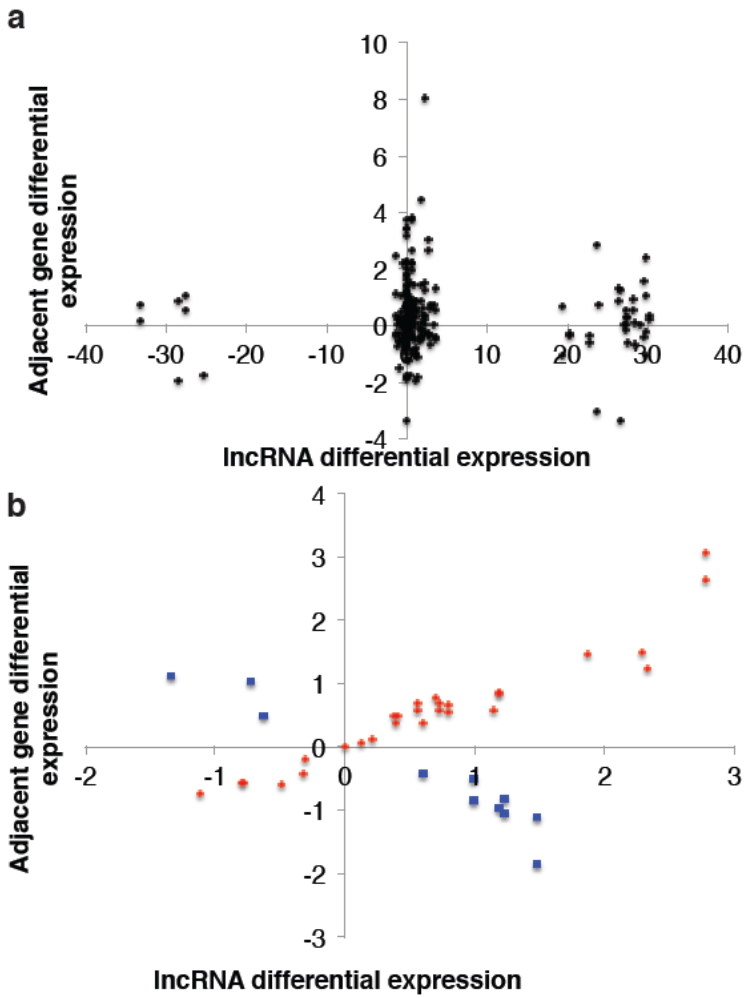
a
Adjacent gene differential expression
lncRNA differential expression
b
Adjacent gene differential expression
lncRNA differential expression

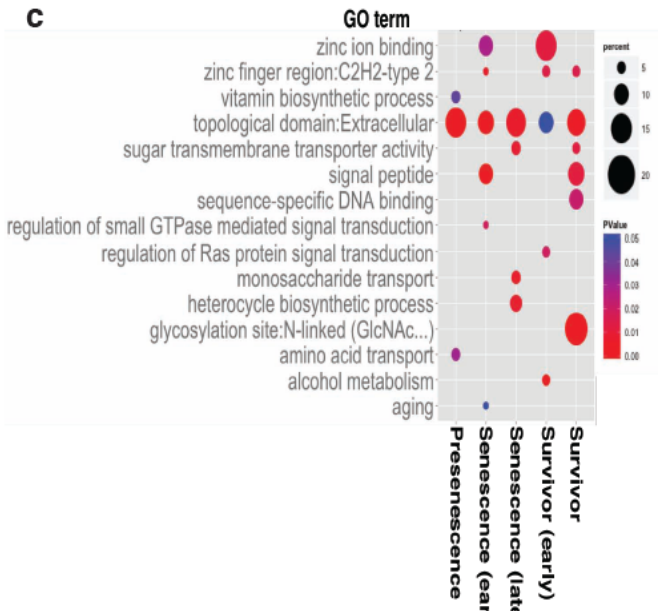
c
GO term
zinc ion binding
zinc finger region:C2H2-type 2
vitamin biosynthetic process
topological domain:Extracellular
sugar transmembrane transporter activity
signal peptide
sequence-specific DNA binding
regulation of small GTPase mediated signal transduction
regulation of Ras protein signal transduction
monosaccharide transport
heterocycle biosynthetic process
glycosylation site:N-linked (GlcNAc...)
amino acid transport
alcohol metabolism
aging
Presenescence
Senescence (early)
Senescence (late)
Survivor (early)
Survivor
percent
PValue

Figure 3-7. Correlation analysis of lncRNAs and adjacent genes.

(a) Differential expression of lncRNAs plotted against differential expression of adjacent genes. (b) Subset of lncRNAs and corresponding adjacent genes showing correlated expression at each time point. Negatively correlated pairs shown in blue, positively correlated pairs shown in red.

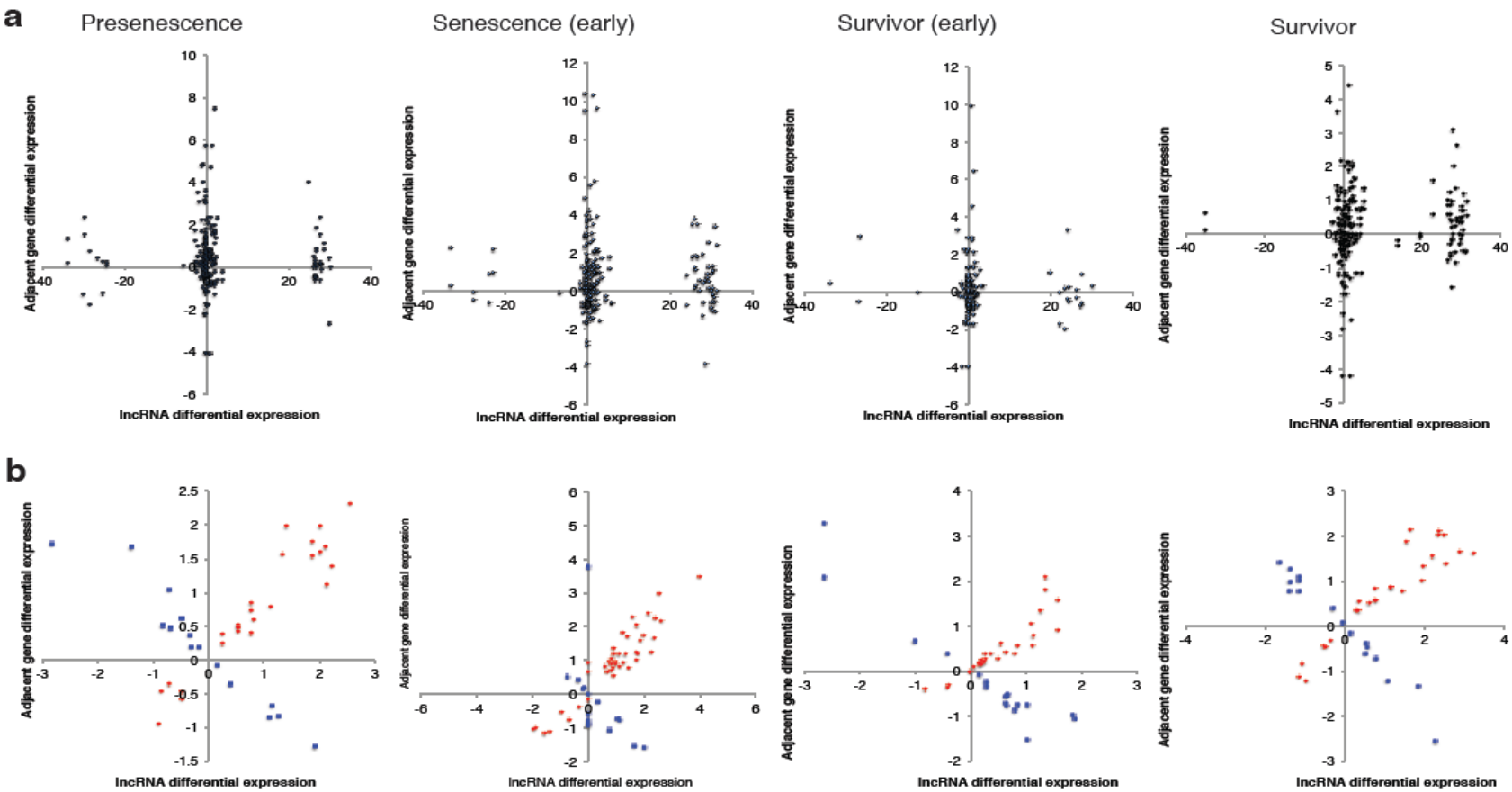
a
Presenescence
Senescence (early)
Survivor (early)
Survivor
Adjacent gene differential expression
lncRNA differential expression
b
Adjacent gene differential expression
lncRNA differential expression

Table 0-2. Percent difference in the value of observed vs. expected correlated genes.

5 independent random datasets were generated using the maximum and minimum observed differential expression values as limits. The described correlation analysis was performed on each generated dataset. The number of negatively or positively correlated values in each random dataset was averaged to generate the number of values “expected” by random chance. Percent difference in the value of observed vs. expected correlated genes ($p < 0.001$). Expected values calculated using a randomly generated dataset. P value calculated using Chi-squared test.

	Presenescence	Senescece (early)	Senescece (late)	Survivor (early)	Survivor
negatively correlated	-31	4	-50	-18	-22
postively correlated	38	11	55	38	50

3.3.6 Genes showing correlated expression with adjacent lncRNA are enriched for membrane proteins

To further explore the potential relevance of the lncRNAs I tested if the correlated lncRNAs could be regulating genes with related functions. I analyzed the gene list using the Database for Annotation, Visualization and Integrated Discovery (DAVID) (Dennis, et al., 2003) functional annotation tool. I found a

strong enrichment for extracellular and membrane proteins in most time points (Figure 3-6b). These groups are also enriched among the differentially expressed genes more broadly (discussed in the next chapter) in every time point, suggesting lncRNAs may be contributing to the coordinated changes in expression of membrane and extracellular proteins in telomerase-negative cells.

3.4 Discussion

The close association of lncRNAs with both cancer and aging suggests they may also be involved in the cellular response to telomerase deletion and subsequent changes in telomere length. We have used RNA-seq to identify 112 putative novel lncRNAs in telomerase-negative yeast. The transcripts are unlikely to encode proteins and have a median length of 467 nt, which is well above the generally accepted 200-nt threshold for classification as a lncRNA. Most of the lncRNAs were upregulated in at least one time point in the telomerase-negative cells and, in fact, many were undetectable in wild-type cells, which may explain why they have not been observed previously. Previous approaches to identify novel lncRNAs have generally utilized RNA-degradation mutants to stabilize transcripts(Samanta, et al. 2006; van Dijk, et al., 2011; Wyers, et al., 2005). However, our work reveals that, despite extensive study, there are undiscovered lncRNAs in *S. cerevisiae* that may become expressed as part of cellular

responses to specific conditions, such as loss of telomerase and dysfunctional telomeres.

It is currently unclear what the functional role of these lncRNAs is or even if these RNA molecules themselves are important, as opposed to transcriptional activity at their gene locations. Transcription of the ncRNAs *SRG1* and *IME4* is sufficient to mediate silencing of nearby genes via an interference mechanism(Martens, et al., 2004). Alternatively, a noncoding RNA generated from the telomeric repeats, TERRA, has been shown to interact with the yeast telomerase RNA, and may facilitate recruitment of telomerase to critically short telomeres (Cusanelli, et al., 2013). Given the number of novel transcripts, we believe it is most likely that the lncRNAs are modulating the expression of genes involved in the adaptive response to telomerase deletion. We find many of the lncRNAs are strongly correlated with the expression of adjacent genes, suggesting they act as cis-regulatory elements. Further testing will be required to fully elucidate the exact mechanism of action.

The genes showing correlated expression with a neighboring lncRNA are strongly enriched for both extracellular and membrane proteins (Fig. 5c). It has previously been reported that telomerase-negative cells undergo mitochondrial proliferation (Nautiyal, et al. 2002; Xie, et al. 2015) and may require changes in expression of membrane proteins as a result. Also, approximately half of the membrane and extracellular proteins are present at the telomere or subtelomere. Silencing at the subtelomere decreases as telomeres shorten(Buck, et al., 1995;

Kyrion, et al., 1993), suggesting a potential link between telomere length and expression of novel lncRNAs from the subtelomeric DNA. Since these lncRNAs also show correlated expression with neighboring genes, it could indicate a programmed expression pathway that is initiated only when most telomeres are critically short, potentially mediated by Rap1 loss from subtelomeres during senescence (Platt, et al., 2013). Additionally, since these functional groups are enriched at every stage, this may represent an additional feature of the previously described telomerase-deletion response (Nautiyal, et al. 2002). The correlated genes involved in cell-wall maintenance overlap somewhat with genes regulated by MUTs in meiotic cells (Lardenois, et al. 2011), which may indicate some similarities between the telomerase-deletion response and the meiotic program in yeast.

Some of the lncRNAs we observe at the subtelomere may overlap or behave similarly to those described previously in cells deficient for nonsense-mediated decay (NMD)(Toesca, et al. 2011), referred to as Cytoplasmically Degraded Cryptic Unstable Transcripts (CD-CUTs). In particular, we see increased transcription 5′ of the zinc transporter, Zrt1. However we do not observe any changes in expression of the major components of the NMD pathway, suggesting the expression and stabilization of these transcripts may be the result of a parallel pathway in telomerase-negative cells. One possible explanation is that transcription at this locus is promoted in part by shortened telomeres. Cells lacking the central NMD component Upf1 do exhibit shortened

telomeres in addition to NMD defects (Askree, et al., 2004; Gatbonton, et al., 2006).

Interestingly, the most differently expressed lncRNAs did not show any correlation with neighboring genes that might be expected either due to cis-regulation or spurious transcription. Thus, this group represents the lncRNAs most likely to act functionally as RNAs with targets elsewhere in the cell. Further studies will be required to determine the function of this relatively small (<20 transcripts) group of lncRNAs, potentially beginning with localization studies to determine whether they remain in the nucleus or are exported to the cytoplasm.

Our analysis adds to the growing body of evidence that pervasive transcription of ncRNAs in yeast is an important component in the ability of the cell to adapt to both internal and external changes. In this case, telomerase-deletion initiates a series of adaptive changes from cell-cycle arrest to initiation of alternative methods of telomere lengthening and we observe changes in lncRNA expression at each of these stages.

Defining the distinct transcriptional response to short-telomere induced senescence

4.1 Senescence and quiescence in yeast

In the absence of function telomerase cells experience progressive telomere shortening and eventually experience a specific cell-cycle arrest, known as senescence. However, senescence is somewhat unique as it is not experienced as a uniform arrest (Xie, et al. 2015), and is instead characterized by transient activation of DNA damage checkpoints for variable amounts of time. Consequently, it is likely distinct from other quiescent or arrested states in ways that are poorly characterized.

In the previous chapter I discussed the identification of novel lncRNAs, many of which are only expressed in telomerase-negative yeast. These lncRNAs represent only a small portion of the transcriptional response to telomerase deletion. Previous studies have examined the global expression response to shortening telomeres (Greenall, et al. 2008; Mandell, et al. 2005; Nautiyal, et al. 2002), however the lack of a consensus from these analyses have made any kind of definitive description of altered gene expression during senescence difficult.

Part of this difficulty arises from the similarities between senescence and other quiescent-like states. For example, during senescence cells exhibit a substantially slowed growth rate. Many genes in yeast show growth-rate dependent expression (Airoldi, et al., 2009; Brauer, et al., 2008) so many features of senescence may, in fact, be byproducts of this slow growth rate.

Similarly, the transient activation of DNA damage checkpoints likely initiates a transcriptional response that largely overlaps with the DNA damage signature, rather than being specific to senescence.

In this chapter, I define the distinct transcriptional response to senescence using RNA-seq to monitor gene expression changes during and after senescence. I then subsequently compared my findings with well characterized transcriptomes from other quiescent-like states including G2/M arrest, DNA damage response and slow growth cells. I find that the senescence state is largely characterized by an increase the expression of putative proteins, suggesting these proteins may play an important role only during this specific condition. Additionally, senescence includes widespread metabolic reprogramming, including a decrease in glucose uptake and increase in autophagy. Likely, these features of senescence promote survival until a means to lengthen telomeres can be restored.

4.2 Materials and methods

4.2.1 Generation of telomerase negative yeast

Strains were generated and characterized as described in chapter 3.

4.2.2 RNA isolation

RNA isolation was carried out using hot-phenol method, as previously described (Kohrer, et al. 1991).

4.2.3 Library preparation and RNA sequencing

Library preparation and sequencing were performed as previously described.

4.2.4 Data analysis

Differentially expressed genes were identified using the edgeR package (Robinson, et al., 2010) with the Benjamini and Hochberg algorithm to control the false discover rate and $p < 0.05$. Heatmaps were generated as described in chapter 3.

4.2.5 Glucose uptake assays

Glucose levels were measured in the media before and after yeast growth as an indirect measure of glucose uptake. I measured glucose using the glucose GO assay kit from Sigma (cat# GAGO20-1KT). I then normalized the consumed glucose to the number of doublings resulting in “grams of glucose consumed per doubling.”

4.2.6 Stress resistance assays

Cells were resuspended in YPAD media to A_{600} = 1.0 prior to treatment. For the heat shock treatment, cells were incubated at 45°C or 30°C for five minutes prior to plating. Equal numbers of cells from each condition were plated onto YPAD media and colonies were allowed to form. Relative growth was determined by comparing the number of colonies resulting from the heat shock to those that were maintained at 30°C. Oxidative stress resistance was determined in the same manner, except the cells were treated with either 1 mM H_2O_2 or water for 45 minutes prior to plating.

To determine changes in cell wall integrity cells were resuspended in phosphate buffer prior to treatment with 10 U zymolyase or water for 30 minutes. A_{600} readings were then taken. Comparison of the zymolyase-treated cells to the no treatment control resulted in relative zymolyase resistance.

4.2.7 Cell death staining

An aliquot of each culture was resuspended in a solution containing 0.1 mg/mL propidium iodide (Sigma cat# 81845). A minimum of 100 cells were counted to obtain percent death.

4.2.8 Monitoring GFP-ATG8 localization

Autophagy measurements were carried out as previously described (Welter, et al., 2010).

4.3 Results

4.3.1 Transcriptional response to telomerase deletion

To characterize the transcriptional response to telomerase deletion we generated and characterized a strain lacking the telomerase RNA component (TLC1) as previously described in chapter 3. RNA was isolated from five time points representing (1) presenescence, (2) senescence (early), (3) senescence (late), (4) survivor (early) and (5) survivor samples. Total RNA was isolated, ribosomal RNA was depleted and the samples were sequenced. Differentially expressed genes were identified using the EdgeR package and read count data generated by our collaborator. The replicates showed good overall correlation, despite being harvested at different concentrations and the general heterogeneity of telomerase-negative cells (Xie, et al. 2015)(Figure4-1). 3525 genes were differentially expressed in at least one time point (Figure4-2a).

4.3.2 Many genes show phase-specific changes in gene expression

I was interested in examining any temporal differences in gene expression so I compared the differentially expressed genes from each time point. I identified

a group of 110 genes that are differentially expressed in every time point and belong to the general telomerase deletion response(Nautiyal, et al. 2002). Each time point has a characteristic set of genes that are only significantly differentially expressed during that phase (Figure 4-2b). Functional enrichment analysis using DAVID (Dennis, et al. 2003) revealed a variety of processes in the phase-specific responses (Figure 4-3). Interestingly, both the senescence and early survivor time points show enrichment for genes involved in response to temperature stimulus which is consistent with the previously described general stress response of senescent cells (Nautiyal, et al. 2002). The cells show surprisingly rapid changes in gene expression with little overlap otherwise, even between samples collected 12 hours apart.

Figure 4-1. Replicates show good agreement at every time point.

FPKM values for each biological replicate are plotted against one another. The time point is indicated on the left, cell type is above. The nutrient-matched WT samples are on the right.

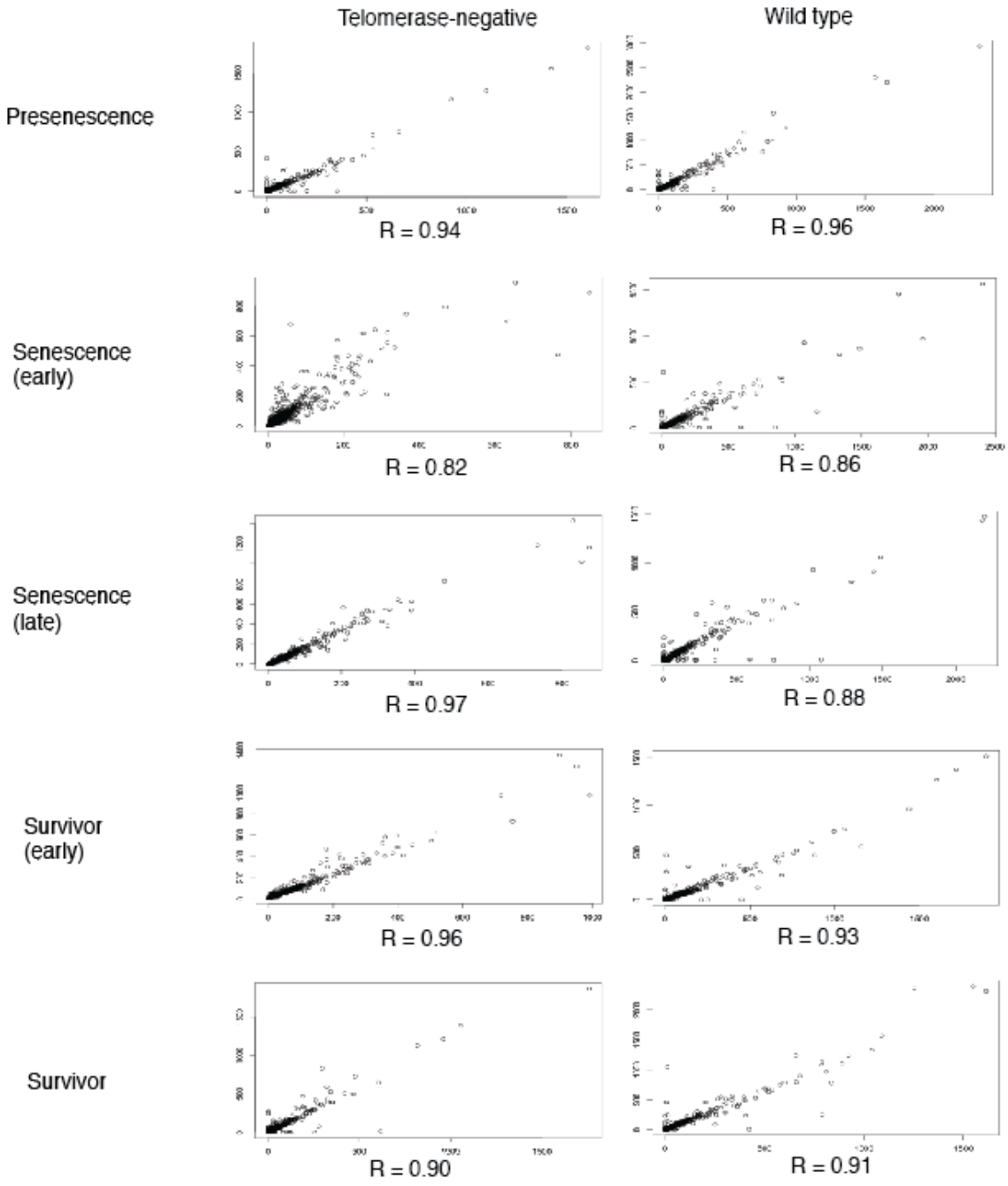

Figure 4-2. Telomerase-negative cells exhibit phase-specific differential expression.

(a) Many genes are differentially expressed in at least one time point. Volcano plot showing the log2(Fold change) in expression relative to wild type against the –log10(P Value). Points in the upper corners show the greatest differential expression with the highest significance. Colored points indicate a gene that was determined to be significantly differentially expressed ($P < 0.05$, fold change > 2). Colors correspond to different time points. Red = presenescence, orange = early senescence, yellow = late senescence, blue = early survivor and purple = survivor. (b) Many genes are differentially expressed in a phase-specific manner. Heat map showing genes that are significantly differentially expressed in only one time point. Any color indicates a change in expression of two-fold or more.

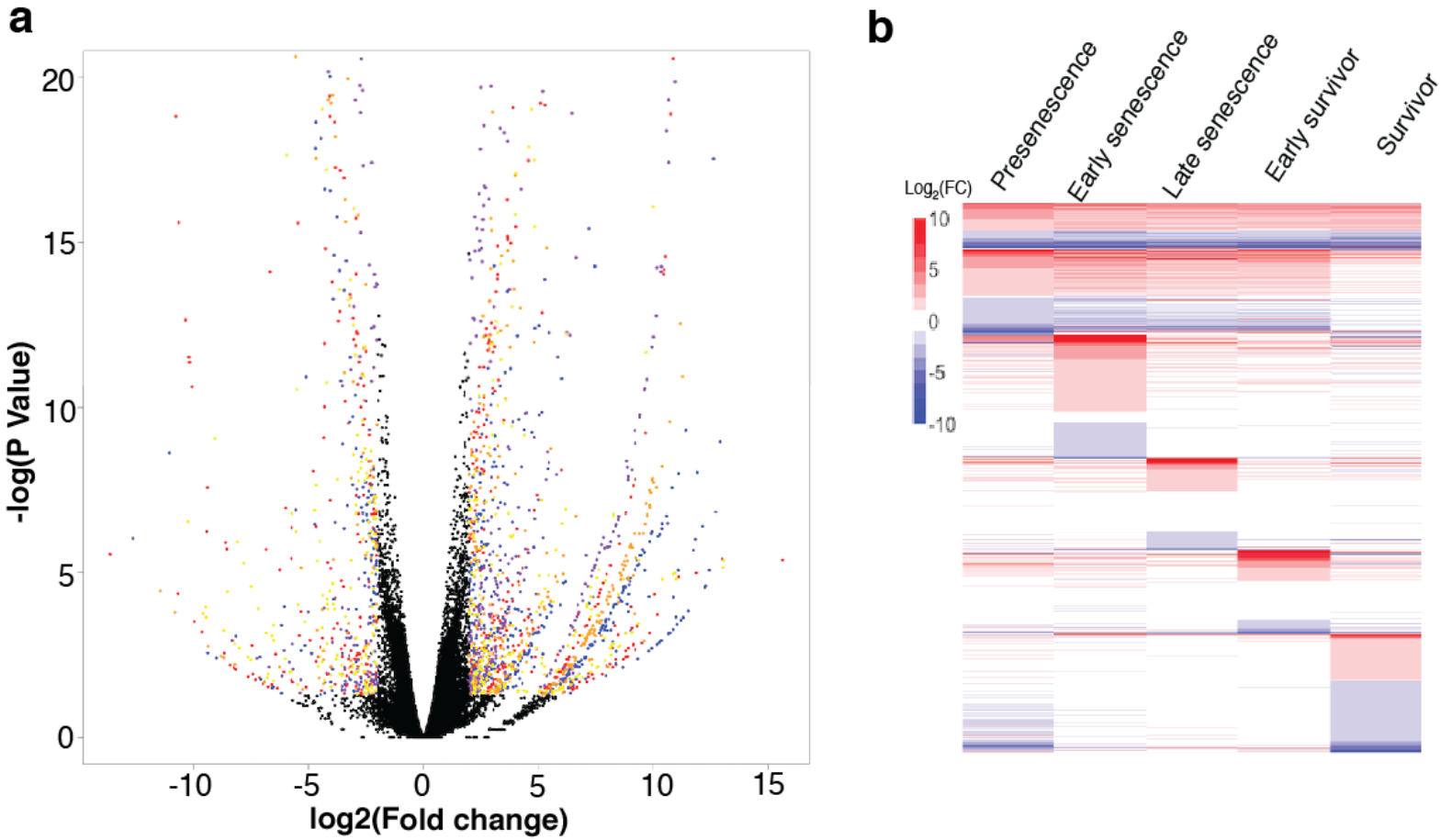
a
-log(P Value)
log2(Fold change)
20
15
10
5
0
-10
-5
0
5
10
15
b
Presenescence
Early senescence
Late senescence
Early survivor
Survivor
Log2(FC)
10
5
0
-5
-10

4.3.3 Telomerase-negative cells show decreased glucose uptake during senescence

Since genes involved in carbohydrate metabolism were enriched during senescence we were interested in investigating glucose sensing and uptake more closely. Closer examination of the changes in glucose monitoring and metabolism genes revealed changes in the expression of hexose transport machinery consistent with a starvation response. (Figure 4-4a). Since the cells were grown in abundant glucose we tested glucose uptake by monitoring the amount of glucose present before and after growth at each time point. The cells consume glucose at WT levels in the presenescent and survivor time points but show a significant decrease in glucose consumption during the senescence time points (Figure 4-4b). This provides a potential explanation for the observed transcriptional starvation response.

Figure 4-3. Functional enrichment analysis of phase-specific genes.

Genes showing phase-specific expression were submitted to DAVID for functional analysis. The top 5 categories are shown for each time point as well as for genes that are differentially expressed in every time point (All)

All
Presenescent
Senescence (early)
Senescence (late)
Survivor (early)
Survivor
tricarboxylic acid cycle
topological domain:Extracellular
Sulfur metabolism
ribosome biogenesis
Ribosome
ribosomal protein
response to temperature stimulus
regulation of translation
pyridoxal phosphate
nitrogen compound biosynthetic process
monosaccharide metabolic process
isopeptide bond
integral to plasma membrane
gpi-anchor
glycolysis
glutamine family amino acid metabolic process
glucose catabolic process
fungal-type cell wall
extracellular region
cytosolic ribosome
cross-link:Glycyl lysine isopeptide (Lys-Gly) (interchain with G-Cter in ubiquitin)
cellular amino acid biosynthetic process
cell wall
cell fraction
carbohydrate catabolic process
arginine biosynthetic process
amino-acid biosynthesis
amino acid transporter
PValue
0.005
0.004
0.003
0.002
0.001
0.000
percent
5
10
15
20

Figure 4-4. Senescing cells consume less glucose and initiate a starvation response.

(a) Genes involved in carbohydrate metabolism show altered expression during senescence. Heat map showing differential expression of genes involved in carbohydrate metabolism at every time point. Most genes are differentially expressed during early senescence in a pattern consistent with a starvation response. **(b) Senescing cells consume less glucose.** Glucose uptake per cell division over a 12 hour time course. Glucose consumption drops during senescent time points while being largely unaffected in presenescent and survivor time points.

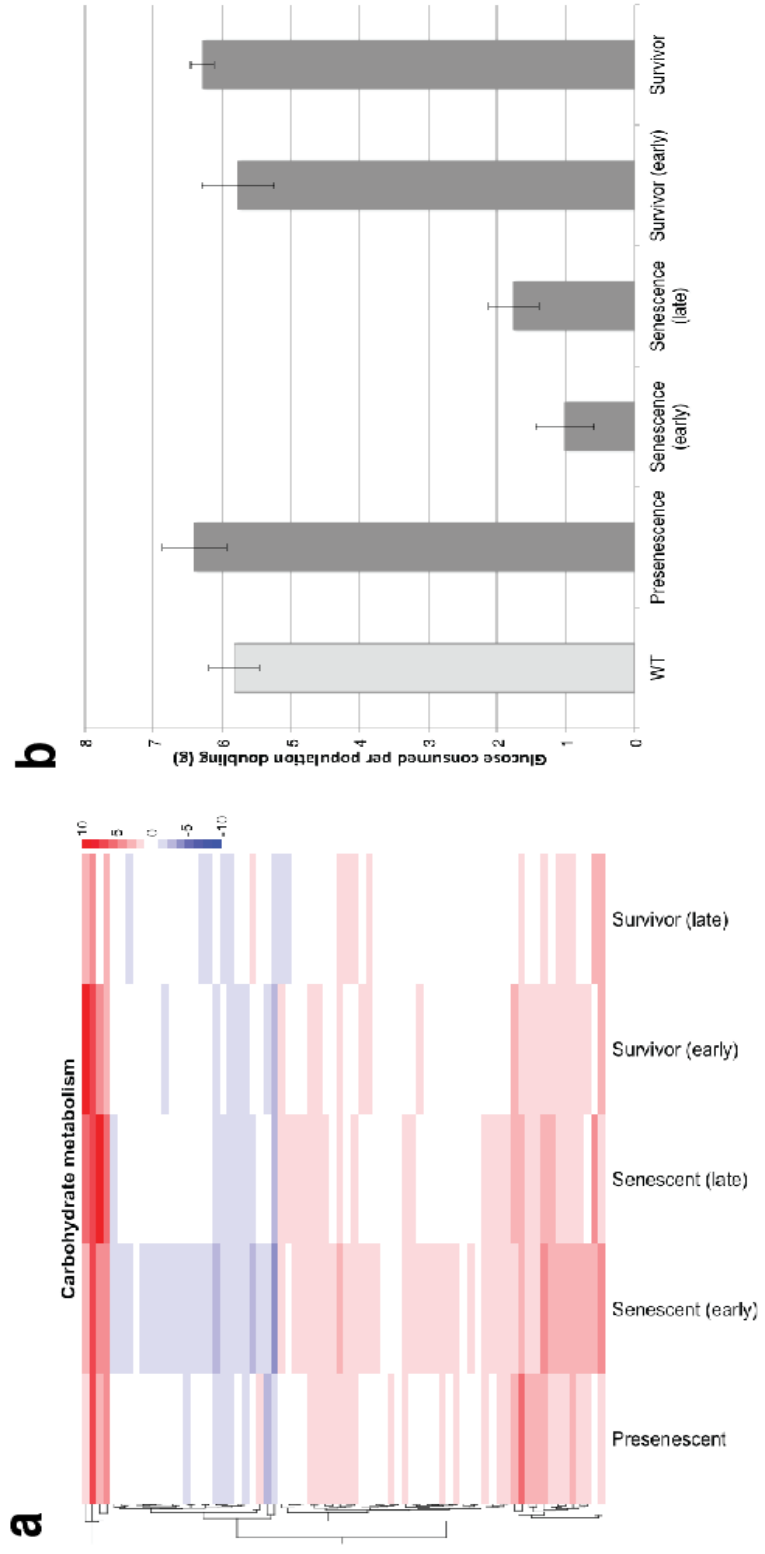
b
Glucose consumed per population doubling (g)
0
1
2
3
4
5
6
7
8
WT
Presenescence
Senescence (early)
Senescence (late)
Survivor (early)
Survivor
a
Carbohydrate metabolism
10
5
0
-5
-10
Survivor (late)
Survivor (early)
Senescent (late)
Senescent (early)
Presenescent

4.3.4 Upregulation of autophagy during short-telomere induced senescence

Since the senescing samples were not consuming glucose I examined the expression of autophagy genes as an alternative energy source. Approximately half of the genes involved in autophagy are upregulated during the early senescence time point (Figure 4-5a). Additionally, we qualitatively assayed autophagy by monitoring the localization of GFP-Atg8. Atg8 is the yeast homolog of human LC3 and is recruited to the phagophore assembly site (PAS) where it is incorporated into the autophagosome and transported to the vacuole (ref). Here, GFP-Atg8 is degraded; since GFP is resistant to degradation within the vacuole autophagy can be monitored by measuring the levels of free GFP (Welter, et al. 2010). We observe increased GFP localization to the vacuole during senescence, consistent with an increase in autophagy (Figure 4-5b). Interestingly, I also observed a sharp increase in cell death during senescence (Figure 4-6) although it is currently unclear whether this represents a programmed response.

Figure 4-5. Telomerase-negative cells show increased autophagic activity.

(a) Differential expression of autophagy-related genes during senescence.

(b) Fluorescence microscopy analysis of GFP-ATG8 vacuolar delivery.

Strains were transformed with the plasmid pRS313-GFP-ATG8 and monitored throughout the senescence time course. WT in complete and SC-N media is shown. Images were taken on an Axiovert 200 LM inverted scope with a 100x objective and an FITC filter. Scale bar represents 5 μM.

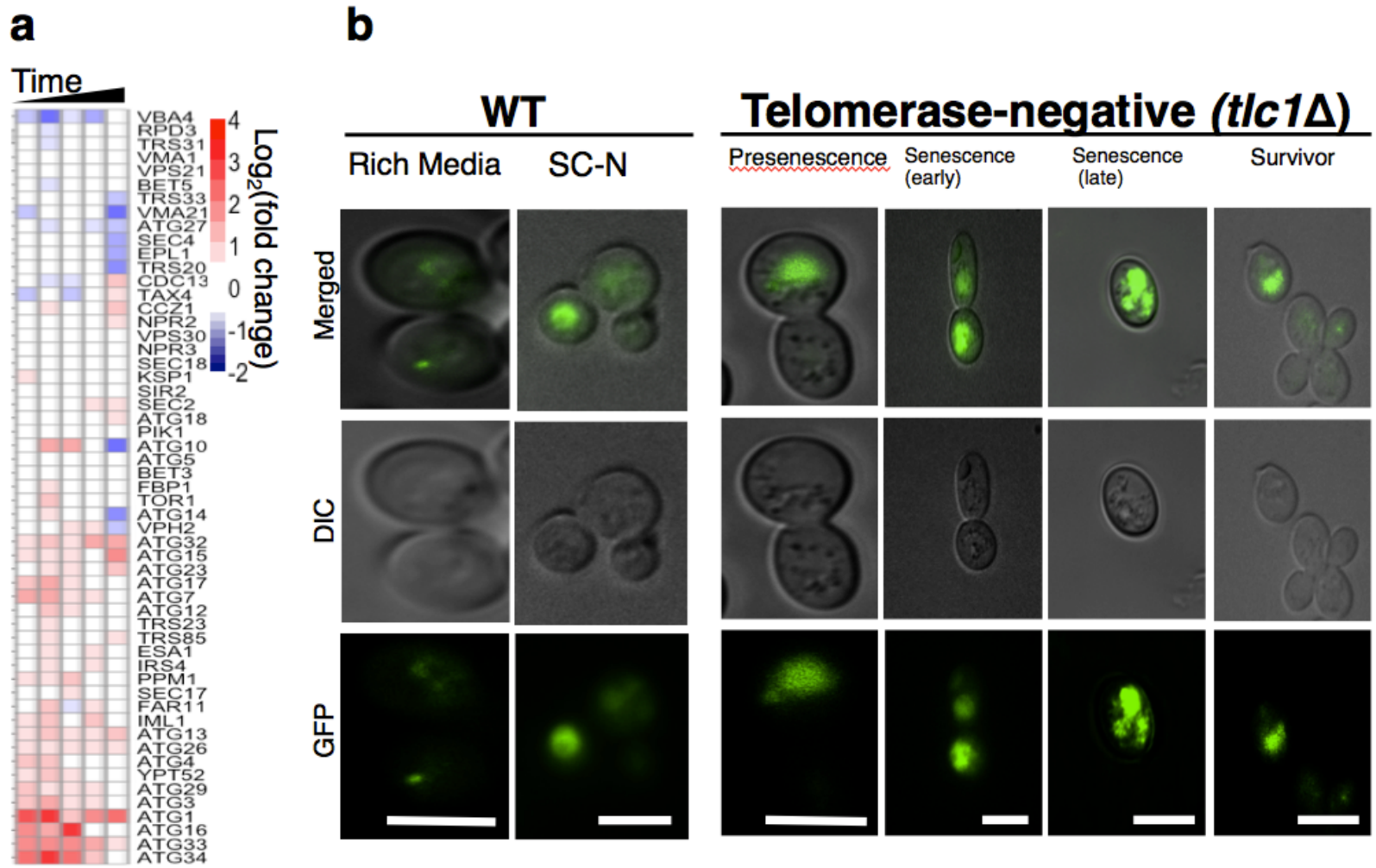
a
Time
VBA4
RPD3
TRS31
VMA1
VPS21
BET5
TRS33
VMA21
ATG27
SEC4
EPL1
TRS20
CDC13
TAX4
CCZ1
NPR2
VPS30
NPR3
SEC18
KSP1
SIR2
SEC2
ATG18
PIK1
ATG10
ATG5
BET3
FBP1
TOR1
ATG14
VPH2
ATG32
ATG15
ATG23
ATG17
ATG7
ATG12
TRS23
TRS85
ESA1
IRS4
PPM1
SEC17
FAR11
IML1
ATG13
ATG26
ATG4
YPT52
ATG29
ATG3
ATG1
ATG16
ATG33
ATG34
4
3
2
1
0
-1
-2
Log2(fold change)
b
WT
Telomerase-negative (tlc1Δ)
Rich Media
SC-N
Presenescence
Senescence (early)
Senescence (late)
Survivor
Merged
DIC
GFP

Figure 4-6. An increase in cell death during senescence.

Cell death, as measured by propidium iodide staining, peaks during senescence. A and B represent biological replicates.

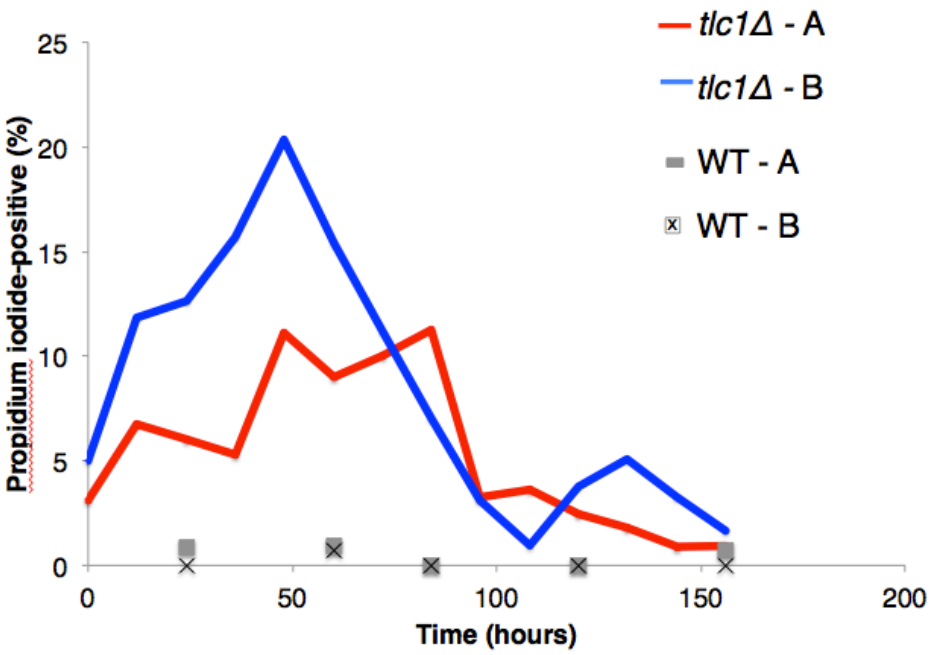

4.3.5 The transcriptional response to telomerase deletion overlaps with the response to slow growth

I wanted to identify any other conditions that might result in an increase in autophagy and a decrease in glucose uptake so I compared our transcriptional profile with previous studies. The transcriptional response of senescing cells overlaps substantially with cells slowly growing cells (Figure 4-7a), which also

show increased autophagy and a transcriptional response consistent with glucose starvation (Airoldi, et al. 2009; Brauer, et al. 2008).

Senescing cells have increased doubling time so this overlap is not surprising. So I was next interested in examining whether the senescent samples were phenotypically distinct from slowly growing cells. Low growth rate is correlated with increased resistance to a variety of stress conditions including heat shock, oxidative stress, and cell wall integrity (Klosinska, et al. 2011). I subjected the cells to each condition at every time point (Figure 4-8). Senescing cells showed increased resistance to both heat shock and cell wall stress, but were particularly sensitive to oxidative stress. This shows that despite substantial overlap with the response to slow growth, senescence is unique both transcriptionally and phenotypically. Previous studies have reported abnormal mitochondrial morphology in telomerase negative cells (Nautiyal, et al. 2002) but mutations in mitochondrial machinery do not appear to impact senescence or the senescence timeline. These data suggest mitochondrial function is compromised, and the cells may be relying on autophagy or fermentation rather than respiration.

4.3.6 The senescence response overlaps with DNA damage and G2/M arrest

Since the senescence response has been reported to also overlap with the DNA damage response and G2/M arrested cells we compared our results with previous studies examining these conditions. While the senescing cells did show significant overlap with each condition 572 genes were only differentially expressed during early senescence with 563 genes differentially expressed during late senescence, supporting the conclusion that senescence is a distinct quiescence-like state (Figure 4-7a). Interestingly, only 271 genes overlap between the two senescence time points (Figure 4-7d) and the majority of the common genes are dubious ORFs or Ty elements.

Figure 4-7. Senescence is a distinct transcriptional state.

(a) The transcriptional response to senescence overlaps with other stress-induced or quiescent states while having its own distinct signature. Comparison of differentially expressed genes in short-telomere induced senescence, G2/M arrested cells (Spellman, et al. 1998), starvation-induced quiescence (Klosinska, et al. 2011), slow growth (Airoldi, et al. 2009; Brauer, et al. 2008), and DNA damage (Fry, et al. 2006; Gasch, et al. 2001). The early senescence time point is shown. Despite some overlap with other conditions senescence has a distinct transcriptional signature, which includes 572 genes. **(b) Most of the uniquely differentially expressed genes in senescence are putative proteins**. Comparison of the top groups of differentially expressed genes within the 572 senescence-specific gene signature. Approximately 40% are dubious/putative ORFs (blue) with the next highest groups corresponding to sexual reproduction (red) and transcription regulation (purple). All other groups (yellow) comprised <5% of the total list. **(c) Genes involved in sexual reproduction are enriched in the senescence-state.** Functional enrichment analysis of the senescence-specific genes using DAVID (Dennis, et al. 2003). Groups are ordered according to significance based on P value. **(d) Comparison of early- and late-senescence specific genes.** Approximately half of the genes overlap between these two time points. Functional enrichment analysis of the unique early senescence, common, and unique late senescence genes **(e,f,g respectively)** revealed that sexual reproduction is overrepresented in both time

points suggesting this is likely an important feature of short-telomere induced senescence.

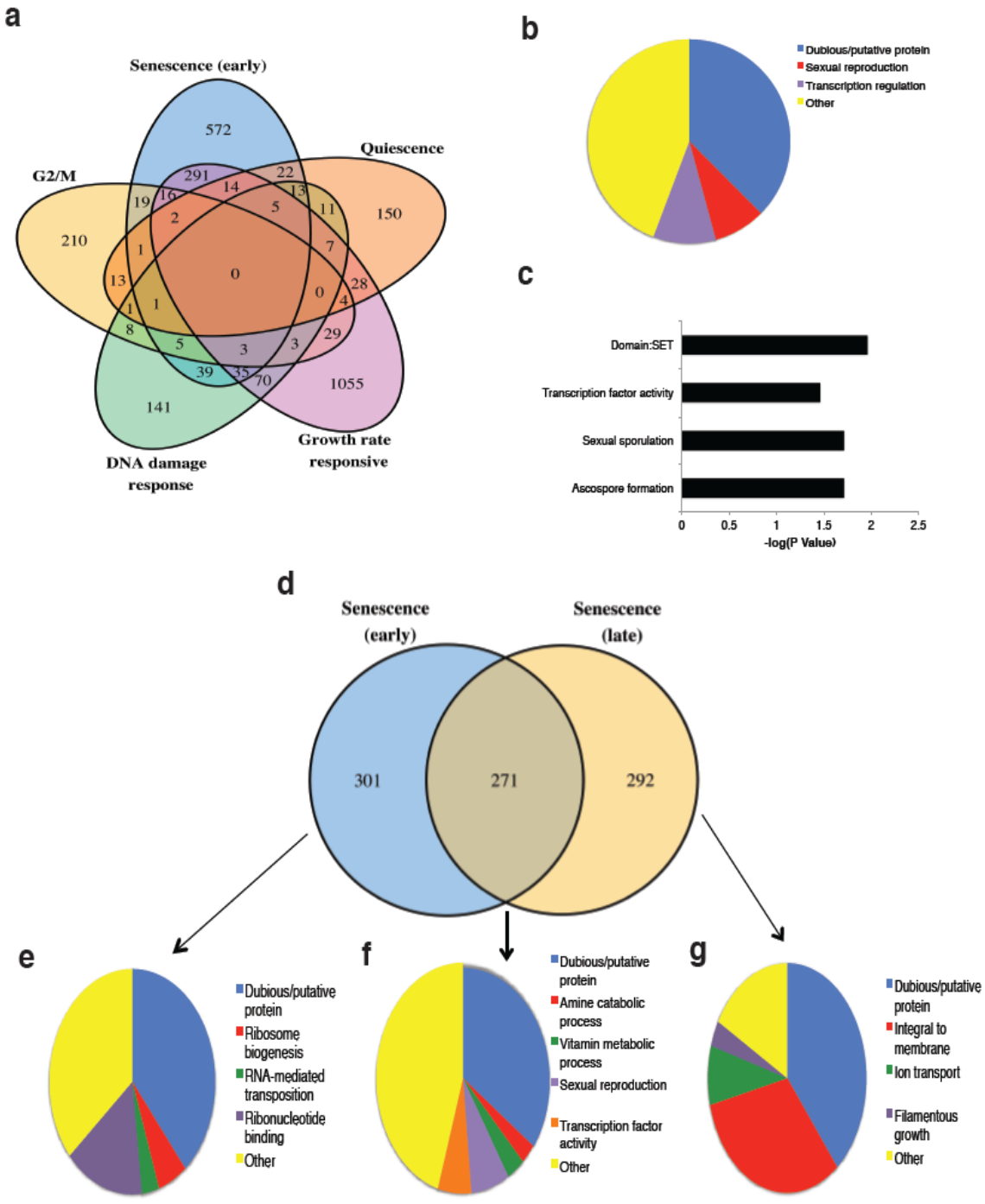

Figure 4-8. Senescence is phenotypically distinct from other quiescent states.

(a) Telomerase-negative cells show increased resistance to zymolyase treatment. Cells were treated with either 0 or 20 units of zymolyase for one hour at 30°C followed by an absorbance measurement (A_{600}). Telomerase-negative cells were assayed in biological triplicate every 12 hours, time-points corresponding to specific phases are shown. Standard deviations are shown. Telomerase-negative cells are more resistant to zymolyase treatment than WT at every time point, with maximum resistance coinciding with senescence. **(b) Telomerase-negative cells are more resistant to heat shock.** Cells were incubated at either 30°C or 45°C for 5 minutes prior to plating for single colonies. Resistance to heat shock was determined based on the growth relative to the 30°C culture. Cells were assayed in biological triplicate, standard deviation shown. **(c) Telomerase-negative cells are sensitive to oxidative stress.** Cells were treated with either 0 or 1mM H_2O_2 for one hour at 30°C followed by plating for single colonies on YPAD media. Sensitivity to oxidative stress was determined using the growth relative to the no treatment control sample. Biological triplicates tested, standard deviations shown.

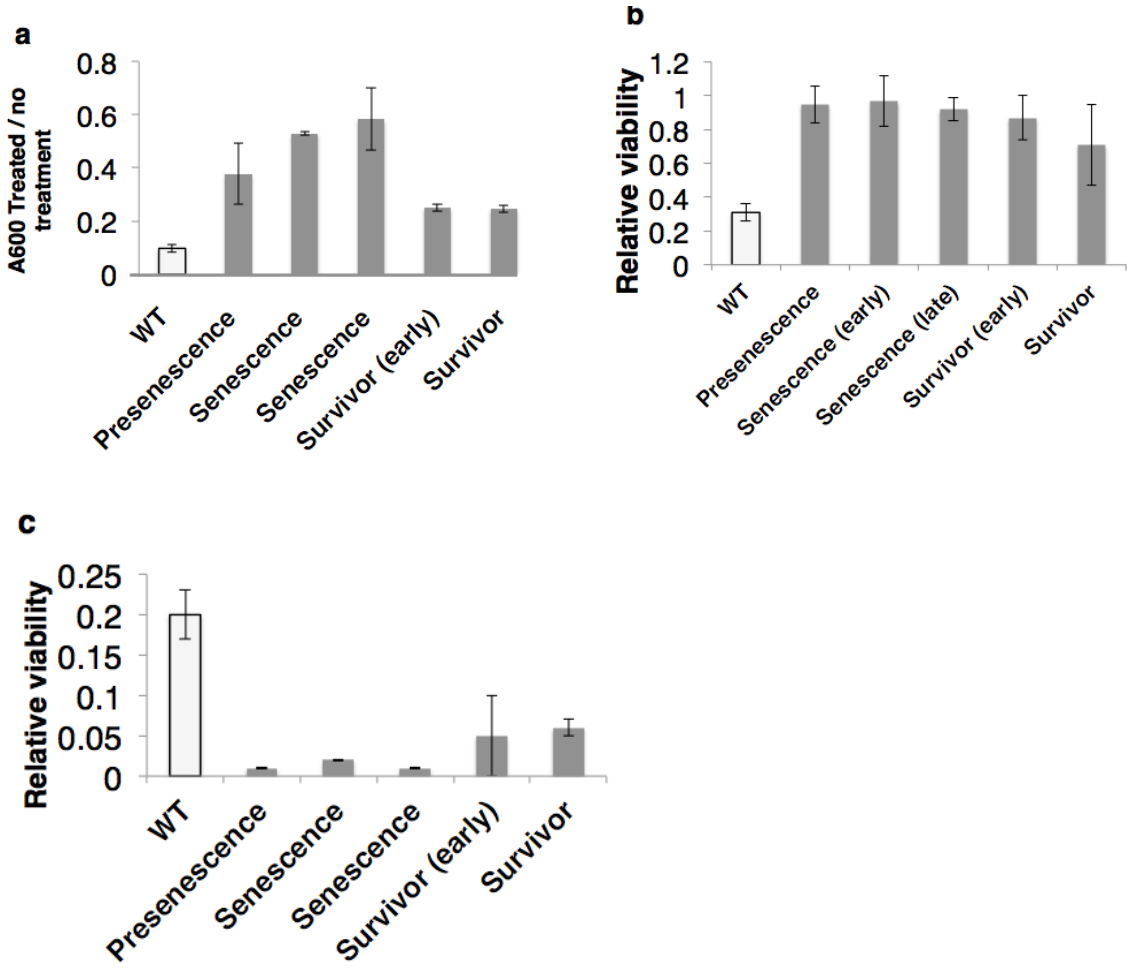

4.3.6 The transcriptional response of senescing cells is dominated by dubious or putative ORFs

I next wanted to characterize the unique transcriptional state of senescing cells so I performed a functional enrichment analysis of the genes only differentially expressed in the senescing cells (Figure 4-7e,f,g). Almost 40% of the differentially expressed genes were either dubious ORFs or putative proteins with unknown functions (Figure 4-7b). This was also true in the late senescent

time point (Figure 4-7d). This could reflect a general increase in transcription in senescing cells or simply further highlight how little is known about the response to telomerase deletion. The other time points also show enrichment for dubious ORFs although to a lesser extent than the senescing time points (~25%). Genes involved in sexual reproduction and meiosis comprised the next most significant category, and were enriched in both the early and late senescent time points (Fig 4-7b,f). This suggests there is some overlap between meiotic reprogramming and senescence.

4.3.7 Translational machinery shows evidence of co-regulated expression

To identify any coordinated changes in gene expression in response to telomerase deletion I calculated the Pearson correlation coefficient for each pair of genes and then performed hierarchical clustering (Figure 4-9). Clustering revealed two groups with strong positive correlation (1) ribosomal proteins, tRNAs and mitochondrial components and (2) Ribosome biogenesis, rRNA processing and proteins involved in polarized growth. The two groups are anticorrelated with one another, which is somewhat surprising since ribosomal proteins appear in a separate group from ribosome biogenesis factors.

Figure 4-9. Ribosomal proteins show anticorrelated expression from ribosomal processing machinery.

Pearson correlation coefficients were calculated between each gene pair and the resulting matrix was used for k-means clustering analysis. The clustered matrix is shown as a heat map with red corresponding to positive correlation in expression and blue indicating anticorrelation. Functional enrichment analysis of the two largest clusters (indicated by a red and blue line on the left) revealed anticorrelated expression between ribosomal proteins, tRNAs (red) and ribosomal biogenesis and processing machinery (blue).

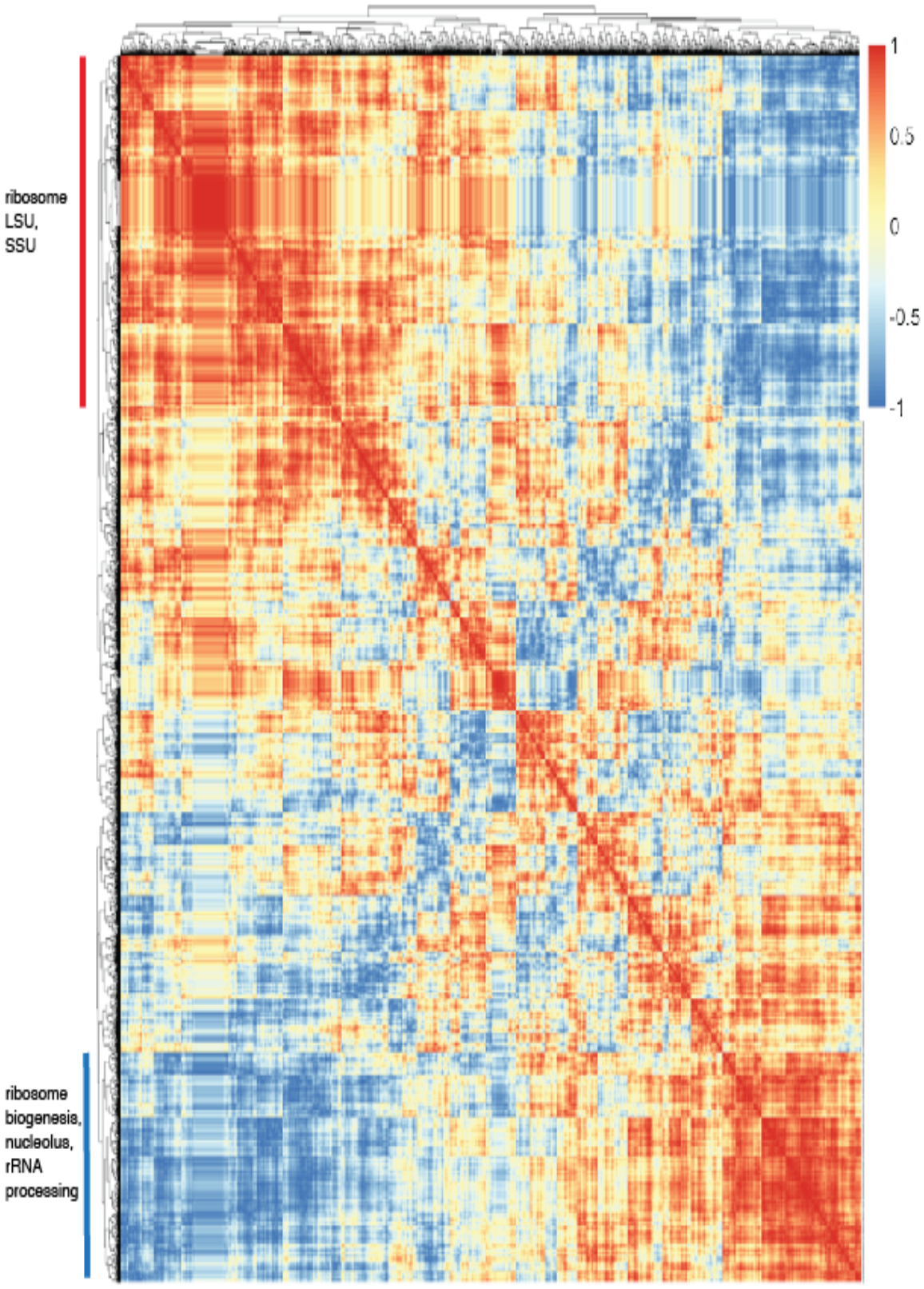
ribosome
LSU,
SSU
ribosome
biogenesis,
nucleolus,
rRNA
processing
1
0.5
0
-0.5
-1

4.4 Discussion

Short-telomere induced senescence shares many features both transcriptionally and phenotypically with previously described stress-states in yeast, such as DNA damage, heat stress and glucose starvation. Previous work identified a telomerase-deletion response that was separable from other stress responses (Nautiyal, et al. 2002), in this chapter I described work that has further refined this signature specifically to the state of senescence. The senescence-state is characterized by a marked decrease in glucose consumption in addition to an increase in resistance to zymolyase treatment. Interestingly, while slow-growing cells are generally more resistant to zymolyase treatment glucose-starved cells are surprisingly sensitive to this stress (Klosinska, et al. 2011). This underscores my conclusion that senescence is a unique state, sharing features with other stress-response states while not completely overlapping with any.

The telomerase-negative cells showed remarkable sensitivity to oxidative stress at every time point tested, indicating compromised mitochondrial function is a feature of the general telomerase deletion response. Previous work has shown that starvation survival is correlated with resistance to oxidative stress (Petti, et al., 2011) so the increase in cell death during senescence may be attributable in part to compromised mitochondrial function. Morphologically the mitochondria in senescing cells have been shown to appear fragmented (Nautiyal, et al. 2002) as though the fusion-fission balance has shifted towards

fission. This is consistent with mitochondrial behavior during times of stress, and could explain the extreme sensitivity of telomerase-negative cells to oxidative stress.

The anti-correlated expression of ribosomal proteins and ribosome biogenesis machinery may be an additional unique feature of telomerase-negative cells. Interestingly, most ribosomal genes are downregulated in presenescent, early senescent and survivor cells while the specific subset of positively correlated translation machinery is upregulated during both senescence time points (Figure 4-8). Previous studies in yeast have shown that translational machinery undergoes alternative targeting during starvation through an as-yet undetermined mechanism. The differing patterns of expression between ribosomal modification and processing machinery and the components themselves could be due to apparent specialization of ribosomes under these conditions, where a both composition and modification status are altered.

A previous study using a similar experimental design but monitoring differential expression by microarray also identified changes in ribosome and mitochondrial biogenesis gene expression (Nautiyal, et al. 2002). Our analysis results in an overlap with half of the genes previously identified during senescence (Figure 4-10), although we identify a larger total amount of differentially expressed genes. Potentially this is due to the greater statistical power of RNA-seq relative to microarray for low and high expression genes. Alternatively, given the large percentage of dubious ORFs that are differentially

expressed it is also possible that early microarrays weren't as well suited to examining the expression of poorly characterized genes.

Figure 4-10. Comparison of differentially expressed genes identifed during senescence in two independent studies.

(a) Venn diagram comparison of differentially expressed genes. Differentially expressed genes identified in the early senescence time point from this study (left) and differentially expressed genes identified from the equivalent time point (as determined by telomere Southern blot) in the Nautiyal et al. study. shown **(b) Functional enrichment analysis of common genes identified in both studies as determined by DAVID**. Groups are ordered by significance and are enriched for stress response and mitochondrial proteins.

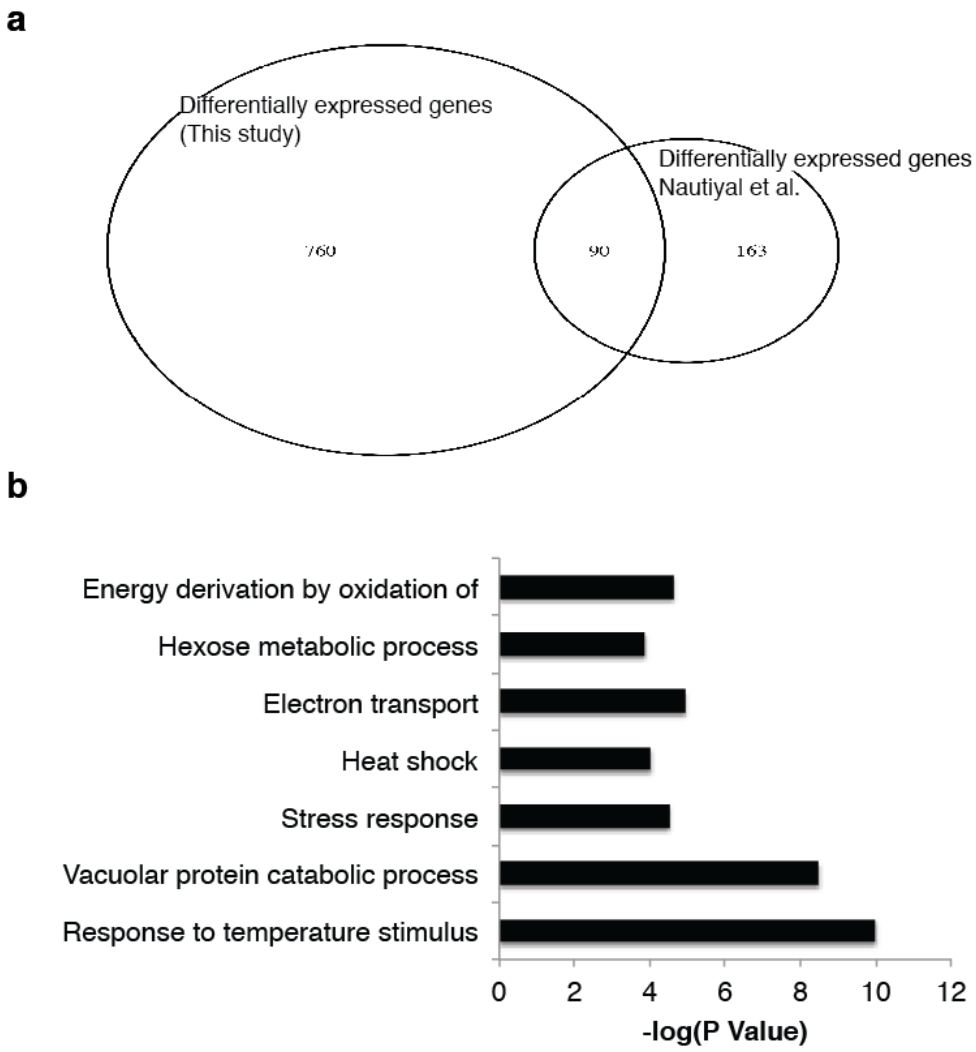

The transcriptional response to short-telomere induced senescence is predominantly characterized by changes in the expression of dubious ORFs. This could point to some undiscovered functions for the dubious ORFs, but may be more likely the result of broadly increased transcription in telomerase negative cells. In the previous chapter I described my identification of novel lncRNAs in telomerase-negative cells and noted a concurrent general increase in transcription. Increased transcription has been noted during meiosis as well as in the absence of RNA processing machinery such as exosome or nonsense

mediated decay components. Additionally, I noted a putative overlap between noncoding RNAs expressed during meiosis and the lncRNAs expressed in telomerase-negative cells. We also observe a functional enrichment of meiosis-related protein coding genes in senescing cells further strengthening the connection between these two conditions. Potentially the functional glucose starvation is enough to induce expression of the meiosis machinery in telomerase-negative cells, but it could also indicate a functional overlap between the processes. For example, it is interesting to speculate that expression of meiotic recombination machinery could prime survivor formation in yeast. Similarly, appropriate expression of meiotic proteins has been speculated to require downregulation of ribosomal proteins (Munding, et al., 2013) due to competition for splicing machinery. We do observe altered expression of both ribosomal proteins and ribosome modification components suggesting these processes may be occurring in senescing cells. This process could have been co-opted by cells as a survival strategy for dealing with life without telomerase.

5.1 Final conclusions

The telomerase RNP maintains the ends of linear chromosomes in most eukaryotes, protecting the ends from progressive shortening and thereby promoting genome integrity. Telomerase RNA plays a critical role in this process by not only providing the template for reverse transcription, but also by binding accessory proteins and likely coordinating catalysis within the core. Defects in either the folding or function of telomerase RNA are associated with a variety of diseases (Armanios 2009; Dokal, et al., 2008; Wong, et al., 2006). This is due to either a partial or complete loss of telomerase activity in the affected cells, which then have to respond and adapt to increasingly short telomeres resulting in either arrest, cell death or, in many cases, cancer (Blasco 2005).

My thesis focused on two aspects of telomerase biology: (1) the structure of telomerase RNA and its role in enzyme function and (2) the cellular response to telomerase dysfunction or absence.

5.1.1 The yeast and human TR cores do not require protein binding to adopt active conformations

In Chapter 2 I showed that unlike ciliate TR (Mihalusova, et al. 2011), both the human and yeast TR cores can adopt catalytically competent conformations

without TERT binding. SHAPE analysis suggests that both RNAs form a stable pseudoknot, a single-stranded template and the catalytically important base triples (Figures 2-2, 2-3). The human RNA requires slightly more Magnesium than the yeast, potentially due to more intricate tertiary interactions surrounding the hTR base triples. Alternatively, this could be the result of the different orientation or lack of a *bona fide* TBE in the human core.

I hypothesize that the reduced requirement for protein binding relative to the ciliate TR, is due to increased thermodynamic stability resulting from more extensive base-triples and larger pseudoknots. The ciliate pseudoknot is relatively small, with one stem only consisting of four base pairs (Cole, et al. 2012; Jiang, et al., 2013; Richards, et al. 2006; Theimer, et al., 2006). The ciliate RNA also binds more proteins in the core (Jiang, et al. 2013) than the larger TRs, potentially indicating a more intimate relationship between protein binding and RNA folding than is necessary in the larger RNAs.

Additionally, the ciliate RNA includes fewer base triples than either the yeast or human RNA. I have shown that the yeast RNA, in fact, forms an additional five base triples that had not appeared in previous models. This set of base triples is phylogenetically conserved, and likely adds substantial stability to the pseudoknot. They may also play a role in substrate positioning, as they are located adjacent to the catalytically important base-triples within stem 2 of the pseudoknot. My working model (shown in Figure 2-10) is that these triples interact with the CCC residues showing low SHAPE reactivity within the template.

This as yet uncharacterized interaction could position the template within the active site for nucleotide addition.

5.1.2 Human and yeast TR cores show a common SHAPE reactivity pattern

Structural conservation within the telomerase core suggests enzyme coordination within the core is also conserved (Lin, et al. 2004). However, without accurate secondary structure predictions it has been difficult to examine structure-function relationships in detail. Using SHAPE, I have shown that in addition to generally conserved structural elements the yeast and human TR cores also show common reactivity patterns. Notably, both cores show high reactivity between the pseudoknot and core-enclosing helix as well as 3' of the template. Additionally, both RNAs show low reactivity 5' of the template (Figure 2-10).

This observation has led to a model where the regions of high reactivity may serve as flexible “hinge points” allowing the substrate to move through the active site as telomerase adds nucleotides to the end of the substrate. The region of low reactivity 5' of the template would then serve as a fixed element to guide the template through the core. Taken together these regions would support the “accordion model” for template positioning, which was recently proposed based on FRET data in the ciliate TR (Berman, et al., 2011).

Alternatively, the less flexible nucleotides 5' of the template could play a role in template-boundary definition, which would be consistent with previous studies in hTR (Box, et al., 2008; Chen, et al. 2003). Disruption mutants in the TBE allow copying past the template by a few nucleotides, but do not completely abolish template definition (Seto, et al., 2003). This could be because of the additional boundary element provided by the low reactivity nucleotides. If this is the case I would expect that modulating physical flexibility in this region using nucleoside analogs would alter template boundary definition. Specifically, in the absence of the TBE I would expect increasing flexibility to reduce boundary definition while a decrease in flexibility should improve fidelity.

5.1.3 Reverse transcriptase-RNA interactions: unique features of telomerase

Among reverse transcriptases, TERT may be unique in its interactions with its RNA template. Specifically, in contrast to other reverse transcriptases like the HIV-1 RT, TERT only copies a small portion of the RNA template and must do so iteratively. Most viral reverse transcriptases must copy an RNA genome in its entirety, so the template boundary definition achieved by the telomerase enzyme is unnecessary.

However, TERT is structurally very similar to a viral reverse transcriptase (Gillis, et al., 2008). TERT is broadly organized into two subdomains, known as the fingers and palm domains. These subdomains are well known and also

commonly observed in RNA and DNA polymerases as well as retroviral reverse transcriptases. One notable difference is the TERT-specific IFD (Insertion in Fingers Domain) motif, which, as the name suggests, is located within the fingers domain (Lue, et al., 2003). However, this motif appears to be involved in processivity rather than template boundary definition.

With no obvious TERT domains that could be involved in template definition, the RNA is the most likely component to step into this role. While the TBD helix is clearly important in providing a steric block to end reverse transcription, it is unlikely that this alone is sufficient for boundary definition given that these kinds of short hairpins are probably common in viral RNA genomes without blocking reverse transcription. Indeed, as previously stated, when this helix is disrupted TERT is still only able to copy a few nucleotides past the end of the template (Seto, et al. 2003). Additionally, the TBE in human telomerase is located 8 nts away from the end of the template (Figure 2-7). Based on my SHAPE data I have suggested that the unreactive and therefore likely conformationally-constrained nts 5' of the template are contributing to template boundary definition. If this model is correct reducing flexibility 5' of any short hairpins in a viral RNA genome should prevent further copying. Consistent with this model, the majority of the short hairpins in the HIV-1 genome have unstructured and highly reactive nts 5' (Watts, et al., 2009).

5.1.4 Loss of telomerase results in metabolic reprogramming in yeast

Loss of telomerase results in increased genome instability due to progressive telomere shortening. Here I've shown that this state also results in widespread metabolic reprogramming including a decrease in glucose uptake and concurrent increase in autophagy (Figures 4-4, 4-5). The decrease in glucose consumption is particularly striking, as it was observed exclusively in the senescence time points (Figure 4-4). This likely represents a survival strategy for the arrested yeast. In previous studies under conditions where a particular amino acid was limiting, the rate of glucose consumption after biomass accumulation had ceased was correlated with survival (Boer, et al., 2008; Brauer, et al. 2008; Petti, et al. 2011). This could also provide an explanation for the marked increase in cell death observed during senescence (Figure 4-6), as the majority of the PI-positive cells appeared swollen. It's possible these cells somehow continued to consume glucose and gain biomass despite the cell cycle arrest and eventually died.

Currently it is unclear what initiates the decrease in glucose uptake, but the most likely candidate is the slow growth rate itself. Many of the starvation-associated glucose transporters, such as HXT5 (Verwaal, et al., 2002), are also induced by a decrease in growth rate. This is consistent with a model where the transient cell-cycle arrests associated with senescence manifest as slow growth,

which decreases glucose uptake, this, in turn, upregulates autophagy to maintain the energy requirements of the cell without increasing the biomass. Cells that are unable to initiate this starvation response, therefore, are unlikely to survive senescence.

5.1.5 Telomerase-negative cells are incredibly sensitive to oxidative stress

Consistent with induction of a general “survival” response, telomerase-negative cells upregulate many genes involved in environmental stress response and show increased resistance to both heat shock and cell wall digestion (Figure 4-8). However, unlike the other stress conditions, telomerase-negative cells showed increased sensitivity to oxidative stress (Figure 4-8). One potential explanation is that the cells may already have saturated levels of reactive oxygen species (ROS), due to alterations in cellular metabolism. However, a previous study found that ROS levels are not significantly altered in telomerase-negative cells, irrespective of telomere length (Xie, et al. 2015).

Another possibility is that mitochondrial function has been compromised. Yeast strains lacking mitochondrial function are also sensitive to oxidative stress (Grant, et al., 1997). In many ways this seems counterintuitive, as mitochondria are one of the major sources of ROS in the cell. However, it appears that the process of respiration may also induce the expression of many antioxidants, and

it is the loss of these components that render cells unable to withstand oxidative stress without functioning mitochondria. Interestingly, the Blackburn lab had previously noted gross abnormalities in mitochondrial morphology in telomerase-negative cells (Nautiyal, et al. 2002). Dysfunctional mitochondria would explain the low levels of ROS, the extreme sensitivity to oxidative stress as well as the shift away from growth and accumulation of biomass to quiescence. However, mitochondrial function has also been correlated with survival during nutrient deprivation (Petti, et al. 2011), so it is difficult to fully reconcile these observations.

Future studies examining mitochondrial function in more detail would help to fully elucidate the metabolic changes that occur during senescence. For example, mitochondrial function during senescence has yet to be directly measured. Additionally, it would be interesting to examine the senescence timeline for cells grown on non-fermentable carbon sources, which would force the cells to respire. If respiration is promoting survival during the induced starvation response, cells grown under this condition should show a decrease in cell death during this time. Conversely, if mitochondrial function is compromised or absent during this time we should observe little to no effect.

5.1.6 Induction of lncRNAs in telomerase-negative cells

In yeast, expression of specific lncRNAs has been associated with a variety of specific cell states, such as meiosis or growth in the absence of metal ions (Lardenois, et al. 2011; Toesca, et al. 2011); while in humans lncRNA expression has been associated with a variety of diseases from aging to cancer (Abdelmohsen, et al. 2013; Guil, et al. 2012; Yang, et al. 2014). In chapter 3, I used RNA-seq to identify 112 novel lncRNAs. I did not observe any changes in the expression of any components of the exosome, or termination machinery suggesting that these are stable transcripts not RNAs that have simply escaped degradation.

Of the 112, 40 are exclusively expressed in telomerase-negative cells. Like the lncRNAs expressed during meiosis, it is likely that these represent the programmed expression of specific lncRNAs in response to the lack of telomerase function. A subset of this group shows correlated expression with a neighboring gene, suggesting these lncRNAs may be cis-regulators of nearby gene expression (Figure 3-6, 3-7). Functional enrichment analysis of the correlated protein-coding genes revealed than many are involved in cell wall synthesis. This represents a potential link between the observed increase in resistance to cell wall digestion and expression of these lncRNAs.

The remaining lncRNAs did not show correlated expression with a neighboring gene and their current functions remain unknown. It will be

interesting to examine the sequence of these RNAs in more detail to try and identify any sequence motifs to predict protein binding. Some clues may also be found by examining the localization of these lncRNAs in more detail, do they remain in the nucleus or are they exported to the cytoplasm? Do they associate with other RNA partners or ribosomes? There are not many well-characterized lncRNAs in yeast so this represents an exciting area for future study.

References:

Abdelmohsen K, *et al.* 2013. Senescence-associated lncRNAs: senescence-associated long noncoding RNAs. *Aging Cell* **12**, 890-900

Airoldi EM, *et al.* 2009. Predicting cellular growth from gene expression signatures. *PLoS computational biology* **5**, e1000257

Antal M, *et al.* 2002. Analysis of the structure of human telomerase RNA in vivo. *Nucleic Acids Res* **30**, 912-20

Armanios M. 2009. Syndromes of telomere shortening. *Annu Rev Genomics Hum Genet* **10**, 45-61

Askree SH, *et al.* 2004. A genome-wide screen for Saccharomyces cerevisiae deletion mutants that affect telomere length. *Proc Natl Acad Sci U S A* **101**, 8658-63

Berman AJ, *et al.* 2011. The RNA accordion model for template positioning by telomerase RNA during telomeric DNA synthesis. *Nat Struct Mol Biol* **18**, 1371-5

Blasco MA. 2005. Telomeres and human disease: ageing, cancer and beyond. *Nat Rev Genet* **6**, 611-22

Boer VM, *et al.* 2008. Influence of genotype and nutrition on survival and metabolism of starving yeast. *Proc Natl Acad Sci U S A* **105**, 6930-5

Box JA, *et al.* 2008. A flexible template boundary element in the RNA subunit of fission yeast telomerase. *J Biol Chem* **283**, 24224-33

Brauer MJ, *et al.* 2008. Coordination of growth rate, cell cycle, stress response, and metabolic activity in yeast. *Mol Biol Cell* **19**, 352-67

Buck SW, *et al.* 1995. Action of a RAP1 carboxy-terminal silencing domain reveals an underlying competition between HMR and telomeres in yeast. *Genes Dev* **9**, 370-84

Campisi J. 2001. From cells to organisms: can we learn about aging from cells in culture? *Exp Gerontol* **36**, 607-18

Cash DD, *et al.* 2013. Pyrimidine motif triple helix in the Kluyveromyces lactis telomerase RNA pseudoknot is essential for function in vivo. *Proc Natl Acad Sci U S A* **110**, 10970-5

Cervantes RB, *et al.* 2002. Mechanisms of chromosome-end protection. *Current opinion in cell biology* **14**, 351-6

Chandra A, *et al.* 2001. Cdc13 both positively and negatively regulates telomere replication. *Genes Dev* **15**, 404-14

Chen JL, *et al.* 2000. Secondary structure of vertebrate telomerase RNA. *Cell* **100**, 503-14

Chen JL, *et al.* 2003. Template boundary definition in mammalian telomerase. *Genes Dev* **17**, 2747-52

Chen Q, *et al.* 2001. Two survivor pathways that allow growth in the absence of telomerase are generated by distinct telomere recombination events. *Mol Cell Biol* **21**, 1819-27

Chen Y, *et al.* 2006. Structure of stem-loop IV of Tetrahymena telomerase RNA. *EMBO J* **25**, 3156-66

Cole DI, *et al.* 2012. New models of Tetrahymena telomerase RNA from experimentally derived constraints and modeling. *J Am Chem Soc* **134**, 20070-80

Coller HA, *et al.* 2006. A new description of cellular quiescence. *PLoS Biol* **4**, e83

Cusanelli E, *et al.* 2013. Telomeric noncoding RNA TERRA is induced by telomere shortening to nucleate telomerase molecules at short telomeres. *Mol Cell* **51**, 780-91

Dandjinou AT, *et al.* 2004. A phylogenetically based secondary structure for the yeast telomerase RNA. *Curr Biol* **14**, 1148-58

Das R, *et al.* 2005. SAFA: semi-automated footprinting analysis software for high-throughput quantification of nucleic acid footprinting experiments. *RNA* **11**, 344-54

Deigan KE, *et al.* 2009. Accurate SHAPE-directed RNA structure determination. *Proc Natl Acad Sci U S A* **106**, 97-102

Dennis G, Jr., *et al.* 2003. DAVID: Database for Annotation, Visualization, and Integrated Discovery. *Genome Biol* **4**, P3

Diede SJ, *et al.* 1999. Telomerase-mediated telomere addition in vivo requires DNA primase and DNA polymerases alpha and delta. *Cell* **99**, 723-33

Dokal I. 2000. Dyskeratosis congenita in all its forms. *Br J Haematol* **110**, 768-79

Dokal I, *et al.* 2008. Inherited aplastic anaemias/bone marrow failure syndromes. *Blood Rev* **22**, 141-53

Fan X, *et al.* 1997. Coordinate regulation of G- and C strand length during new telomere synthesis. *Mol Biol Cell* **8**, 2145-55

Forstemann K, *et al.* 2005. Telomerase limits the extent of base pairing between template RNA and telomeric DNA. *EMBO Rep* **6**, 361-6

Fry RC, *et al.* 2006. The DNA-damage signature in Saccharomyces cerevisiae is associated with single-strand breaks in DNA. *BMC genomics* **7**, 313

Gasch AP, *et al.* 2001. Genomic expression responses to DNA-damaging agents and the regulatory role of the yeast ATR homolog Mec1p. *Mol Biol Cell* **12**, 2987-3003

Gatbonton T, *et al.* 2006. Telomere length as a quantitative trait: genome-wide survey and genetic mapping of telomere length-control genes in yeast. *PLoS Genet* **2**, e35

Gilley D, *et al.* 1999. The telomerase RNA pseudoknot is critical for the stable assembly of a catalytically active ribonucleoprotein. *Proc Natl Acad Sci U S A* **96**, 6621-5

Gillis AJ, *et al.* 2008. Structure of the Tribolium castaneum telomerase catalytic subunit TERT. *Nature* **455**, 633-7

Grant CM, *et al.* 1997. Mitochondrial function is required for resistance to oxidative stress in the yeast Saccharomyces cerevisiae. *FEBS Lett* **410**, 219-22

Gray JV, *et al.* 2004. "Sleeping beauty": quiescence in Saccharomyces cerevisiae. *Microbiology and molecular biology reviews : MMBR* **68**, 187-206

Greenall A, *et al.* 2008. A genome wide analysis of the response to uncapped telomeres in budding yeast reveals a novel role for the NAD+ biosynthetic gene BNA2 in chromosome end protection. *Genome Biol* **9**, R146

Guil S, *et al.* 2012. Cis-acting noncoding RNAs: friends and foes. *Nat Struct Mol Biol* **19**, 1068-75

Hengesbach M, *et al.* 2012. Single-molecule FRET reveals the folding dynamics of the human telomerase RNA pseudoknot domain. *Angew Chem Int Ed Engl* **51**, 5876-9

Jacquier A. 2009. The complex eukaryotic transcriptome: unexpected pervasive transcription and novel small RNAs. *Nat Rev Genet* **10**, 833-44

Jiang J, *et al.* 2013. The architecture of Tetrahymena telomerase holoenzyme. *Nature* **496**, 187-92

Kavanaugh LA, *et al.* 2009. Non-coding RNA prediction and verification in Saccharomyces cerevisiae. *PLoS Genet* **5**, e1000321

Kim NK, *et al.* 2010. Effect of pseudouridylation on the structure and activity of the catalytically essential P6.1 hairpin in human telomerase RNA. *Nucleic Acids Res* **38**, 6746-56

Kim NK, *et al.* 2014. Structure and sequence elements of the CR4/5 domain of medaka telomerase RNA important for telomerase function. *Nucleic Acids Res* **42**, 3395-408

Kim NK, *et al.* 2008. Solution structure and dynamics of the wild-type pseudoknot of human telomerase RNA. *J Mol Biol* **384**, 1249-61

Klosinska MM, *et al.* 2011. Yeast cells can access distinct quiescent states. *Genes Dev* **25**, 336-49

Kohrer K, *et al.* 1991. Preparation of high molecular weight RNA. *Methods in enzymology* **194**, 398-405

Kong L, *et al.* 2007. CPC: assess the protein-coding potential of transcripts using sequence features and support vector machine. *Nucleic Acids Res* **35**, W345-9

Kyrion G, *et al.* 1993. RAP1 and telomere structure regulate telomere position effects in Saccharomyces cerevisiae. *Genes Dev* **7**, 1146-59

Langmead B, *et al.* 2012. Fast gapped-read alignment with Bowtie 2. *Nature methods* **9**, 357-9

Lardenois A, *et al.* 2011. Execution of the meiotic noncoding RNA expression program and the onset of gametogenesis in yeast require the conserved exosome subunit Rrp6. *Proc Natl Acad Sci U S A* **108**, 1058-63

Lebo KJ, *et al.* 2015. A second essential function of the Est1-binding arm of yeast telomerase RNA. *RNA*,

Leeper T, *et al.* 2003. The solution structure of an essential stem-loop of human telomerase RNA. *Nucleic Acids Res* **31**, 2614-21

Leeper TC, *et al.* 2005. The structure of an enzyme-activating fragment of human telomerase RNA. *RNA* **11**, 394-403

Levy MZ, *et al.* 1992. Telomere end-replication problem and cell aging. *J Mol Biol* **225**, 951-60

Lin J, *et al.* 2004. A universal telomerase RNA core structure includes structured motifs required for binding the telomerase reverse transcriptase protein. *Proc Natl Acad Sci U S A* **101**, 14713-8

Liu F, *et al.* 2012. Thermodynamic characterization of the Saccharomyces cerevisiae telomerase RNA pseudoknot domain in vitro. *RNA* **18**, 973-91

Lue NF, *et al.* 2003. A conserved telomerase motif within the catalytic domain of telomerase reverse transcriptase is specifically required for repeat addition processivity. *Mol Cell Biol* **23**, 8440-9

Lundblad V, *et al.* 1993. An alternative pathway for yeast telomere maintenance rescues est1- senescence. *Cell* **73**, 347-60

Lundblad V, *et al.* 1989. A mutant with a defect in telomere elongation leads to senescence in yeast. *Cell* **57**, 633-43

Ly H, *et al.* 2003. Comprehensive structure-function analysis of the core domain of human telomerase RNA. *Mol Cell Biol* **23**, 6849-56

Mandell JG, *et al.* 2005. Global expression changes resulting from loss of telomeric DNA in fission yeast. *Genome Biol* **6**, R1

Martens JA, *et al.* 2004. Intergenic transcription is required to repress the Saccharomyces cerevisiae SER3 gene. *Nature* **429**, 571-4

Martin-Rivera L, *et al.* 2001. Identification of functional domains and dominant negative mutations in vertebrate telomerase RNA using an in vivo reconstitution system. *J Biol Chem* **276**, 5856-65

McClintock B. 1941. The Stability of Broken Ends of Chromosomes in Zea Mays. *Genetics* **26**, 234-82

Mefford MA, *et al.* 2013. RNA connectivity requirements between conserved elements in the core of the yeast telomerase RNP. *EMBO J* **32**, 2980-93

Merino EJ, *et al.* 2005. RNA structure analysis at single nucleotide resolution by selective 2'-hydroxyl acylation and primer extension (SHAPE). *J Am Chem Soc* **127**, 4223-31

Mihalusova M, *et al.* 2011. Functional importance of telomerase pseudoknot revealed by single-molecule analysis. *Proc Natl Acad Sci U S A* **108**, 20339-44

Mozdy AD, *et al.* 2006. Low abundance of telomerase in yeast: implications for telomerase haploinsufficiency. *RNA* **12**, 1721-37

Munding EM, *et al.* 2013. Competition between pre-mRNAs for the splicing machinery drives global regulation of splicing. *Mol Cell* **51**, 338-48

Nagalakshmi U, *et al.* 2008. The transcriptional landscape of the yeast genome defined by RNA sequencing. *Science* **320**, 1344-9

Nautiyal S, *et al.* 2002. The genome-wide expression response to telomerase deletion in Saccharomyces cerevisiae. *Proc Natl Acad Sci U S A* **99**, 9316-21

Petti AA, *et al.* 2011. Survival of starving yeast is correlated with oxidative stress response and nonrespiratory mitochondrial function. *Proc Natl Acad Sci U S A* **108**, E1089-98

Platt JM, *et al.* 2013. Rap1 relocalization contributes to the chromatin-mediated gene expression profile and pace of cell senescence. *Genes Dev* **27**, 1406-20

Prescott J, *et al.* 1997. Telomerase RNA mutations in Saccharomyces cerevisiae alter telomerase action and reveal nonprocessivity in vivo and in vitro. *Genes Dev* **11**, 528-40

Putnam CD, *et al.* 2009. Perspectives on the DNA damage and replication checkpoint responses in Saccharomyces cerevisiae. *DNA repair* **8**, 974-82

Qi H, *et al.* 2000. The Saccharomyces telomere-binding protein Cdc13p interacts with both the catalytic subunit of DNA polymerase alpha and the telomerase-associated est1 protein. *Genes Dev* **14**, 1777-88

Qiao F, *et al.* 2008. Triple-helix structure in telomerase RNA contributes to catalysis. *Nat Struct Mol Biol* **15**, 634-40

Ramakrishnan S, *et al.* 1997. Characterization of human telomerase complex. *Proc Natl Acad Sci U S A* **94**, 10075-9

Richards RJ, *et al.* 2006. Structure of the Tetrahymena thermophila telomerase RNA helix II template boundary element. *Nucleic Acids Res* **34**, 816-25

Richards RJ, *et al.* 2006. Structural study of elements of Tetrahymena telomerase RNA stem-loop IV domain important for function. *RNA* **12**, 1475-85

Roberts A, *et al.* 2011. Identification of novel transcripts in annotated genomes using RNA-Seq. *Bioinformatics* **27**, 2325-9

Robinson MD, *et al.* 2010. edgeR: a Bioconductor package for differential expression analysis of digital gene expression data. *Bioinformatics* **26**, 139-40

Samanta MP, *et al.* 2006. Global identification of noncoding RNAs in Saccharomyces cerevisiae by modulating an essential RNA processing pathway. *Proc Natl Acad Sci U S A* **103**, 4192-7

Seto AG, *et al.* 2002. A bulged stem tethers Est1p to telomerase RNA in budding yeast. *Genes Dev* **16**, 2800-12

Seto AG, *et al.* 2003. A template-proximal RNA paired element contributes to Saccharomyces cerevisiae telomerase activity. *RNA* **9**, 1323-32

Shefer K, *et al.* 2007. A triple helix within a pseudoknot is a conserved and essential element of telomerase RNA. *Mol Cell Biol* **27**, 2130-43

Singer MS, *et al.* 1994. TLC1: template RNA component of Saccharomyces cerevisiae telomerase. *Science* **266**, 404-9

Smets B, *et al.* 2010. Life in the midst of scarcity: adaptations to nutrient availability in Saccharomyces cerevisiae. *Curr Genet* **56**, 1-32

Spellman PT, *et al.* 1998. Comprehensive identification of cell cycle-regulated genes of the yeast Saccharomyces cerevisiae by microarray hybridization. *Mol Biol Cell* **9**, 3273-97

Steen KA, *et al.* 2012. Fingerprinting noncanonical and tertiary RNA structures by differential SHAPE reactivity. *J Am Chem Soc* **134**, 13160-3

Team RC. R: A language and environment for statistical computing. R Foundation for Statistical Computing, Vienna,
Austria.; 2014.

Teng SC, *et al.* 1999. Telomere-telomere recombination is an efficient bypass pathway for telomere maintenance in Saccharomyces cerevisiae. *Mol Cell Biol* **19**, 8083-93

Theimer CA, *et al.* 2005. Structure of the human telomerase RNA pseudoknot reveals conserved tertiary interactions essential for function. *Mol Cell* **17**, 671-82

Theimer CA, *et al.* 2006. Structure and function of telomerase RNA. *Curr Opin Struct Biol* **16**, 307-18

Theimer CA, *et al.* 2003. Mutations linked to dyskeratosis congenita cause changes in the structural equilibrium in telomerase RNA. *Proc Natl Acad Sci U S A* **100**, 449-54

Theimer CA, *et al.* 2007. Structural and functional characterization of human telomerase RNA processing and cajal body localization signals. *Mol Cell* **27**, 869-81

Toesca I, *et al.* 2011. Cryptic transcription mediates repression of subtelomeric metal homeostasis genes. *PLoS Genet* **7**, e1002163

Trapnell C, *et al.* 2012. Differential gene and transcript expression analysis of RNA-seq experiments with TopHat and Cufflinks. *Nat Protoc* **7**, 562-78

Trapnell C, *et al.* 2010. Transcript assembly and quantification by RNA-Seq reveals unannotated transcripts and isoform switching during cell differentiation. *Nat Biotechnol* **28**, 511-5

Tzfati Y, *et al.* 2000. Template boundary in a yeast telomerase specified by RNA structure. *Science* **288**, 863-7

Tzfati Y, *et al.* 2003. A novel pseudoknot element is essential for the action of a yeast telomerase. *Genes Dev* **17**, 1779-88

van Dijk EL, *et al.* 2011. XUTs are a class of Xrn1-sensitive antisense regulatory non-coding RNA in yeast. *Nature* **475**, 114-7

Verwaal R, *et al.* 2002. HXT5 expression is determined by growth rates in Saccharomyces cerevisiae. *Yeast* **19**, 1029-38

Vulliamy T, *et al.* 2001. The RNA component of telomerase is mutated in autosomal dominant dyskeratosis congenita. *Nature* **413**, 432-5

Watts JM, *et al.* 2009. Architecture and secondary structure of an entire HIV-1 RNA genome. *Nature* **460**, 711-6

Wei C, *et al.* 2003. Protecting the terminus: t-loops and telomere end-binding proteins. *Cellular and molecular life sciences : CMLS* **60**, 2283-94

Weinert TA, *et al.* 1988. The RAD9 gene controls the cell cycle response to DNA damage in Saccharomyces cerevisiae. *Science* **241**, 317-22

Welter E, *et al.* 2010. Quantification of nonselective bulk autophagy in S. cerevisiae using Pgk1-GFP. *Autophagy* **6**, 794-7

Wickham H. ggplot2: elegant graphics for data analysis. New York: Springer; 2009.

Wilkinson KA, *et al.* 2006. Selective 2'-hydroxyl acylation analyzed by primer extension (SHAPE): quantitative RNA structure analysis at single nucleotide resolution. *Nat Protoc* **1**, 1610-6

Wong JM, *et al.* 2006. Telomerase RNA level limits telomere maintenance in X-linked dyskeratosis congenita. *Genes Dev* **20**, 2848-58

Wu J, *et al.* 2012. Non-coding RNAs in Saccharomyces cerevisiae: what is the function? *Biochemical Society transactions* **40**, 907-11

Wyers F, *et al.* 2005. Cryptic pol II transcripts are degraded by a nuclear quality control pathway involving a new poly(A) polymerase. *Cell* **121**, 725-37

Xie Z, *et al.* 2015. Early telomerase inactivation accelerates aging independently of telomere length. *Cell* **160**, 928-39

Xu Z, *et al.* 2009. Bidirectional promoters generate pervasive transcription in yeast. *Nature* **457**, 1033-7

Yang G, *et al.* 2014. LncRNA: a link between RNA and cancer. *Biochimica et biophysica acta* **1839**, 1097-109

Yassour M, *et al.* 2009. Ab initio construction of a eukaryotic transcriptome by massively parallel mRNA sequencing. *Proc Natl Acad Sci U S A* **106**, 3264-9

Yeoman JA, *et al.* 2010. RNA conformation in catalytically active human telomerase. *J Am Chem Soc* **132**, 2852-3

Zappulla DC, *et al.* 2004. Yeast telomerase RNA: a flexible scaffold for protein subunits. *Proc Natl Acad Sci U S A* **101**, 10024-9

Zappulla DC, *et al.* 2005. A miniature yeast telomerase RNA functions in vivo and reconstitutes activity in vitro. *Nat Struct Mol Biol* **12**, 1072-7

Zhang Q, *et al.* 2011. Architecture of human telomerase RNA. *Proc Natl Acad Sci U S A* **108**, 20325-32

Zhang Q, *et al.* 2010. Structurally conserved five nucleotide bulge determines the overall topology of the core domain of human telomerase RNA. *Proc Natl Acad Sci U S A* **107**, 18761-8

Vita

Rachel O. Niederer

rnieder1@jhu.edu
Department of Biology
Johns Hopkins University
Baltimore, MD 21218-2685
(410) 516-7316 (lab)

Education

PhD 2015	**Johns Hopkins University**, Program in Cell, Molecular, Developmental Biology, and Biophysics
BS 2009	**University of Maryland, College Park**, Cell biology and molecular genetics (with high honors)
BS 2009	**University of Maryland, College Park**, Biochemistry

Research experience

2009 – present	**Johns Hopkins University, Department of biology** PhD research Research focus: Structure-function relationships in telomerase RNA Transcriptional response to telomerase deletion in yeast Faculty mentor: Dr. David Zappulla
2007 – 2009	**University of Maryland, Department of cell biology and molecular genetics** Undergraduate honors research Research focus: Protein and rRNA modification in ribosome assembly and function Faculty Mentor: Dr. Jonathan Dinman
2006 – 2007	**University of Virginia, Department of biochemistry and molecular genetics** Research focus: Regulatory mechanisms of RNA polymerase I Faculty Mentor: Dr. Jeffrey Smith

Publications

Niederer, R.O., Papadopoulos, N., Zappulla, D.C. Identification of novel lncRNAs in telomerase-negative yeast by RNA-seq (Under review at *Scientific Reports*)

Niederer R.O., Zappulla D.C. (2015) Refined secondary structure models of the core of yeast and human telomerase RNAs directed by SHAPE. *RNA*. 21(2):254-61

Lebo, K.J., **Niederer, R.O.,** Zappulla, D.C. (2015) A second essential function of the Est1-binding arm of yeast telomerase. *RNA*. Epub 2015 Mar 3.

Jack K, Bellodi C, Landry D.M., **Niederer R.O.**, Meskauskas A, Musalgaonkar S, Kopmar N, Krasnykh O, Dean A.M., Thompson S.R., Ruggero D, Dinman J.D. (2011). rRNA pseudouridylation defects affect ribosomal ligand binding and translational fidelity from yeast to human cells. *Mol Cell*. 44(4):660-6

Hontz, R.D., **Niederer, R.O.**, Johnson, J.M., Smith, J.S. (2009). Genetic Identification of Factors that Modulate Ribosomal DNA Transcription in Saccharomyces cerevisiae. *Genetics.* 182(1):105-19

Manuscripts in preparation

Niederer, R.O., Gelsinger, D.R., Papadopoulos, N., Zappulla, D.C. Defining the distinct transcriptional response to short telomere-induced senescence

Posters and Presentations

2015 Telomeres and Telomerase, Cold Spring Harbor, NY
Niederer, R.O., Wang, Y., Papadopoulos, N., Zappulla, D.C. Defining the distinct transcriptional response to short telomere-induced senescence (Poster)

2015 RNA Biology, NIH, Bethesda, MD
Niederer, R.O., Wang, Y., Papadopoulos, N., Zappulla, D.C. Global changes in transcription and rna processing during short telomere-induced senescence in yeast identified by RNA-seq (Poster)

2013 RNA Society meeting, Davos, Switzerland
Niederer, R.O., Zappulla, D.C. Investigating the structures of the yeast and human telomerase RNAs by SHAPE (Poster)

2008 Bioscience Day, University of Maryland, College Park
Niederer, R.O., Dinman J.D. Genetic Characterization of CBF5 mutants: implications with regard to Dyskeratosis congenita (Poster)

2007 Summer Research Symposium, University of Virginia
Niederer R.O., Smith, J.S. A Role for DNA replication in the inheritance of rDNA silencing (Talk)

2006 Summer Research Symposium, University of Virginia
Niederer, R.O., Smith, J.S. Regulatory mechanisms of RNA Polymerase I (Talk)

Teaching experience

2015 Intersession instructor, RNA in disease
Johns Hopkins University
Proposed and developed the course covering:
- Molecular mechanisms underlying RNA-based diseases
- Practical, hands on experience processing gene expression datasets using Tuxedo suite tools and R

2014 Guest lecturer, Eukaryotic molecular biology
Professor: Van Moudrianakis
Johns Hopkins University
Designed and taught 5 lectures covering
- DNA replication and repair
- Transcription
- RNA processing & nuclear export
- Translation and mRNA decay
- Methods in molecular biology including high-throughput sequencing technologies

2012 - 2014 Participant
Symposium on Excellence in Teaching and Learning in the Sciences, Johns Hopkins University

2014 Teaching assistant, lecture
Cell biology, Johns Hopkins University
Duties: grading problem sets & exams, led 4 recitation sessions

2013 Teaching assistant, lab
Genetics, Johns Hopkins University

Duties: Introduced weekly lab concepts and techniques, supervised experimental procedures, graded lab reports, held office hours

2011 Teaching assistant, lab
Cell biology, Johns Hopkins University
Duties: Introduced weekly concepts and techniques, supervised experimental procedures, graded weekly lab reports, held optional review for final exam

2010 Teaching assistant, lab
Biochemistry, Johns Hopkins University
Duties: Introduced weekly concepts and techniques, supervised experimental procedures, graded weekly lab reports

2005 Teaching assistant, lab and lecture
General biology, Cabrillo College, Aptos, CA
Duties: Held weekly office hours, graded lab reports, problem sets and weekly quizzes, supervised experimental procedures

Mentoring experience

2009 – present Johns Hopkins University
Graduate students: Michael Bemben, Josh Spurrier, Justin Brodie-Kommit, Jessica Winger, Diego Gelsinger

Undergraduate students: Jeffrey Nelson, Praneeth Sadda, Michael Setteducato, Eduardo Urias (BioREU participant)

Awards and honors

2013 **RNA society travel fellowship**
2008 – 2009 **HHMI Undergraduate Research Fellow**
University of Maryland, College Park
2008 **Tau Sigma Honor Society**
University of Maryland, College Park
2008 **Primmanum Honor Society**
University of Maryland, College Park
2007 – 2009 **Cell Biology and Molecular Genetics Honors Program**
University of Maryland, College Park
2006 – 2007 **SRIP undergraduate research fellowship**
University of Virginia, Charlottesville, VA

2004 – 2006 **Deans List**
Cabrillo College, Aptos, CA
2005 **Cornelia Ackley Memorial Biology Scholarship**
Cabrillo College, Aptos, CA
2003 – 2004 **Founders Scholarship Level II**
Tulane University, New Orleans, LA
2003 – 2004 **St. Johns Hospital Scholarship**
Tulane University, New Orleans, LA

Professional memberships

2014 – present American Society of Cell Biology (ASCB)
2013 – present RNA society